Synchrony and Bifurcations in Coupled Dynamical Systems and Effects of Time Delay

Dissertation
zur Erlangung des akademischen Grades

doctor rerum naturalium

(Dr. rer. nat.)

Im Fach Mathematik

eingereicht an der Mathematisch-Naturwissenschaftlichen Fakultät
der Humboldt-Universität zu Berlin

von

Diplom-Mathematiker
Jan Philipp Pade

Präsident der Humboldt-Universität zu Berlin

Prof. Dr. Jan-Hendrik Olbertz

Dekan der Mathematisch-Naturwissenschaftlichen Fakultät

Prof. Dr. Elmar Kulke

Gutachter/innen:

1. Prof. Dr. Caren Tischendorf
2. Prof. Dr. Zhao Liang
3. Dr. Serhiy Yanchuk

Tag der mündlichen Prüfung: 22.07.2015

Acknowledgements

I did most of the work contained in this thesis in Berlin, as a member of the Junior Research Group "Applied Analysis, Dynamics and Synchronisation of Complex Systems" under the leadership of my supervisor Dr. Serhiy Yanchuk. So first of all I want to thank Serhiy for the great communicative and inspiring atmosphere he created. He had literally always time for questions and long discussions and he taught me a great deal about how to approach, solve and present problems. I also want to thank my supervisor Prof. Dr. Zhao Liang from São Paulo and Tiago Pereira from London for sharing their knowledge and for making my guest stays in their groups so enjoyable and fruitful.

I want to thank my colleague Leonhard Lücken for all the inspiring discussions - it was a pleasure to work with him. Furthermore I thank Petar Tomov, Michael Zaks, Lutz Recke, Irina Kmit and Dmitry Puzyrev for the great atmosphere in the Applied Analysis group.

I want to thank Regina, Jochen, Tamina and Jonas for having supported me so carefully.

This work would not have been possible without the funding of the DFG in the framework of the International Research Training Group (IRTG) 1740, "Dynamical Phenomena in Complex Networks".

Finally, I want to thank Dr. S. Yanchuk, Prof. Dr. L. Zhao and Prof. Dr. Caren Tischendorf for reading this thesis. I hope you enjoy some of it.

Thank you!

Philipp

Abstract

Since a couple of decades, dynamics on networks is a rapidly growing branch of mathematics with applications in various disciplines such as physics, biology or sociology. The functioning of many networks heavily relies on the ability to synchronize the network's nodes. More precisely, the existence and the transverse stability of the synchronous manifold are essential properties. It was only in the last few years that people tried to understand the entangled relation between the coupling structure of a network, given by a (di-)graph, and the stability properties of synchronous states. This is the central theme of this dissertation. I first present results towards a classification of the links in a directed, diffusive network according to their impact on the stability of synchronization. Then I investigate a complex bifurcation scenario observed in a directed ring of Stuart-Landau oscillators. I show that under the addition of a single weak link, this scenario is persistent. Subsequently, I investigate synchronous patterns in a directed ring of phase oscillators coupled with time delay. I discuss the coexistence of multiple of synchronous solutions and investigate their stability and bifurcations. I apply these results by showing that a certain time-shift transformation can be used in order to employ the ring as a pattern recognition device. Next, I investigate the same time-shift transformation for arbitrary coupling structures in a very general setting. I show that invariant manifolds of the flow together with their stability properties are conserved under the time-shift transformation. Furthermore, I determine the minimal number of delays needed to equivalently describe the system's dynamics. Finally, I investigate a peculiar phenomenon of non-continuous transition to synchrony observed in certain classes of large random networks, generalizing a recently introduced approach for the description of large random networks to the case of delayed couplings.

Abstrakt

Dynamik auf Netzwerken ist ein mathematisches Feld, das in den letzten Jahrzehnten schnell gewachsen ist und Anwendungen in zahlreichen Disziplinen wie z.B. Physik, Biologie und Soziologie findet. Die Funktion vieler Netzwerke hängt von der Fähigkeit ab, die Elemente des Netzwerkes zu synchronisieren. Mit anderen Worten, die Existenz und die transversale Stabilität der synchronen Mannigfaltigkeit sind zentrale Eigenschaften. Erst seit einigen Jahren wird versucht, den verwickelten Zusammenhang zwischen der Kopplungsstruktur und den Stabilitätseigenschaften synchroner Zustände zu verstehen. Genau das ist das zentrale Thema dieser Arbeit. Zunächst präsentiere ich erste Ergebnisse zur Klassifizierung der Kanten eines gerichteten Netzwerks bezüglich ihrer Bedeutung für die Stabilität des synchronen Zustands. Folgend untersuche ich ein komplexes Verzweigungsszenario in einem gerichteten Ring von Stuart-Landau Oszillatoren und zeige, dass das Szenario persistent ist, wenn dem Netzwerk eine schwach gewichtete Kante hinzugefügt wird. Daraufhin untersuche ich synchrone Zustände in Ringen von Phasenoszillatoren die mit Zeitverzögerung gekoppelt sind. Ich bespreche die Koexistenz synchroner Lösungen und analysiere deren Stabilität und Verzweigungen. Weiter zeige ich, dass eine Zeitverschiebung genutzt werden kann, um Muster im Ring zu speichern und wiederzuerkennen. Diese Zeitverschiebung untersuche ich daraufhin für beliebige Kopplungsstrukturen. Ich zeige, dass invariante Mannigfaltigkeiten des Flusses sowie ihre Stabilität unter der Zeitverschiebung erhalten bleiben. Darüber hinaus bestimme ich die minimale Anzahl von Zeitverzögerungen, die gebraucht werden, um das System äquivalent zu beschreiben. Schließlich untersuche ich das auffällige Phänomen eines nichtstetigen Übergangs zu Synchronizität in Klassen großer Zufallsnetzwerke indem ich einen kürzlich eingeführten Zugang zur Beschreibung großer Zufallsnetzwerke auf den Fall zeitverzögerter Kopplungen verallgemeinere.

Contents

List of Figures

CHAPTER 1

Introduction

"The real voyage of discovery consists
not in seeking new landscapes,
but in having new eyes."
Marcel Proust, In search of lost time

In the introduction of my thesis I motivate central questions and quantities from dynamical systems on networks. Along this first chapter we will encounter all the problems I treat in my thesis. As soon as such a problem is mentioned here I will refer to the corresponding chapter. I begin with a short introduction in the history of dynamical systems on networks.

1.1. Dynamical systems on networks

Compared to classical mathematical disciplines such as algebra, complex analysis or even differential equations, dynamical systems on networks is a rather young discipline. It locates in the intersection of dynamical systems, graph theory and probabilistic theory. In order to motivate the approach, I describe one of the first impulses which was given by Smale in 1976 [**163**]. Smale took up an idea introduced by Turing [**173**] who modeled two biological cells interacting via diffusion past a membrane. Each of these cells is supposed to be "dead", i.e. inactive when left alone. In mathematical terms, the individual dynamics are modelled by a globally stable fixed point. However, Turing observed that when these dead cells were coupled they began pulsing. In other words, a globally stable periodic orbit emerged through a Hopf bifurcation. When Smale took up this study, he investigated the simplest case of two cells first. Only after having discussed this case, he asked under which general conditions this phenomenon can be observed when coupling more than two cells. To be more precisely, in [**163**] he investigated the following problem. Consider the equations

$$\dot{\boldsymbol{x}}_i = \boldsymbol{f}(\boldsymbol{x}_i) + \sum_{j=1}^{N} a_{ij}\boldsymbol{\Gamma}(\boldsymbol{x}_j - \boldsymbol{x}_i) \qquad \boldsymbol{x}_i \in \mathbb{R}^m,\ 1 \leq i \leq N \tag{1.1.1}$$

where the identical single cell dynamics is given by a vector field $\boldsymbol{f} : \mathbb{R}^m \to \mathbb{R}^m$, admitting a globally stable fixed point. The network structure $A = \{a_{ij}\}$ is given by the $a_{ij} \in \{0, 1\}$ where the cell j is coupled to cell i iff $a_{ij} = 1$. The local coupling is given by a diagonal matrix $\boldsymbol{\Gamma} \in \mathbb{R}^{m\times m}$. For which triples

$(\boldsymbol{A}, \boldsymbol{f}, \boldsymbol{\Gamma})$ does the coupled system admit a globally stable periodic orbit? Even for the case of two coupled cells Smale was not able to characterize the pairs $(\boldsymbol{f}, \boldsymbol{\Gamma})$ which do so, and to my knowledge the general problem is not solved until today.

Smale's article could be seen as the birth of dynamical systems on networks. Here, it serves as an illustration for the fact that looking at ordinary differential equations from another point of view, i.e. treating the coupling as a separate structure can lead to new problems and to new solutions of old problems. It highlights the fact that bifurcations due to the network structure can be an important factor in applications: there are coupling schemes for which the cells won't oscillate, but will rather stay at the fixed points. By adding or even deleting connections in the network, the system might undergo a (Hopf) bifurcation which yields stable oscillations. This is where graph theory comes into play, and again, this is what distinguishes dynamical systems from dynamical systems on networks: the point of view. Indeed, we could understand Eq. (1.1.1) as a system of first order ordinary differential equations like scientists have done for a long time. However, for many questions concerning the existence and stability of special states such as equilibria, periodic orbits or synchronous motions, it turns out that the coupling structure understood as a graph plays a major role. More specifically, quantities associated to algebraic properties of the graph will show up in the stability criteria. Or, to put it in rather simple terms: in some cases we might be able to state results by just looking at the graph, without any further specific knowledge of the local dynamics. Technically, the theory of dynamical systems still delivers the main tools. However, step by step, tools and notions from graph theory and recently developed network measures **[129]** find their way into this interdisciplinary field of research. In the line of research initiated by Smale, the most prominent contributions came from Ermentrout and Kopell who investigated coupled oscillators with non-weak coupling **[53, 6]** and Golubitsky and Stewart who founded a whole mathematical theory for the dynamics on networks with symmetries **[65, 66, 37, 36]**.

Another line of research was initiated by Wiener in 1958 **[181]**. He made first attempts to mathematically describe self organization in networks and investigate existence and stability of synchronous states, in which all the elements of a network behave in the same manner. These states were observed in nature quite early, for instance in ensembles of south-east Asian fireflies **[25, 75]**, but their generating mechanism remained in the dark for a long time. However, the description by Wiener, consisting of coupled nonlinear limit-cycle oscillators, was far too complex to understand basic mechanisms of synchronization. In 1967, Winfree took up this thread and made a huge step forward by essentially reducing the underlying describing differential equations **[182]**. Firstly, he considered states of limit cycle oscillators which were close to the limit cycle. Secondly, he assumed that the interaction between elements

was weak enough not to kick the individual oscillators away from the limit cycle. Under these assumptions, the amplitude of each element could be neglected and its state variable reduced to a scalar variable describing the phase of the oscillator in the limit cycle - the birth of phase oscillators. The next seminal step in this line of research was the introduction of the much acclaimed Kuramoto model by Kuramoto in 1975 together with a thorough bifurcation analysis [**101**]. The main simplification consisted in a reduction to sinusoidal coupling and a neglect of higher harmonics, resulting in the tractable equations

$$\dot{\varphi}_i = \omega_i + \frac{K}{N} \sum_{j=1}^{N} \sin\left(\varphi_j - \varphi_i\right)$$

for the oscillator's phases φ_i. The introduction of this model in the scientific community was followed by a sustained research activity on exhibited dynamics of the model and derived models in various fields ranging from Biology and Physics to Mathematics. Two of the most important contributors were certainly S. Strogatz and R. Mirollo who were first capable of proving a conjecture made by Kuramoto about the stability of the incoherent state [**168**]. By now, a countless number of publications on probably any imaginable variant of the Kuramoto exists: Systems with non-global coupling, with stochastic terms, with time delays, continuum limits and many more [**3, 167, 20**]. However, I remark that even for the rather simple case of global coupling, a stability analysis of partially synchronized states was only done in 2005 [**123**]. Furthermore, a conjecture by Kuramoto about the persistence of the bifurcation scenario when the number of oscillators N goes to infinity was only proved in 2010, using elaborate function analytic techniques [**32, 33**]. Therefore, it should be no surprise that oscillators coupled in a non-global fashion are still heavily investigated. Unfortunately, unless the network admits some kind of symmetry, these systems are much more complicated to study and new tools are still being developed. In this thesis all the questions are related to non-global coupling in general. From the applied point of view it is crucial to understand the dynamical behaviour of non-globally coupled systems. Our everyday lives are dominated by networks many of which do neither have a global nor a constant coupling topology. For instance social networks, the internet and economic networks are under constant evolution [**79, 135, 119**]. The connections between nerve cells are changing due to synaptic plasticity [**77, 1**], and our power-grid is not only under constant evolution, but right now subject to a considerable change due to the inclusion of renewable energy sources [**57**]. I remark that in many cases the evolution of the network is on a slower time scale than the node dynamics, so it can be neglected in dynamical models. In these cases, it is desirable to develop a theory which can predict stability changes induced by network modifications. I investigate questions related to this problem in **Chapters 2** and **3**.

1.2. Synchrony in networks of coupled elements

As in the line of research initiated by Wiener, I will mainly be interested in the existence and stability of particular states such as equilibria and synchronous states[1]. Here, in general the term synchronization refers to the state where all the nodes of a network behave identically. However, it can refer to different phenomena. For instance, when oscillators synchronize their frequencies, whereas the phases are not identical, one would speak about frequency-synchronization [**88**], or in the opposite case, where the phases are synchronized while the amplitudes differ, one speaks about phase synchronization [**141, 151**]. Motivated by the observation that the function of many real world networks heavily relies on their synchronization properties, the last few years have shown a steep increase in publications investigating (stability) properties of synchronous states in networks [**141, 136, 12**]. Examples for the importance of network synchronization in our everyday lives stem from various applications. In power grids, power stations must keep a proper synchronization to avoid energy supply disturbances and blackouts [**125, 47**]. Sensor networks rely on synchronization among sensors to transmit information [**134**]. In the brain, epileptic seizures and motor diseases such as Dystonia and Parkinson are a strong manifestation of synchronization of subcortical brain areas [**122, 165, 73**]. On the other hand, it is strongly hypothesized that synchronization is the main mechanism through which distant brain areas connect, even in such complex tasks as human cognition [**97, 62**]. Further examples can be found in consensus formation [**146, 31**] where different parties try to reach a common state.

Here, I will consider systems for which the set of synchronous motions is invariant. in other words, if the network's nodes move in synchrony and are not perturbed, they will stay synchronized for all times. Now in general, invariant sets of dynamical systems can be very complicated and must not be smooth at all, even for very simple dynamical rules. A famous example is Smale's horseshoe, an invariant set which contains a dense set of periodic orbits and a dense orbit and which since it's discovery in 1967 serves as a paradigmatic structure for chaotic dynamics [**162**]. However, under mild assumptions some of the invariant sets turn out to be submanifolds of the phase space, such as the synchronous manifold, the set given by all the solution curves of synchronous motion. In mathematical terms, most of the problems connected to synchrony in networks deal in one way or another with the transverse stability of invariant manifolds in dynamical systems. Once an invariant manifold is shown to be stable one can investigate the dynamics restricted to the manifold and thereby essentially reduce the dimension of the dynamical system. In general, invariant manifolds together with their stability properties have been studied

[1]Here, synchronous states includes synchronization where the individual node dynamics are chaotic.

in various systems, ranging from difference equations to ordinary differential equations [**58**] up to abstract dynamical systems in Banach spaces [**35, 171**]. Although sharp criteria for the transverse stability of the synchronous manifold have been found, it was only in the last few decades that these have been connected to properties of the underlying coupling structure. One way to do so is the Master-Stability formalism [**136**]. This approach relies on a decoupling of the linearised system which enables one to study the long-term behaviour of perturbations transverse to the synchronization manifold. The transverse directions in turn are exclusively determined by the coupling structure. A disadvantage of this approach is that it uses Maximal Lyapunov Exponents (MLE) in order to infer stability properties for the linearised system. However, it is known that for non-autonomous system, in general, a negative maximal MLE does not induce stability of the nonlinear system, nor does a positive MLE induce instability of the nonlinear system [**110**]. One of the reasons for the success of the Master-Stability formalism is that it can simply be implemented for numerical calculations and allows for a broad range of coupling functions. So for (relative) equilibria it is well suited. We will employ this formalism in **chapter 3**. Another approach which was recently introduced relies on the use of exponential dichotomies for non-autonomous systems [**137, 38**]. This approach delivers conditions for exponential contraction towards the synchronous manifold in the nonlinear system.

1.3. Time delays in networks

A quantity which does not appear in the above examples, but which is an important factor in many of the above mentioned real life networks is time delay. More precisely, the connections between the nodes can be delayed, that is the input of a node i at time t is the state of a node j at time $t-\tau$ for some $\tau > 0$. From the point of view of modelling, there are several motivations for including time delay in the network's connections. In neuronal dynamics, delays incorporate the time a neuronal spike needs to travel along an axon to the next neuron [**27**]. In laser dynamics, delays correspond to the propagation time of the light [**188, 177**], and in population models, delays incorporate times needed for maturing and gesturing [**100**]. Now, in order to solve a given delay differential equation (DDE) uniquely, it is not sufficient to impose an initial condition from some $\mathbb{R}^n$, but one has to supply an initial function on the whole interval $[-\tau, 0]$ (in the case of a single delay). In other words, the phase space is infinite dimensional. Here, I remark that DDEs can be seen as a special case of hyperbolic partial differential equations (see Appendix C) where one can think of the solution operator as a transport of the initial function segment on the interval $[-\tau, 0]$. A consequence is, that in general, results or techniques from ordinary differential equations cannot be applied to this class of equations. So mathematically, the incorporation of delays poses new problems and asks for new tools. Not only will delays ask for new methods,

but also the qualitative behaviour can be very different from the associated ordinary differential equation which is obtained by setting the delays to zero. To see this, consider for instance the following example from **[100]** (p.11)

$$\dot{x}(t) + 2\dot{x}(t-\tau) = -x(t).$$

For $\tau = 0$ it is easy to see that the origin is a stable equilibrium. However, for any $\tau > 0$ it becomes unstable (See **[100]** for further examples). Fortunately though, generically, small delays will have small effects for the class of non-neutral delay equations ([**34**]), that is equations which do not involve delays in the highest order derivative.

A rather unexplored task within the theory of delay equations consists in the investigation of equations with multiple delays. This is in contrast to the fact that in many applications one is confronted with a large number of different delays. In mesoscale brain models the transmission delays depend on the distance between distant connected brain areas [**42, 69**] . Even in network models of single cells it is known that due to myelination of the axons transmission times can vary independently of the axon's length[**27, 28**]. In gene regulatory networks time delays model the duration of biochemical reaction chains [**40, 111**]. When treated as system parameters, this multitude of delays makes analytic approaches harder in many senses. It is known that the dimension as well as the number of attractors increase linearly with the delay [**189, 48, 18**]. In numerical studies every additional delay drastically increases the computational costs. So independent of the approach, it is desirable to reduce the number of different delays, a task which was only addressed for some examples so far [**9, 117, 138, 142**]. In **chapter 5** I treat this problem and related stability questions in a very general setting.

Despite the problems multiple delays can cause in investigations, they might be a main ingredient in the functioning of complex networks such as the brain [**42, 69**]. Indeed, delays can be a used as a tool for constructing complex dynamics in relatively simple models. In [**142, 190**] it was shown that tuning the delays in a ring of delay coupled oscillators, one can produce almost arbitrary patterns. I use this idea in **chapter 4** to construct a pattern recognition device from a ring of delay coupled oscillators. But even with a scalar equation with a single delay, one can construct a pattern recognition device as shown in [**107**]. Other ideas to construct pattern recognition devices using time delays with pulse-coupled elements can be found in [**81, 115**]. Finally, I want to mention that by introducing a time delayed control term in ordinary differential equations, one can stabilize unstable (periodic) orbits [**144, 94, 60, 59**] in a non-invasive fashion, which means the control vanishes once the desired state is attained.

1.4. Large random networks

Another challenge in many applications is the mere size of the networks. The human brain consists of around $8 \cdot 10^{10}$ neurons [**78**], social networks expand over the whole globe and food-webs can include thousands of species. In some cases it is useful to approximate a large system with an appropriate infinite dimensional system. For instance, in the case of phase oscillators subject to external noise, when increasing the number of oscillators, the system can be described by a partial differential equation called Fokker-Planck equation [**176, 155**]. Motivated by terminology from statistical physics, the limit process of increasing the dimension of the system to infinity is also called taking the thermodynamic limit. A similar case of a thermodynamic limit is treated in **chapter 6**. Here, the distribution of the phases θ_k of a large ensemble of oscillators is described by a smooth density function $f(\theta, t)$ which again fulfils a partial differential equation. Although at first glance it might appear that the infinite dimensional problem is harder to solve, which in general is true, in many cases it allows for more insight. The reason is that, as in an asymptotic analysis, the finite size irregularities are smoothed out in the thermodynamic limit. For illustration consider the sum $\sum_{k=1}^{N} \sqrt{k}$. It is not clear how to calculate this sum other than with the help of a computer. However, if we suppose N is large, we can use the approximation with an upper integral to write $\int_0^1 \sqrt{x} dx \approx \frac{1}{N} \sum_{k=1}^{N} \sqrt{\frac{k}{N}}$. Now the integral can easily be computed by hand and we obtain $\sum_{k=1}^{N} \sqrt{k} \approx \frac{2}{3} N^{3/2}$. I remark that infinite dimensional systems can in general be approximated by finite dimensional systems. In contrast, the other way around is not always possible as for instance in **chapter 3** where I consider a unidirectional ring of oscillators which can not be understood as discretization of a spatially extended system. Surprisingly enough, the phenomenon observed in this finite size network is similar to one observed in a spatially extended system, namely the Eckhaus instability in reaction-diffusion systems [**172, 85**]. And even more, a finite dimensional network can exhibit very different dynamics from its infinite dimensional counterpart. Such a case was observed in [**128**] where the authors investigate a discretization of a reaction-diffusion equation. The discrete and the continuous equation both exhibit a destabilization of the homogeneous state through a Turing instability. However, the bifurcation scenario observed in the finite dimensional system, given by a network of diffusively coupled nodes (such as in **chapter 2**) is very different from the classical Turing instability in spatially extended systems. Partly, this relies on the special coupling topology that was chosen for the network, namely a scale-free topology. Roughly speaking, such random networks consist of few nodes with many links and many nodes with few links. I will go into more detail in **chapter 6** where I investigate the dynamics of phase oscillators in this class of networks. Since the early 2000s they have been discovered to be an important structure in applications such as the world-wide

web or social networks [**4, 112**]. It is remarkable that, although the theory of dynamics on networks has been a growing field in the last decades, it has only been in the beginning of this millennium that the importance of special topologies like scale-free networks was discovered and dynamics on these structures were studied extensively [**20**]. Another important class of random networks I want to mention here are small-world networks. These networks became famous after the American scientist S. Milgram claimed in the late 1960s that the human society is a small-world network . This claim was supported by an experiment which showed that an American citizen was acquainted with any other American citizen through at most five people. The coupling topology of a small-world network is given by a graph in which every node is coupled to its k nearest neighbours and additionally a few random connections are added. Since then, small-world networks were discovered in various disciplines such as sociology, biology and neuroscience [**4, 124, 158**]. I will investigate the dynamics of limit-cycle oscillators on such a network in **chapter 3**. Although they won't appear in this thesis, for the sake of completeness I want to mention another important class of random networks given by Erdös-Renyi graphs. These graphs can be constructed by taking N unconnected nodes, browsing through all possible connections and setting a link with (independent) probability p. Thus, the number of Erdös-Renyi graphs with N nodes and k links is $p^k (1-p)^{\binom{N}{2}-k}$. An important question is how the dynamics exhibited by networks with these different types of coupling structures differ qualitatively or even quantitatively [**167**]. This problem was often investigated regarding the stability of synchronous states. Unfortunately, there is no easy takehome message, but there are partial results. It was shown for a large class of systems that heterogeneity in the coupling structure yields better synchronizability than a regular coupling structure such as lattices [**93, 63**]. Indeed, heterogeneity decreases the average path length in the graph, so the network becomes "smaller" and can be expected to be easier to synchronize. However, to make matters more complicated, it was shown shortly after that within a certain class of scale-free networks, higher heterogeneity leads to worse synchronization properties [**127, 126**]. And to make things even more complicated, it was shown in [**7**] that it is by far not enough to consider given degree distributions in order to infer stability properties of the synchronous state. More precisely, for a given degree distribution corresponding to one of the above mentioned random graph classes one is able to construct a network which is arbitrarily close to desynchronization. The reason for this variety of behaviours is that the stability of synchronization really depends on a fine interplay between three ingredients: the coupling topology, the coupling function and the individual node dynamics. In **chapter 2** I show how these three interact for a large class of dynamics and

arbitrary coupling topologies. Summarizing, the relation between the dynamics of a network and its coupling topology is very entangled and corresponding statements should be made with great care.

1.5. Basic definitions, notations and results

Here, we give some basic definitions and results which will be used throughout the thesis. If not stated otherwise we will consider the euclidean norm on $\mathbb{R}^N$, so

$$\|\boldsymbol{x}\| := \sqrt{x_1^2 + \ldots + x_N^2}, \quad x \in \mathbb{R}^N.$$

The corresponding scalar product $(\boldsymbol{x}, \boldsymbol{y}) = \sum_{k=1}^{N} x_k y_k$ will simply be denoted by $\boldsymbol{xy}$. For vectors and matrices we will use bold face symbols, for instance $\boldsymbol{x} \in \mathbb{R}^N$ and $\boldsymbol{A} \in \mathbb{R}^{N\times N}$. For the identity mapping of a space $\mathbb{R}^N$ we write $\boldsymbol{I}_N$. If no confusion can arise we just write $\boldsymbol{I}$. We will also use notions from both, the theory of dynamical systems and graph theory.

1.5.1. Dynamics. Let us consider the equation

$$\dot{\boldsymbol{x}}(t) = \boldsymbol{f}(\boldsymbol{x}(t)) \tag{1.5.1}$$

where we assume either $\boldsymbol{x} \in \mathbb{R}^N$ or $\boldsymbol{x} \in \mathbb{T}^N = S^1 \times S^1 \times \ldots \times S^1$. I mentioned in the introduction that there are different notions of synchronization. Here, we define as follows

Definition 1. We say a solution $\boldsymbol{x}(t)$ of (1.5.1) is synchronous, if $x_i(t) = x_j(t)$ for all $i, j \leq N$ and for all $t > 0$. The solution $\boldsymbol{x}(t)$ synchronizes if we have

$$\|x_i(t) - x_j(t)\| \to 0$$

for $t \to \infty$ and all $i, j \leq N$.

For systems of coupled phase oscillators, the degree of synchrony can be measured with a real variable r between zero and one.

Definition 2. For $\boldsymbol{x} \in \mathbb{T}^N$ we define the order parameter r as

$$r(\boldsymbol{x}) = \frac{1}{N}\left|\sum_{j=1}^{N} e^{ix_j}\right|.$$

Suppose $\boldsymbol{x}(t) \in \mathbb{T}^N$ is a solution of Eq. (1.5.1). Then we call $\boldsymbol{x}$ the incoherent state if $r(\boldsymbol{x}) = 0$. This corresponds to a solution for which the oscillator's phases are equally distributed along the circle. In contrast, in the synchronous state all the phases coincide, so $x_j = x_s$ for some $x_s(t) \in S^1$ and all j, and we have $r(\boldsymbol{x}) = \left|e^{ix_s}\right| = 1$.

1.5.2. Graph Theory and Algebra.

Definition 3. A digraph $\mathcal{G} = (\mathcal{N}, \mathcal{E})$ is a set of nodes $\mathcal{N} \subset \mathbb{N}$ together with links $\ell \in \mathcal{E}$ given as a set of ordered pairs of nodes. A weighted digraph

$\mathcal{G} = (\mathcal{N}, \mathcal{E}, c)$ is a triple of nodes and links together with a map $c : \mathcal{E} \to \mathbb{R}$ called weights.

For undirected graphs, the concept of connectedness is very natural. However, directed graphs can have a more complicated structure. We differentiate between different types of connectedness [**10**]

DEFINITION 4. A digraph $\mathcal{G} = (\mathcal{N}, \mathcal{E})$ is strongly connected if every node is reachable from every other node through a directed path. That is

$$\forall i, j \in \mathcal{N}\, \exists l_k \in \mathcal{E}\ k = 1, 2, \ldots r\ :\ l_1(2) = j,\ l_r(1) = i,\ l_k(1) = l_{k+1}(2)\,.$$

The digraph is weakly connected if it is not strongly connected and the underlying graph which is obtained by ignoring the links' directions is connected. A strongly connected subdigraph of a weakly connected digraph is called strongly connected component, or short strong component. A set of links which connects two strong components is called cutset.

Obviously, for undirected graphs, the two notions of connectedness are equivalent. Furthermore, with these new notions it is clear that any link in a digraph $\mathcal{G}$ belongs either to a strong component, or to a cutset.

When analysing the dynamics on networks, algebraic properties of graphs will play an essential role. The following definition introduces a natural connection between graphs and algebra

DEFINITION 5. Let $\mathcal{G} = (\mathcal{N}, \mathcal{E})$ be an unweighted digraph. Set $W_{ij} = 1$ if there is a link $\ell \in \mathcal{E}$ such that $\ell(1) = j$ and $\ell(2) = i$ and $W_{ij} = 0$ otherwise. Then we call $\boldsymbol{W} = \{W_{ij}\}$ the adjacency matrix of $\mathcal{G}$. Equivalently, for a weighted digraph $\mathcal{G} = (\mathcal{N}, \mathcal{E}, c)$ set $W_{ij} = c(\ell)$ if there is a link $\ell \in \mathcal{E}$ such that $\ell(1) = j$ and $\ell(2) = i$ and $W_{ij} = 0$ otherwise.

Closely related to the adjacency matrix is the so called graph Laplacian.

DEFINITION 6. Let $\mathcal{G}$ be a weighted digraph with adjaceny matrix $\boldsymbol{W}$. Then we call

$$\boldsymbol{L} = \boldsymbol{D_W} - \boldsymbol{W}$$

the graph Laplacian. Here, we defined the diagonal matrix $\boldsymbol{D_W}$ as

$$(\boldsymbol{D_W})_{ij} = \begin{cases} \sum_{k=1}^{n} W_{ik} & j = i \\ 0 & \text{else} \end{cases}\,.$$

This definition generalizes the notions of adjacency matrix and graph Laplacian which are usually used in the context of simple graphs without weights. In the context of synchronization, an important property of the Laplacian is that by definition its row sums vanish as will turn out later. Now, we can define the term network properly.

DEFINITION 7. A network $\mathcal{M} = (\mathcal{G}, \boldsymbol{f}, \boldsymbol{H})$ is a triple consisting of a digraph $\mathcal{G}$, local dynamics $\boldsymbol{f} = (f_1, f_2, \ldots, f_N)$ with $f_k : \mathbb{R}^m \to \mathbb{R}^m$ and a coupling function $\boldsymbol{H} : \mathbb{R}^m \to \mathbb{R}^m$.

I emphasize that if no confusion can arise about the dynamics $\boldsymbol{f}$ and the coupling function $\boldsymbol{H}$, we will identify the terms network and graph. However, one should always keep in mind this definition as most of the difficulties in dynamics on networks arise from the close entanglement of these three objects. The next result by Gershgorin is of purely algebraic nature and concerns the location of the eigenvalues of a matrix [**106**].

THEOREM 8. *(Gershgorin) Let* $\boldsymbol{A} \in \mathbb{C}^{N\times N}$ *and*

$$d_i = \sum_{k=1}^{N} |a_{ik}|,$$

then every eigenvalue of A lies in at least one of the disks

$$\{z| \, |z - a_{jj}| \leq d_j\}, \qquad j = 1, 2, \ldots, N$$

Finally, we will need a very useful theorem concerning the spectrum of a special class of matrices, namely the Perron-Frobenius theorem [**17**]. In order to state the theorem we first need to introduce the notion of reducibility of a matrix. We call a matrix $\boldsymbol{A} \in \mathbb{R}^{N\times N}$ reducible if there is an $N \times N$ permutation matrix $\boldsymbol{P}$ (i.e. a matrix which is obtained by an interchange of rows and columns of the identity matrix) such that

$$\boldsymbol{P}^t \boldsymbol{A} \boldsymbol{P} = \begin{pmatrix} \boldsymbol{A} & \boldsymbol{B} \\ \boldsymbol{0} & \boldsymbol{C} \end{pmatrix}$$

for square matrices $\boldsymbol{A}$ and $\boldsymbol{B}$. If no such $\boldsymbol{P}$ exists $\boldsymbol{A}$ is irreducible [**106**]. It is worth mentioning that the adjacency matrix $\boldsymbol{A}$ of a digraph $\mathcal{G}$ is irreducible if and only if $\mathcal{G}$ is strongly connected. Now we can state the theorem.

THEOREM 9. *Let* $\boldsymbol{A} \in \mathbb{R}^{N\times N}$ *be a nonnegative matrix, i.e.* $a_{ij} \geq 0$ *for all* $i, j \leq N$. *Assume further that* $\boldsymbol{A}$ *is irreducible. Then* $\boldsymbol{A}$ *possesses a maximal, positive, real and simple eigenvalue and there exist corresponding nonnegative left and right eigenvectors.*

CHAPTER 2

Synchronization Loss in Directed Networks with Diffusive Coupling

"The Paradox of Choice has a simple
yet profoundly life-altering message
for all Americans."
Philip G. Zimbardo

2.1. Introduction

In this chapter we investigate a network of identical elements which are coupled in a diffusive manner, by which we mean that the dynamics of a node does not depend on its mere input but rather on the difference between its own state and the input[1]. This class of equations is used to model a multitude of applications such as the voltage of cell membranes in neuronal cell dynamics [**90**], the phase of generators in power-grids [**47**] and the state in consensus formation [**146**]. Also, we will repeatedly encounter this class in this thesis. As mentioned in the main introduction, in all these applications the existence and stability properties of synchronous states play a major role for their proper functioning. Here, our main concern is the change of stability when the network's coupling structure is modified. For spatially extended diffusive systems such as the heat equation it is easy to see that increasing the diffusion coefficient makes the system more stable in terms of relaxation rates towards the homogeneous state[2]. In networks, the homogeneous state corresponds to the synchronous state and increasing the connection density or the link's weights corresponds to increasing the diffusion coefficient. Now surprisingly enough, this property is still present in certain networks even though in general, the coupling structure does not represent a simple discretization of some continuum. It was previously shown for certain classes of undirected networks with diffusive coupling that increasing the homogeneity or the number of connections can enhance synchronization [**86, 92, 126**]. Here, we show

[1]The term diffusion is indeed inherited by spatially extended systems. Technically, it relies on the fact that a discretization of the Laplace operator yields diffusive coupling in the network sense.

[2]This can be seen for instance by looking at the fundamental solution of the homogeneous heat equation.

in a very general setting that adding links or increasing weights in diffusively coupled networks yields better synchronizability.

However, networks found in nature are often directed and weighted. For example, electrical synapses in neuron networks have asymmetric conductance [**95**], which makes the underlying network directed. Recent work has provided sufficient conditions to guarantee the stability of synchronization in directed networks in terms of the network structure and nature of the interaction [**16, 137, 130**]. Nonetheless, understanding the impact of structural modifications, such as changing weights and adding or deleting links on synchronization remains an open problem.

Here, we show that in contrast to undirected networks, improving the network connectivity structure in directed networks can lead to a synchronization loss. We show that the spectrum of the network Laplacian plays a crucial role in this desynchronization mechanism and use eigenvalue perturbation methods in order to relate the stability changes to the coupling structure. This will allow us to identify a class of links in directed networks for which increasing the weights enhances synchronization, namely the cutset. This constitutes a first step in classifying the links of a network according to their dynamical importance.

2.2. Stability of synchronization in networks with diffusive coupling

We consider directed networks of identical elements with diffusive interaction. The theory we develop here can include networks of non-identical elements with minor modifications [**137**]. The network dynamics is described by

$$\dot{\boldsymbol{x}}_i = \boldsymbol{f}(\boldsymbol{x}_i) + \alpha \sum_{j=1}^{N} W_{ij} \boldsymbol{H}(\boldsymbol{x}_j - \boldsymbol{x}_i) \qquad i = 1, 2, \ldots, N, \tag{2.2.1}$$

where $\boldsymbol{f} : \mathbb{R}^m \to \mathbb{R}^m$ describes the local node dynamics, $\alpha \geq 0$ is the overall coupling strength, and the matrix $\boldsymbol{W}$ describes the network structure, i.e., $W_{ij} \geq 0$ measures the strength of interaction from node j to node i. Furthermore, let $\boldsymbol{L}$ be the graph Laplacian associated to the adjacency matrix $\boldsymbol{W}$ (see Def. 6). As described in the introduction, we are interested in the stability of the synchronization subspace $\boldsymbol{\gamma}(t) = \boldsymbol{x}_1(t) = \boldsymbol{x}_2(t) = \cdots = \boldsymbol{x}_N(t)$, with $\dot{\boldsymbol{\gamma}}(t) = \boldsymbol{f}(\boldsymbol{\gamma}(t))$ which exists under the assumption $\boldsymbol{H}(0) = 0$. Although this type of equations is heavily used in the context of network synchronization, it was only very recently that a stability result was established [**137**] for the general case of time-dependent solutions. In order to prove the main result, Pereira et al. make the following

Assumptions

A1: $\boldsymbol{f} : \mathbb{R}^m \to \mathbb{R}^m$ is continuous and there exists a bounded, positively invariant open set $U \subset \mathbb{R}^m$ such that f is continuously differentiable in U and there

exists a $\varrho > 0$ such that

$$\|d\boldsymbol{f}(\boldsymbol{x})\| \leq \varrho \qquad \forall x \in U.$$

A2: The local coupling function $\boldsymbol{H}$ is smooth satisfying $\boldsymbol{H}(\boldsymbol{0}) = \boldsymbol{0}$ and the eigenvalues β_j of $d\boldsymbol{H}(0)$ are real.
A3: The eigenvalues λ_i of $\boldsymbol{L}$ and β_j of $d\boldsymbol{H}(0)$ fulfil

$$\gamma := \min_{\substack{2 \leq i \leq N \\ 1 \leq j \leq m}} \Re(\lambda_i \beta_j) > 0.$$

Let us shortly discuss these assumptions to see that they are somehow natural. The first assumption guarantees that the node dynamics admit an invariant compact set, for instance an equilibrium, a periodic orbit or a chaotic synchronous orbit. The second condition guarantees that the synchronous state $\boldsymbol{x}_1(t) = \boldsymbol{x}_2(t) = \cdots = \boldsymbol{x}_N(t)$ is a solution of the coupled equations for all values of the overall coupling strength α: when starting with identical initial conditions the coupling term vanishes and all the nodes behave in the same manner. In order to prove the theorem (10) we do not need the assumption that the eigenvalues β_j are real. However, it will make subsequent considerations clearer. Also, we remark that in many applications, this is the case (for instance in the Smale case **[163]** discussed in the introduction, where $\boldsymbol{H}$ is a real diagonal matrix). The last condition is a little more involved, at least for the general case of complex β_i. Assume for illustrational purposes the special case in which all the β_j are one. Then this assumption reduces to $\min_{2 \leq i \leq N} \Re(\lambda_i) > 0$. Now, for undirected graphs it can be shown that the zero eigenvalue of a Laplacian is non-simple iff the underlying graph is disconnected **[24]**. In this case the stability condition would be violated, and indeed, in order to observe synchronization it is clear that one should consider at least weakly connected networks. Having made these assumptions one can prove the following theorem **[137]**.

THEOREM 10. *Consider the network of diffusively coupled equation (2.2.1) satisfying assumptions **A1-A3**. Then there exists a $\rho = \rho(\boldsymbol{f}, d\boldsymbol{H}(0))$ such that for all coupling strengths*

$$\alpha > \frac{\rho}{\gamma} \tag{2.2.2}$$

the network is locally uniformly synchronized. This means that there exists a $\delta > 0$ and a constant $C = C(\boldsymbol{L}, d\boldsymbol{H}(0)) > 0$ such that if $\boldsymbol{x}_i(t_0) \in U$ and $\|\boldsymbol{x}_i(t_0) - \boldsymbol{x}_j(t_0)\| \leq \delta$ for any $1 \leq i, j \leq N$, then

$$\|\boldsymbol{x}_i(t) - \boldsymbol{x}_j(t)\| \leq Ce^{-(\alpha\gamma - \rho)(t - t_0)} \|\boldsymbol{x}_i(t_0) - \boldsymbol{x}_j(t_0)\| \qquad \forall t \geq t_0.$$

So the constant γ which represents the coupling structure is directly related to the contraction rate towards the synchronous manifold. Let us define this as a measure of synchronizability.

DEFINITION 11. We say a system is synchronizable when it admits an exponential estimate as in Theorem 10. Furthermore, by higher synchronizability we mean a larger contraction rate towards the synchronous manifold.

One of the steps in the proof is to show that the linearisation of Eq. (2.2.1) along $\boldsymbol{\gamma}(t)$ can be decomposed into n blocks of the form

$$\dot{\boldsymbol{\xi}}_i = \left[D\boldsymbol{f}(\boldsymbol{\gamma}(t)) - \alpha\lambda_i d\boldsymbol{H}(0)\right]\boldsymbol{\xi}_i \quad i = 1, \ldots, N \tag{2.2.3}$$

independently of $\boldsymbol{L}$ being diagonalizable or not. This has the main advantage that these are decoupled m-dimensional equations which only differ by the Laplacian eigenvalues λ_i. So next we have a closer look at these eigenvalues.

THEOREM 12. *Let $\boldsymbol{W} \in \mathbb{R}^{N\times N}$ be a nonnegative matrix. Then, the eigenvalues λ_i of the corresponding Laplacian $\boldsymbol{L} = \boldsymbol{D_W} - \boldsymbol{W}$ have nonnegative real parts, i.e. they can be ordered according to their real parts*

$$0 = \lambda_1 \leq \Re(\lambda_2) \leq \ldots \leq \Re(\lambda_N).$$

An eigenvector of the zero eigenvalue is given by $\mathbf{1}$.

PROOF. This is a simple consequence of the Gershgorin theorem (see Thm. 8) which implies that each eigenvalue lies in a disk of the form

$$\{z \,|\, |z - l_{jj}| \leq l_{jj}\}$$

with $l_{jj} = \sum_{k=1}^{N} w_{jk} \geq 0$. The second statement is clear because a Laplacian has zero row sum. □

Hence, the eigenvector of the zero eigenvalue corresponds to motion in the synchronous manifold, whereas the eigenvectors of eigenvalues with non-zero real parts correspond to motion transverse to the synchronization manifold. Therefore, if we assume that γ is time independent and the corresponding equations (2.2.3) for $i > 1$ have stable trivial solutions, synchronization in Eq. (2.2.1) is stable. This observation led to the introduction of the so called Master Stability Function (MSF) in 1998 [**136**], which maps a complex number z to the maximal Lyapunov exponent of the time dependent operator $D\boldsymbol{f}(\boldsymbol{\gamma}(t)) - zd\boldsymbol{H}(0)$. By definition, the region of stability is the domain where the MSF has negative real part. Clearly, the MSF approach is well suited for computational investigations and covers a broad range of coupling functions. For autonomous systems it also yields contraction rates towards the (relative) equilibria. However, in the non-autonomous case we consider here, the stability of the nonlinear system can in general not be deduced by the location of the Maximal Lyapunov Exponent of the linearised system due to Perron effects [**110**]. In this case, the use of exponential dichotomies is preferable as it yields exponential estimates for the nonlinear flow as in Thm. 10. Furthermore, it has the advantage that structural stability follows naturally, and under stronger assumptions one even obtains estimates for the size of the basin of attraction [**137**].

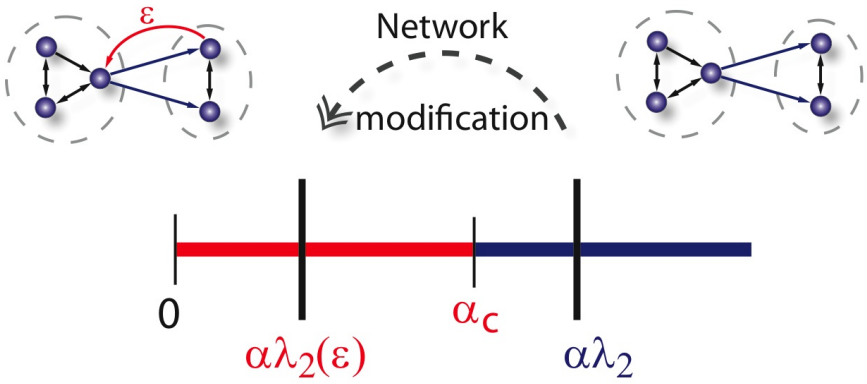

FIGURE 2.2.1. In a schematic representation we illustrate the motion of the spectral gap λ_2 under structural modifications in case $\lambda_2(\varepsilon)$ is real. The network on the right has a spectral gap such that $\alpha\lambda_2 > \alpha_c$. Adding a link as indicated decreases the gap to $\lambda_2(\varepsilon)$, which violates the stability condition (2.2.4).

Now, as we mentioned above, the theorem is still valid if we do not assume that the β_j are real. However, this assumption simplifies condition (2.2.2) essentially. By using the structure of the Laplacian spectrum the condition (2.2.2) for stable synchronous motion writes as

$$\alpha \Re(\lambda_2) \min_{1\le j\le m} \beta_j > \rho. \tag{2.2.4}$$

More involved stability conditions can be tackled, but the analysis becomes more technical without providing new insight into the phenomenon. Condition (2.2.4) shows that the spectral gap λ_2 plays a central role for synchronization properties of the network. Structural changes which decrease the real part of λ_2 can destabilize the synchronous state, see Fig. 2.2.1. This establishes a strong connection between the coupling topology of a network and the stability of synchronous states in the network. In the case of directed graphs, very few is known about the connection between the coupling structure and the spectral gap. However, for undirected graphs there is a well developed theory.

2.3. Motion of the spectral gap and stability in undirected networks

One of the first who investigated the spectral gap of Laplacians of graphs was M. Fiedler [**61**]. He established the following result

LEMMA 13. *Let $\mathcal{G}$ and $\mathcal{G}'$ be unweighted and undirected graphs such that $\mathcal{G} \subset \mathcal{G}'$. Then we have*

$$\lambda_2(\mathcal{G}) \le \lambda_2(\mathcal{G}').$$

As a simple consequence we have

COROLLARY 14. *In the setting of the main theorem for an unweighted graph, increasing the connection density in the graph yields higher synchronizability.*

However, to establish a similar result for weighted and directed graphs we have to employ a different approach [**84**].

LEMMA 15. *Let λ be a simple eigenvalue of $\boldsymbol{L} \in \mathbb{R}^{N\times N}$ with corresponding left and right eigenvectors $\boldsymbol{u}, \boldsymbol{v}$ and let $\tilde{\boldsymbol{L}} \in \mathbb{R}^{n\times n}$. Then, for ε small enough there exists a smooth family $\lambda(\varepsilon)$ of simple eigenvalues of $\boldsymbol{L}+\varepsilon\tilde{\boldsymbol{L}}$ with $\lambda(0) = \lambda$ and*

$$\lambda'(0) = \frac{\boldsymbol{u}\tilde{\boldsymbol{L}}\boldsymbol{v}}{\boldsymbol{u}\boldsymbol{v}}. \tag{2.3.1}$$

PROOF. First, we remark that for the eigenvectors $\boldsymbol{u}, \boldsymbol{v}$ of a simple eigenvalue we have $\boldsymbol{u}\boldsymbol{v} \neq 0$ (see Lemma 6.3.10 in [**84**]). The existence of a family of simple eigenvalues follows from the smooth dependence of eigenvalues on matrix entries. For the second statement, let $\boldsymbol{x}(\varepsilon)$ and $\boldsymbol{y}(\varepsilon)$ be left and right eigenvectors of $\boldsymbol{L}+\varepsilon\tilde{\boldsymbol{L}}$ corresponding to $\lambda(\varepsilon)$. Then, we differentiate the eigenvalue equation $\lambda(\varepsilon)\boldsymbol{x}(\varepsilon)\boldsymbol{y}(\varepsilon) = \boldsymbol{x}(\varepsilon)\left[\boldsymbol{L}+\varepsilon\tilde{\boldsymbol{L}}\right]\boldsymbol{y}(\varepsilon)$ and omit the dependence on ε for simplicity to obtain

$$\lambda'\boldsymbol{x}\boldsymbol{y} + \lambda\left[\boldsymbol{x}'\boldsymbol{y} + \boldsymbol{x}\boldsymbol{y}'\right] = \boldsymbol{x}'\left[\boldsymbol{L}+\varepsilon\tilde{\boldsymbol{L}}\right]\boldsymbol{y} + \boldsymbol{x}\left[\boldsymbol{L}\boldsymbol{y}' + \tilde{\boldsymbol{L}}\boldsymbol{y} + \varepsilon\tilde{\boldsymbol{L}}\boldsymbol{y}'\right].$$

Evaluating this expression in $\varepsilon = 0$ and using that $\boldsymbol{x}(0)$ and $\boldsymbol{y}(0)$ are eigenvectors of $\boldsymbol{L}$ we have

$$\lambda'(0)\boldsymbol{x}(0)\boldsymbol{y}(0) \quad = \quad \boldsymbol{x}(0)\tilde{\boldsymbol{L}}\boldsymbol{y}(0)$$

which is the desired representation. □

Before we proceed to the analysis of a directed network, we mention that by using Lemma 15 we can generalize Lemma 13 to weighted undirected graphs

COROLLARY 16. *Let $\mathcal{G}$ be a weighted graph with Laplacian $\boldsymbol{L}$ and simple spectral gap λ_2. Let $\boldsymbol{L}_p = \boldsymbol{L} + \varepsilon\tilde{\boldsymbol{L}}$ be a perturbed Laplacian with a positive (semi-) definite perturbation $\tilde{\boldsymbol{L}}$ and associated spectral gap $\lambda_2(\varepsilon)$. Then we have $\lambda_2'(0) > 0$ ($\lambda_2'(0) \geq 0$ resp.).*

PROOF. First, we remark that $\boldsymbol{L}$ is symmetric. Consequently, the left and right eigenvectors $\boldsymbol{u}$ and $\boldsymbol{v}$ are dual, i.e. $\boldsymbol{v} = \boldsymbol{u}$. Let $\tilde{\boldsymbol{L}}$ be positive semi-definite, so we have by Lemma 15 $\lambda_2'(0) = \frac{\boldsymbol{u}\tilde{\boldsymbol{L}}\boldsymbol{u}}{\boldsymbol{u}\boldsymbol{u}} \geq 0$. Analogously $\lambda_2'(0) > 0$ if $\tilde{\boldsymbol{L}}$ is positive definite. □

In other words, this Corollary states that increasing weights or adding links with positive weights will generically increase the spectral gap and therefore the synchronizability.

REMARK 17. In the corollary, we do not assume that the perturbation is symmetric. However, if it is we can apply the result repeatedly as long as the spectral gap is simple.

To conclude this section, we have seen that in undirected networks, improving the connection structure in the sense of making it denser and stronger, indeed yields higher synchronizability. Of course, the natural question arises, if we have similar results for the case of directed networks. Before investigating the general case we want to motivate it with some numerical examples.

2.4. Two case studies

Here, we present results of numerical simulations which show that adding links or increasing weights can destabilize the synchronous state in directed networks. The underlying digraph for the first two examples is shown on the top left of Fig. (2.4.1). It consists of two components which are strongly connected, visualized by the grey dotted lines. Again, this means every node is reachable from every other node through a directed path inside these components. Here, the smaller component does not influence the larger component, as there are no links from the smaller to the larger component. Nonetheless, the network still supports stable synchronous dynamics. Now, introducing a new link pointing from node 4 to node 1 improves the connection structure significantly in the sense that the whole network is now strongly connected: any two nodes in the network are connected by a directed path. However, this structural improvement has a surprising consequence for the dynamics: the synchronous state becomes unstable.

In Fig. (2.4.1) a) the local dynamics is given by the Hindmarsh-Rose model, a three dimensional ordinary differential equation which models the membrane potential of a neuron. Neurons are known to exhibit a wide range of dynamical behaviour, such as subthreshold oscillations, regular and chaotic spiking and bursting. Depending on the parameter settings, the Hindmarsh-Rose model exhibits spiking and bursting behaviour [**89**]. The local dynamics $\boldsymbol{f}$ is given by

$$\begin{aligned} \dot{x} &= y + a_1 x^2 - x^3 - z + I \\ \dot{y} &= 1 - 5x^2 - y \\ \dot{z} &= a_2(s(x - x_R) - z). \end{aligned}$$

Here, I is a constant input current. We choose the parameters as follows: $a_1 = 3.01$, $a_2 = 0.006$, $s = 4$, $I = 3.2$ and $x_R = -1.6$. As can be seen in the inset of Fig. 2.4.1 a), in this regime each node exhibits chaotic bursting [**13**]. We consider the electrical synaptic interaction between neurons given by

$$\boldsymbol{H} = \begin{pmatrix} 1 & 0 & 0 \\ 0 & 0 & 0 \\ 0 & 0 & 0 \end{pmatrix},$$

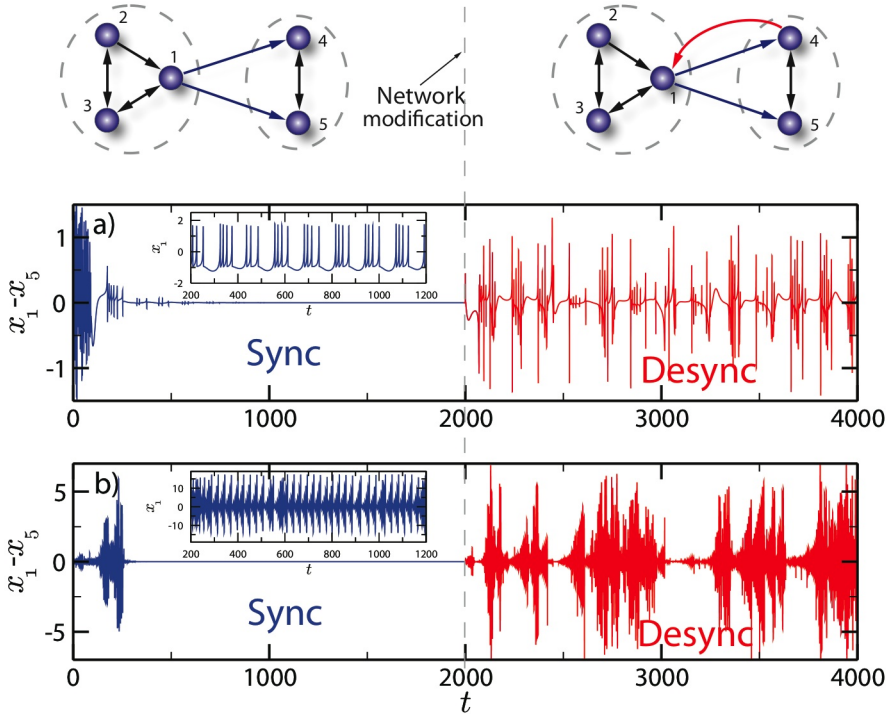

FIGURE 2.4.1. The figures show simulation results for the networks on top. All links in blue have weight one. In the main plots we show the difference of the first component of $\boldsymbol{x}_1$ and the first component of $\boldsymbol{x}_5$. In a) the node dynamics is given by Hindmarsh-Rose (HR) neurons, and in b) by Rössler dynamics. The global coupling α is chosen such that the nodes synchronize chaotically for the original network. This can be seen in the main plots for times until $t = 2000$ in blue. The introduction of the new link $4 \to 1$ with weight 0.4 at time $t = 2000$ leads to a destabilization, displayed in red. The insets show the time series of a single node. For the HR neurons we consider a chaotic bursting mode and for the Rössler dynamics a chaotic state.

so the local coupling is only in the x-component, known as membrane potential. In this case, the assumption **A3** for Theorem 10 is not satisfied. However, the stability condition $\alpha\Re(\lambda_2) > \alpha_c$ can be verified via a master stability function approach [**136**]. All nonzero weights W_{ij} in the network on top left are set to one and in order to achieve stable synchronized motion for the whole network we fixed $\alpha = 0.96$. In the main plot of Fig. 2.4.1 a) we show the difference of the first component of nodes 1 and 5. We observe synchronous dynamics for times $t < 2000$ (in blue). At time $t = 2000$ we add the new link $4 \to 1$ with a weight of $W_{14} = 0.4$, which leads to the strongly connected network on

the top right. As can be seen for times $t > 2000$ (in red) this destabilizes the synchronous state.

In the second example we consider the same network topology, now endowed with Rössler oscillators as local dynamics **[153]**

$$\begin{aligned} \dot{x} &= -y - z \\ \dot{y} &= x + a_1 y \\ \dot{z} &= a_2 + z(x - a_3). \end{aligned}$$

Here we chose $a_1 = 0.2$, $a_2 = 0.2$ and $a_3 = 9$. For these parameters, the isolated nodes exhibit chaotic dynamics, as can be seen in the inset of Fig. 2.4.1 b). We consider the interaction in all variables

$$\boldsymbol{H} = \begin{pmatrix} 1 & 0 & 0 \\ 0 & 1 & 0 \\ 0 & 0 & 1 \end{pmatrix}.$$

In this case, we can apply Theorem 10 and we obtain the stability condition $\alpha\Re(\lambda_2) > \alpha_c$ as in the previous case. Again, all nonzero weights W_{ij} in the network are set to one and in order to achieve stable synchronization we fixed $\alpha = 0.092$. As in the previous example, we observe synchronization for times $t < 2000$, see Fig. 2.4.1 b). The introduction of a new link at time $t = 2000$, however, leads to a desynchronized state.

We remark that these findings are not restricted to networks consisting of strong components connected by a cutset, which corresponds to a so-called master-slave configuration. To illustrate this, we carried out simulations on a strongly connected network with Rössler systems as local dynamics as shown in Fig. 2.4.2. Here, we use the interaction

$$\boldsymbol{H} = \begin{pmatrix} 1 & 0 & 0 \\ 0 & 0 & 0 \\ 0 & 0 & 0 \end{pmatrix}$$

which corresponds to a resistive coupling in the first variable between the oscillators. We remark that taking the identity as interaction function yields similar results though. In a) we choose the global coupling α such that the nodes synchronize chaotically for the network shown on the right. Here again, all weights are set to one. At time $t = 2000$ we increase the weight on the link $2 \to 3$ shown in red. This decreases the spectral gap, which in turn destabilizes the synchronous state. In b), the global coupling is chosen slightly smaller, such that the nodes do not synchronize. Now, introducing the new link $1 \to 2$, shown as a dotted line, increases the spectral gap. And this in turn stabilizes the synchronous state, as can be seen for times $t > 2000$ (in blue). We emphasize that there are different possibilities which stabilize the synchronous state. For instance, increasing the weights on either of the links $2 \to 1$, $2 \to 4$ or $3 \to 1$ yields a similar result.

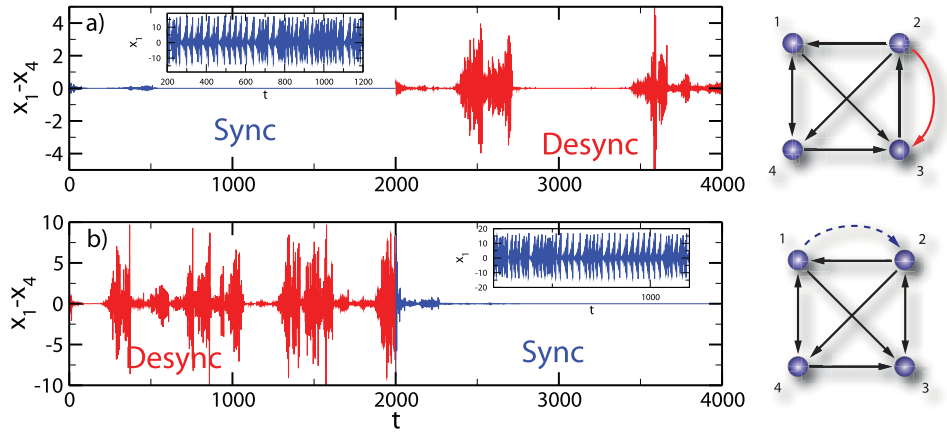

FIGURE 2.4.2. The figures show simulation results for the networks on the right. All links in black have weight one. In the main plots we show the difference of the first component of $\boldsymbol{x}_1$ and the first component of $\boldsymbol{x}_4$. In both a) and b) the node dynamics is given by Rössler dynamics. In a), the global coupling α is chosen such that the nodes synchronize chaotically for the original network. This can be seen in the main plots for times until $t = 2000$ in blue. At time $t = 2000$ the weight on the (red) link $2 \to 3$ is increased by 0.5 which leads to a destabilization, displayed in red. In b), the global coupling α is chosen such that the nodes do not synchronize. At time $t = 2000$ we introduce the dotted link $1 \to 2$ with a weight 0.5. This leads to chaotic synchronization, as can be seen in blue. The insets show the time series of a single chaotic Rössler node.

2.5. Stability of synchronization in directed networks

Let us try to understand the destabilization mechanism in more detail. We consider a directed network composed of two strongly connected components of size N and m as in the example in Fig. 2.4.1. Let again $\boldsymbol{L}$ be the associated graph Laplacian with ordered eigenvalues λ_j (see Theorem 12). Before proceeding further let us make two rather generic assumptions for the coupling structure

Assumptions

A4: The zero eigenvalue $\lambda_1 = 0$ of $\boldsymbol{L}$ is simple.

A5: The spectral gap $\lambda_2 \neq 0$ of $\boldsymbol{L}$ is simple.

Let us shortly discuss these two assumptions. Firstly, the zero eigenvalue is simple if and only if the graph has only one initial strong component (see Prop. 1.7.1 in [**10**]). In particular, this is the case for strongly connected graphs. The next assumption, namely that the eigenvalue λ_2 is simple, is generic in the sense that the set of random graphs which do not have this

property is "very small". For the case of a non-continuous distribution of the matrix entries this means its (Lebesgue) measure tends to zero when the graph size increases. This was conjectured by Babai in the eighties and only proved in the end of 2014 [**170**]. As a consequence, it is also valid for the much used class of Erdös-Rényi random graphs [**52**]. For a continuous distribution it is easier to see that independent of the dimension, the set of matrices with non-simple eigenvalues has zero (Lebesgue) measure. First, we remark that the set of square matrices with pairwise distinct eigenvalues is open and dense as a subset of all square matrices. This is easy to see when looking at a matrix in its Schur triangular form with the eigenvalues on the diagonal [**84**]. However, it does not necessarily mean that this set has full measure. To see it does, consider the discriminant function $f(A) = \prod_{i<j}(\lambda_i - \lambda_j)$ which maps a square matrix on the product of all possible differences of eigenvalues λ_i. Then the set of matrices with non-simple eigenvalues is precisely the preimage of zero under f. By showing that the set of zeros of a nonzero polynomial is a nullset one obtains the result.

Now, in this situation the Laplacian can be written in block form

$$\boldsymbol{L} = \begin{pmatrix} \boldsymbol{L}_1 & \boldsymbol{0} \\ -\boldsymbol{C} & \boldsymbol{L}_2 + \boldsymbol{D}_{\boldsymbol{C}} \end{pmatrix}, \tag{2.5.1}$$

where $\boldsymbol{L}_1 \in \mathbb{R}^{N\times N}$ and $\boldsymbol{L}_2 \in \mathbb{R}^{m\times m}$ are the respective Laplacians of the strong components. $\boldsymbol{C} \in \mathbb{R}^{m\times N}$ is the adjacency matrix of the cutset pointing from one strong component to the other and $\boldsymbol{D}_{\boldsymbol{C}}$ is again a diagonal matrix with the row sums of $\boldsymbol{C}$ on its diagonal. As a consequence of the block structure, eigenvalues of $\boldsymbol{L}$ are either eigenvalues of $\boldsymbol{L}_1$ or eigenvalues of $\boldsymbol{L}_2 + \boldsymbol{D}_c$. Now, our aim is to apply Lemma 15 in order to track the motion of the spectral gap when we perturb the network and therefore the Laplacian. To do so, we first gather some information about the eigenvectors of $\boldsymbol{L}$.

LEMMA 18. *Let λ_2 be a simple eigenvalue of $\boldsymbol{L}$ located in the second component, i.e.* $\det(\lambda_2 \boldsymbol{I} - (\boldsymbol{L_2} + \boldsymbol{D_C})) = 0$. *Then the corresponding left and right eigenvectors of $\boldsymbol{L}$ have the form*

$$\left(\boldsymbol{w}\boldsymbol{C}\left(\boldsymbol{L}_1 - \lambda_2 \boldsymbol{I}\right)^{-1}, \boldsymbol{w}\right) \quad , \quad (0, \boldsymbol{y})$$

where $\boldsymbol{w}$ and $\boldsymbol{y}$ are left and right eigenvectors of $\boldsymbol{L}_2 + \boldsymbol{D}_{\boldsymbol{C}}$.

PROOF. Let $(\boldsymbol{v}, \boldsymbol{w})$ and $(\boldsymbol{x}, \boldsymbol{y})$ be left and right eigenvectors of $\boldsymbol{L}$ corresponding to λ_2. For the left eigenvector we have

$$\begin{aligned} \boldsymbol{0} &= (\boldsymbol{v}, \boldsymbol{w})\,\boldsymbol{L} - \lambda\,(\boldsymbol{v}, \boldsymbol{w}) \\ &= \left(\boldsymbol{v}\left(\boldsymbol{L}_1 - \lambda_2 \boldsymbol{I}\right) - \boldsymbol{w}\boldsymbol{C}, \boldsymbol{w}\left(\boldsymbol{L}_2 + \boldsymbol{D}_{\boldsymbol{C}}\right) - \lambda \boldsymbol{w}\right). \end{aligned}$$

The second component of this equation yields that $\boldsymbol{w}$ is a left eigenvector of $(\boldsymbol{L}_2 + \boldsymbol{D}_{\boldsymbol{C}})$. By assumption λ_2 is simple and consequently not an eigenvalue

of $\boldsymbol{L}_1$, so the first component yields

$$\boldsymbol{v} = \boldsymbol{w}\boldsymbol{C}\left(\boldsymbol{L}_1 - \lambda_2 \boldsymbol{I}\right)^{-1}.$$

The equation for the right eigenvector is

$$\begin{aligned} 0 &= \boldsymbol{L}\begin{pmatrix} \boldsymbol{x} \\ \boldsymbol{y} \end{pmatrix} - \lambda_2 \begin{pmatrix} \boldsymbol{x} \\ \boldsymbol{y} \end{pmatrix} \\ &= \begin{pmatrix} \left(\boldsymbol{L}_1 - \lambda_2 \boldsymbol{I}\right)\boldsymbol{x} \\ -\boldsymbol{C}\boldsymbol{x} + \left(\boldsymbol{L}_2 + \boldsymbol{D}_{\boldsymbol{C}}\right)\boldsymbol{y} - \lambda_2 \boldsymbol{y} \end{pmatrix}. \end{aligned}$$

As $\boldsymbol{L}_1 - \lambda_2 \boldsymbol{I}$ is regular we have $\boldsymbol{x} = 0$. The second component then yields that $\boldsymbol{y}$ is a right eigenvector of $\boldsymbol{L}_2 + \boldsymbol{D}_{\boldsymbol{C}}$. □

Remark 19. We remark that the example from Fig. 2.4.1 is enclosed in this case. Also, the case where the smallest eigenvalue is located in the first component is not interesting for perturbations on the cutset. This can be seen in Eq. (2.5.1). Suppose λ_2 is located in the first component and introduce a perturbation $\boldsymbol{C} + \varepsilon\tilde{\boldsymbol{C}}$ where $\tilde{\boldsymbol{C}}$ is a nonnegative matrix. Then by continuous dependence of the eigenvalues on the matrix entries for ε small enough λ_2 will still be in the first component. But the perturbed Laplacian writes $\boldsymbol{L} = \begin{pmatrix} \boldsymbol{L}_1 & 0 \\ -\boldsymbol{C} - \varepsilon\boldsymbol{\Delta} & \boldsymbol{L}_2 + \boldsymbol{D}_{\boldsymbol{C}+\varepsilon\boldsymbol{\Delta}} \end{pmatrix}$ so λ_2 remains unchanged.

Now observe that the matrix $\boldsymbol{L}_2 + \boldsymbol{D}_{\boldsymbol{C}}$ is nonnegative diagonally dominant [**17, 84**]. This property enables us to find a Perron-Frobenius like result.

Lemma 20. *$\boldsymbol{L}_2 + \boldsymbol{D}_{\boldsymbol{C}}$ has a minimal real positive eigenvalue with corresponding nonnegative left and right eigenvectors.*

Proof. Let $s = \max_i \left\{ d_i + \sum_{j \neq i} a_{ij} \right\}$, then $\boldsymbol{N} = s\boldsymbol{I} - \left(\boldsymbol{L}_2 + \boldsymbol{D}_{\boldsymbol{C}}\right)$ is a nonnegative matrix by definition of s. Furthermore it is irreducible as we assumed that the component associated to $\boldsymbol{L}_2$ is strongly connected. Then, by the Perron-Frobenius theorem (Thm. 9), $\boldsymbol{N}$ has a maximal real eigenvalue Λ with corresponding nonnegative left and right eigenvectors $\boldsymbol{\omega}$ and $\boldsymbol{\eta}$. That is

$$\begin{aligned} \boldsymbol{N}\boldsymbol{\eta} &= \Lambda\boldsymbol{\eta} \\ \iff \left(\boldsymbol{L}_2 + \boldsymbol{D}_{\boldsymbol{C}}\right)\boldsymbol{\eta} &= (s - \Lambda)\,\boldsymbol{\eta}. \end{aligned}$$

As Λ is the maximal eigenvalue and all the eigenvalues of $\boldsymbol{L}_2 + \boldsymbol{D}_{\boldsymbol{C}}$ are obtained by eigenvectors μ of $\boldsymbol{N}$ through $s - \mu$, we must have that $s - \Lambda$ is the minimal real eigenvalue of $\boldsymbol{L}_2 + \boldsymbol{D}_{\boldsymbol{C}}$. Furthermore, the eigenvectors are the same, so the left and right eigenvectors corresponding to $s - \Lambda$ are nonnegative. That the eigenvalue is positive can be seen by looking at the Gershgorin circles. □

This shows that the spectral gap is real in this case. So when changing the coupling structure, the motion of λ_2 will be along the real axis by Lemma 15. Now we can state the first main result of this section

THEOREM 21. *Let a network consist of two strong components with the Laplacian*

$$\boldsymbol{L} = \begin{pmatrix} \boldsymbol{L}_1 & \boldsymbol{0} \\ -\boldsymbol{C} & \boldsymbol{L}_2 + \boldsymbol{D}_{\boldsymbol{C}} \end{pmatrix}.$$

Let the smallest nonzero eigenvalue λ_2 be simple and located in the second component, that is $\det(\lambda_2 - (\boldsymbol{L_2} + \boldsymbol{D_C})) = 0$. *Then, increasing the weights on the cutset never decreases the spectral gap. That is, for ε small enough and a nonnegative perturbation $\boldsymbol{C} + \varepsilon\boldsymbol{\Delta}$ we will have $\lambda_2(\varepsilon) \geq \lambda_2(0)$.*

PROOF. Let $\varepsilon\boldsymbol{\Delta}$ be a perturbation in direction of the cutset, so the perturbed Laplacian $\tilde{\boldsymbol{L}}$ can be written as

$$\begin{aligned} \tilde{\boldsymbol{L}} &= \begin{pmatrix} \boldsymbol{L}_1 & 0 \\ -\boldsymbol{C} - \varepsilon\boldsymbol{\Delta} & \boldsymbol{L}_2 + \boldsymbol{D}_{\boldsymbol{C}+\varepsilon\boldsymbol{\Delta}} \end{pmatrix} = \boldsymbol{L} + \begin{pmatrix} 0 & 0 \\ -\varepsilon\boldsymbol{\Delta} & \boldsymbol{D}_{\varepsilon\boldsymbol{\Delta}} \end{pmatrix} \\ &= \boldsymbol{L} + \varepsilon \begin{pmatrix} 0 & 0 \\ -\boldsymbol{\Delta} & \boldsymbol{D}_{\boldsymbol{\Delta}} \end{pmatrix}. \end{aligned}$$

Using Lemma 15 we have for the spectral gap of the perturbed system

$$\lambda_2'(0) = \frac{\boldsymbol{w}(\boldsymbol{D}_{\boldsymbol{\Delta}}\boldsymbol{y} - \boldsymbol{\Delta}\boldsymbol{x})}{(\boldsymbol{v}, \boldsymbol{w}) \begin{pmatrix} \boldsymbol{x} \\ \boldsymbol{y} \end{pmatrix}}$$

for left and right eigenvectors $(\boldsymbol{v}, \boldsymbol{w})$ and $(\boldsymbol{x}, \boldsymbol{y})$ of $\boldsymbol{L}$. Now, plugging in the representation from Lemma 18 we obtain

$$\lambda_2'(0) = \frac{\boldsymbol{w}\boldsymbol{D}_{\boldsymbol{\Delta}}\boldsymbol{y}}{\boldsymbol{w}\boldsymbol{y}}.$$

By assumption $\boldsymbol{\Delta}$ and therefore $\boldsymbol{D}_{\boldsymbol{\Delta}}$ is nonnegative. Furthermore, Lemma 20 shows that $\boldsymbol{w}$ and $\boldsymbol{y}$ are nonnegative, which concludes the proof. □

The next question is what happens when we introduce a perturbation $\boldsymbol{\Delta}$ opposite to the cutset. In this case, the Laplacian writes as

$$\boldsymbol{L}_p = \begin{pmatrix} \boldsymbol{L}_1 + \boldsymbol{D}_{\Delta} & -\boldsymbol{\Delta} \\ -\boldsymbol{C} & \boldsymbol{L}_2 + \boldsymbol{D}_c \end{pmatrix},$$

where $\boldsymbol{\Delta}$ is the matrix describing the coupling in opposite direction to the cutset. Using Lemma 15 and 18 again yields

$$\lambda_2' = -\frac{\boldsymbol{w}\boldsymbol{M}\boldsymbol{y}}{\boldsymbol{w}\boldsymbol{y}}, \tag{2.5.2}$$

where

$$\boldsymbol{M} = \boldsymbol{C}(\boldsymbol{L}_1 - \lambda_2\boldsymbol{I})^{-1}\boldsymbol{\Delta}$$

takes into account the structural changes $\boldsymbol{\Delta}$. Now again, such a modification will weaken the stability or even lead to instabilities if $\lambda_2' < 0$. Determining the modifications that yield a decrease of the spectral gap is an involved problem, and we shall tackle it elsewhere. Here, we will focus on the example

of Fig. 2.4.1, as it contains the central concepts without technical intricacies. In the example from Fig. 2.4.1, $\boldsymbol{L_2} + \boldsymbol{D}_c$ is symmetric and we have $\boldsymbol{v} = \boldsymbol{w} = -\frac{1}{\sqrt{2}}(1,1)$. Moreover, $\boldsymbol{M} = \frac{1}{2}\begin{pmatrix} 0 & 1 \\ 0 & 1 \end{pmatrix}$ and $\boldsymbol{v}$ and $\boldsymbol{w}$ are eigenvectors of $\boldsymbol{M}$ with eigenvalue $1/2$. Because $\boldsymbol{v}$ is a common eigenvector of both $\boldsymbol{L_2} + \boldsymbol{D}_c$ and $\boldsymbol{M}$ corresponding to a positive eigenvalue we obtain a decrease of the spectral gap with a rate $\lambda_2' = -\frac{1}{2}$. This is a main mechanism that generates instabilities: the eigenvectors of $\boldsymbol{L_2} + \boldsymbol{D}_c$ lie in the space spanned by the eigenvectors of $\boldsymbol{M}$ with positive eigenvalues.

Formally, we can obtain all the structural changes capable for destabilization as a function of the eigenvectors $\boldsymbol{v}, \boldsymbol{w}$ of $\boldsymbol{L}_1$ and $\boldsymbol{L}_2 + \boldsymbol{D}_c$. In contrast to undirected networks where there is a well developed theory relating eigenvectors to the underlying graph structure [**19**], for directed graphs the theory is underdeveloped. Therefore, further analytical insights remain a challenge. From a computational point of view though, we can solve this problem for any given network.

2.6. Discussion

In this chapter we have investigated the effect of the addition of a link and an increase of a link's weight on the transverse stability of the synchronous manifold in diffusively coupled networks. The results reveal that in a broad class of dynamics, directed and undirected networks behave essentially distinct under these structural changes. Namely, assuming the stability condition Eq. (2.2.4), synchronization loss caused by structural improvements is a property inherent to directed networks exclusively. If $\alpha\Re(\lambda_2)\min_{1\leq j\leq m}\beta_j \gg \rho$, the network modification may not destroy synchronization. However, it worsens the quality in the sense that the transient towards synchronization becomes larger. Also, we remark that under additional conditions on the local dynamics f, one can establish estimates for the size of the basin of attraction linearly depending on the quantity $\alpha\Re(\lambda_2)$. Hence, with these assumptions our stability considerations also relate to the newly introduced basin stability [**120**].

Recently, interconnected networks have attracted much attention [**26, 145**], as they can exhibit catastrophic cascades of failures when connections are undirected. Our results suggest that interconnected networks in which interconnections are represented by directed cutsets behave qualitatively different. In game theory, such catastrophic effects of structural improvements on the network function are well known under the name of "Braess's paradox" [**21, 22**]. However, here the effect is due to the fact that the players take rational decisions to optimise their strategies. In the case of complex networks of dynamical systems considered here, the effect is purely dynamical and is a consequence of the motion of eigenvalues of the network Laplacian. Furthermore, our results shed light on how to plan and design network modifications without destroying the network performance, as for instance discussed for power-grids

in [**183, 125**]. And indeed, this phenomenon can be observed experimentally. In [**74**] we consider directed networks of four coupled optoelectronic delay-coupled devices which upon the addition of a link exhibit synchronization loss for periodic and chaotic synchronization. So as a next step, it is desirable to extend our approach to networks with transmission delays. Finally, as mentioned in the main text, there is a rich body of work about the relation between the spectrum of a graph Laplacian and the underlying graph topology, developed in the last century in algebraic graph theory [**61**]. However, there are few attempts to extend these approaches to directed graphs. As shown here, related results would essentially improve our understanding of the dynamical impact of a link in directed networks.

CHAPTER 3

Shortcuts in Rings of Stuart-Landau Oscillators

"Short cuts make long delays."
J.R.R. Tolkien, The fellowship of the ring

3.1. Introduction

In the last chapter we have seen that the addition of a single link can have drastic consequences for the exhibited dynamics if the underlying network is directed. In this chapter, we study the same modification in a special class of networks belonging to the class of small-world networks **[20]**. Namely, we consider unidirectional rings which are perturbed by the insertion of a single non-local link (Fig. 3.1.1). One reason for the interest in ring structures is that they emerge in many natural systems **[98, 149, 169]**. Also, rings can be seen as motifs of larger and more complex networks **[121]**. A lot of research has been done for bidirectional rings in the last few years **[2, 39, 148, 179, 194]**. In contrary, less is known about dynamics in unidirectional rings **[83, 82, 139, 191, 142, 138]**, although these structures play an important role in various applications **[23, 36, 166, 169, 178, 175]**. As a simple, paradigmatic model, we consider unidirectional rings of N identical Stuart-Landau oscillators with an additional shortcut from node ℓ to node N, to which we refer as a perturbation of the homogeneous system. The dynamics on the perturbed ring are then described by the following equations:

$$\begin{aligned} \dot{z}_j(t) &= \left(\mu - |z_j(t)|^2\right) z_j + z_{j+1}(t), \quad j = 1, ..., N-1, \\ \dot{z}_N(t) &= \left(\mu - |z_N(t)|^2\right) z_N + z_1(t) + s z_\ell(t), \end{aligned} \tag{3.1.1}$$

where $\mu = \alpha + i\beta$, $\beta > 0$ and α is the bifurcation parameter. $s > 0$ is the shortcut strength and $z_j(t) \in \mathbb{C}$. We remark that here, the coupling is additive, in contrast to the previous chapter where we considered a diffusive coupling. However, introducing polar coordinates $z_j = |z_j| e^{i\phi_j}$ in Eqs. (3.1.1) one can see that the coupling in the phase variables ϕ_j is diffusive as well. The difference is that here, we also consider variations in the oscillator's amplitudes.

For an unperturbed ring ($s = 0$), the system is highly symmetric. The coupling topology is invariant under the rotational group $\gamma\mathbf{z} = \gamma(z_1, z_2, \ldots, z_N) = (z_2, z_3, \ldots, z_N, z_1)$ which constitutes a spatial symmetry. Furthermore, the system possesses a spatiotemporal symmetry which consists of a phase shift

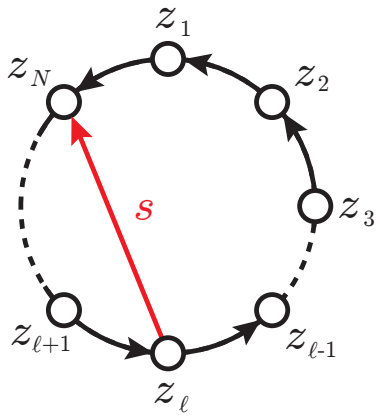

FIGURE 3.1.1. Coupling scheme of a unidirectional ring with a shortcut.

$\mathbf{z} \to e^{i\varphi}\mathbf{z}$ and which can be identified with the symmetry group S^1. So equations (3.1.1) with $s = 0$ constitute an example for a system with spatial and spatiotemporal symmetries. Bifurcations from equilibria and periodic orbits which can occur in these systems were investigated in very general settings in **[104, 105, 44]**. Therein it was shown that due to the symmetry, a certain class of periodic solutions can be transformed into equilibria in rotating coordinates, therefore termed relative equilibria. This essentially simplifies the bifurcation analysis of these solutions and we will use this fact in chapters 4 and 6. The same mechanism was also used in **[191]** where the bifurcations from the zero equilibrium in (3.1.1) are described in much more detail. In particular, when the parameter $\alpha = \Re(\mu)$ in (3.1.1) is increased, the zero equilibrium

$$z_1 = ... = z_N = 0 \tag{3.1.2}$$

loses stability and undergoes a sequence of Hopf bifurcations. The first half of the emerging branches of periodic solutions stabilizes at appropriate values of α (see section 3.2.2). Remarkably, this phenomenon resembles the Eckhaus scenario in spatially extended diffusive systems **[50, 172]** although there is no apparent way to to interpret the network as a discretization of some continuum. The aim of this chapter is to investigate the transformation of this scenario under non-local perturbations which destroy the rotational symmetry of the system. We investigate two different asymptotic cases of small and large perturbation size s. For small s, the Eckhaus scenario persists qualitatively with a modulated Eckhaus line, while for large s, there is a qualitative difference to the unperturbed case that reflects the new network topology, i.e. the existence of a new loop.

The chapter is structured as follows. In section 3.2 we discuss the stability of the zero solution (3.1.2), its spectrum and its bifurcations. In section 3.3 we find asymptotic expressions for the emerging periodic solutions in the case

of small perturbation size s. We also reduce the case of asymptotically large s to the analysis of an inhomogeneous ring. Section 3.4 deals with the stability analysis of the periodic solutions and the results are compared to numerical simulations. Finally, we discuss our findings and give an outlook on possible extensions and applications of the results in section 3.5.

3.2. Stability of the zero solution

To study the stability of system (3.1.1) it is convenient to identify each variable $z_j(t) \in \mathbb{C}$ with a two-dimensional real variable

$$\begin{aligned} \boldsymbol{z}_j(t) &= (z_{j,1}(t), z_{j,2}(t))^\top \\ &= (\Re(z_j(t)), \Im(z_j(t)))^\top \in \mathbb{R}^2 \end{aligned}$$

. Then, system (3.1.1) is equivalent to the real system

$$\begin{aligned} \dot{\boldsymbol{z}}_j(t) &= \left(M_\mu - \left(z_{j,1}^2 + z_{j,2}^2\right)\right)\boldsymbol{z}_j + \boldsymbol{z}_{j+1}, \\ \dot{\boldsymbol{z}}_N(t) &= \left(M_\mu - \left(z_{N,1}^2 + z_{N,2}^2\right)\right)\boldsymbol{z}_N + \boldsymbol{z}_1 + s\boldsymbol{z}_\ell, \end{aligned} \tag{3.2.1}$$

where $\boldsymbol{M}_\mu = \begin{bmatrix} \alpha & -\beta \\ \beta & \alpha \end{bmatrix}$ is the representation of the multiplication with $\mu \in \mathbb{R}^{2\times 2}$.

3.2.1. Spectrum of the equilibrium. We linearize system (3.1.1) in $\boldsymbol{z}_1 = .. = \boldsymbol{z}_N \equiv 0$ and obtain the variational equation

$$\begin{aligned} \frac{d}{dt}\delta\boldsymbol{z}_j(t) &= M_\mu \delta\boldsymbol{z}_j + \delta\boldsymbol{z}_{j+1}(t), \ j = 1, ..., N-1, \\ \frac{d}{dt}\delta\boldsymbol{z}_N(t) &= M_\mu \delta\boldsymbol{z}_N + \delta\boldsymbol{z}_1(t) + s\delta\boldsymbol{z}_\ell(t), \end{aligned}$$

which can be written as

$$\frac{d}{dt}\delta\boldsymbol{Z}(t) = \left[\boldsymbol{I}_N \otimes \boldsymbol{M}_\mu + \boldsymbol{G}_s \otimes \boldsymbol{I}_2\right]\delta\boldsymbol{Z}(t), \tag{3.2.2}$$

where $\delta\boldsymbol{Z} = (\delta\boldsymbol{z}_1, ..., \delta\boldsymbol{z}_N)^\top$, $\boldsymbol{I}_N \in \mathbb{R}^{N\times N}$ is the N-dimensional identity matrix,

$$\boldsymbol{G}_s = \begin{bmatrix} 0 & 1 & & 0 \\ \vdots & \ddots & \ddots & \\ 0 & & \ddots & 1 \\ 1 & 0 & s & 0 \end{bmatrix} \tag{3.2.3}$$

is the coupling matrix of the perturbed ring, $\boldsymbol{A}\otimes\boldsymbol{B}$ denotes the tensor product of the two matrices $\boldsymbol{A}$ and $\boldsymbol{B}$. Eq. (3.2.2) is a simple example of a system, which is treatable by a master stability function (MSF) approach [**136**]. In our case the MSF $M : \mathbb{C} \longrightarrow \mathbb{R}$ simply reads $M(\lambda) = \alpha + \Re(\lambda)$, where λ is an eigenvalue of the coupling matrix $\boldsymbol{G_s}$. Indeed, the spectrum of (3.2.2) is

$$\sigma\left(\boldsymbol{I}_N \otimes \boldsymbol{M}_\mu + \boldsymbol{G}_s \otimes \boldsymbol{I}_2\right) = \sigma(\boldsymbol{M}_\mu) + \sigma(\boldsymbol{G}_s) = \{\mu, \bar{\mu}\} + \sigma(\boldsymbol{G}_s). \tag{3.2.4}$$

Taking the real part, we obtain $M(\lambda) = \alpha + \Re(\lambda)$. The spectrum of the coupling matrix $\boldsymbol{G}_s$ equals the set of solutions of the characteristic equation

$$\chi_{G_s}(\lambda) = \lambda^N - s\lambda^{\ell-1} - 1 = 0. \tag{3.2.5}$$

For $s = 0$, $\sigma(\boldsymbol{G}_0)$ consists of the N roots of unity

$$\gamma_{N,k} = e^{i\frac{2\pi k}{N}},\ k = 0, ..., N-1.$$

For small $s \neq 0$, the roots λ_k, $k = 1, ..., N$, of Eq. (3.2.5) are given (asymptotically) as

$$\lambda_k(s) = \gamma_{N,k} + \frac{s}{N}\gamma_{N,k}^{\ell} + \mathcal{O}\left(s^2\right), \tag{3.2.6}$$

as one can readily compute by applying the implicit function theorem to (3.2.5) with base points $(s_0, \lambda_0) = (0, \gamma_{N,k})$. Hence, the spectrum of $\boldsymbol{G}_s$ is a weak modulation of the spectrum of the circulant matrix $\boldsymbol{G}_0$ (see Fig. 3.2.1 (a), (b)). For large s, $\sigma(\boldsymbol{G}_s)$ can be computed in a similar manner. In Appendix B we show that in this case the spectrum of $\boldsymbol{G}_s$ splits into two parts: there are $\ell - 1$ roots

$$\lambda_{1,k}(s) \approx s^{-1/\ell-1}\gamma_{\ell-1,k},\ k = 0, ..., \ell-2, \tag{3.2.7}$$

located close to an inner circle of amplitude $\sim s^{-1/\ell-1}$ and $N - \ell + 1$ roots

$$\lambda_{2,k}(s) \approx s^{1/N-\ell+1}\gamma_{N-\ell+1,k},\ k = 0, ..., N-\ell, \tag{3.2.8}$$

which are close to an outer circle of amplitude $\sim s^{1/N-\ell+1}$ (see Fig.3.2.1).

3.2.2. Bifurcations of the equilibrium. From the formula (3.2.4) for the spectrum of the equilibrium $\boldsymbol{z}_1 = .. = \boldsymbol{z}_N \equiv 0$, it follows that it is asymptotically stable iff

$$\Re(\lambda) < -\alpha,\ \text{for all } \lambda \in \sigma(\boldsymbol{G}_s). \tag{3.2.9}$$

When the parameter α is increased starting from a value which satisfies (3.2.9), a bifurcation takes place whenever for some $\lambda \in \sigma(\boldsymbol{G}_s)$:

$$\alpha = -\Re(\lambda). \tag{3.2.10}$$

Note that there is always one purely real eigenvalue $\lambda_1(s) = 1 + \frac{s}{N} + \mathcal{O}\left(s^2\right)$ of $\boldsymbol{G}_s$ which has maximal real part among all eigenvalues of $\boldsymbol{G}_s$ by a Perron-Frobenius argument (Thm.9). Therefore, for small $s \geq 0$ the equilibrium switches stability at

$$\alpha_1(s) \approx -\left(1 + \frac{s}{N}\right).$$

Since we assume $\beta \neq 0$, this bifurcation is a Hopf bifurcation and the emerging periodic orbit has frequency β at onset. As for $s = 0$, the bifurcation is supercritical for small $s > 0$, because the cubic term of the corresponding normal form depends continuously on s. Therefore, a branch of stable periodic solutions emerges and exists for $\alpha > \alpha_1(s)$. A further increase of α leads to a sequence of Hopf bifurcations which give rise to $N - 1$ branches of periodic

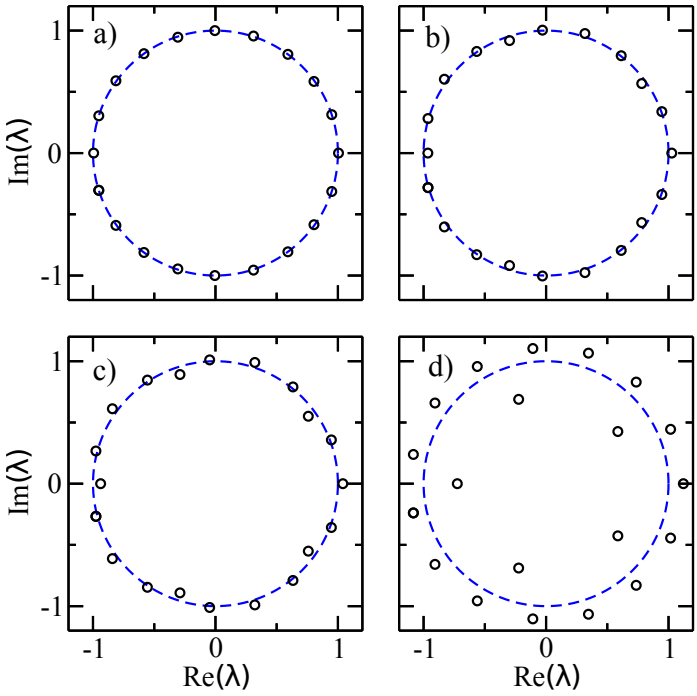

FIGURE 3.2.1. Spectra of the coupling matrix G_s (3.2.3) for $N = 20$ oscillators, a shortcut at node $l = 6$ and for different coupling strengths s: a) $s = 0.1$, b) $s = 0.6$, c) $s = 1$, d) $s = 5$.

solutions. As in the case $s = 0$, all bifurcations are supercritical if $s > 0$ is small (by continuity). The same is true if $s > 0$ is large, as we show in Appendix B. The latter $N-1$ periodic solutions are initially unstable, inheriting instability from the steady state. The initial frequency ω of the emerging periodic solution equals the imaginary part of the crossing eigenvalue, that is $\omega = \beta + \Im(\lambda)$ for the corresponding $\lambda \in \boldsymbol{G}_s$. For the unperturbed ring ($s = 0$) the first $\lfloor (N-1)/2 \rfloor$ ($\lfloor x \rfloor := \max\{n \in \mathbb{N} : n \leq x\}$) branches stabilize when they cross the Eckhaus stabilization line **[191]**

$$\frac{1}{N}|\boldsymbol{Z}|^2 = \frac{3\alpha}{4} + \sqrt{\left(\frac{\alpha}{4}\right)^2 + \frac{1}{2}}, \tag{3.2.11}$$

where $|\boldsymbol{Z}|^2$ is the (constant) amplitude of a periodic solution $\boldsymbol{Z}(t) = (z_1(t), ..., z_N(t))^T$. This observation is in striking analogy with the well known Eckhaus destabilization in diffusive systems **[50, 172]**. Remarkably, it is also found in this unidirectional system which does not extend to a spatially extended system in a natural manner. In section 3.4 we investigate how the added shortcut changes this scenario.

3.3. Emergent periodic orbits

Let $\boldsymbol{Z}(t)$ be a periodic solution of (3.1.1), which emerges from a Hopf bifurcation at

$$\alpha(s) = -\Re(\lambda(s)), \tag{3.3.1}$$

and which is associated to the eigenvalue $\lambda(s)$ of the coupling matrix $\boldsymbol{G}_s$, see (3.2.6)–(3.2.8). Because of the S^1-symmetry of the system, we employ the Ansatz

$$\boldsymbol{Z}(t) = \sqrt{\varepsilon} e^{i\omega(\varepsilon,s)t} \boldsymbol{V}(\varepsilon, s), \tag{3.3.2}$$

where

$$\varepsilon := \alpha - \alpha(s) \geq 0 \tag{3.3.3}$$

is the parameter distance from the bifurcation point,

$$\boldsymbol{V}(\varepsilon, s) = (v_1(\varepsilon, s), ..., v_N(\varepsilon, s))^T \in \mathbb{C}^N, \tag{3.3.4}$$

is the profile vector and the frequency $\omega(\varepsilon, s)$ of $\boldsymbol{Z}(t)$ is

$$\omega(\varepsilon, s) = \beta + \Im(\lambda(s)) + \mathcal{O}(\varepsilon). \tag{3.3.5}$$

The emerging periodic orbit is ε-close to the complex plane spanned by the eigenvector $b(s)$ of $\boldsymbol{G}_s$ corresponding to $\lambda(s)$ and tangential at the bifurcation point itself [**103**]. This means, $\boldsymbol{V}(0, s) = \boldsymbol{b}(s)$ with

$$\boldsymbol{b}(s) = a(s) \cdot \left(1, \lambda(s), \lambda^2(s), ..., \lambda^{N-1}(s)\right)^T, \tag{3.3.6}$$

where one may assume $a(s) \in \mathbb{R}$ due to the S^1-symmetry of the system. Fig. 3.3.1 shows several examples of the profile shapes for different s and λ. For $|\lambda| > 1$ the emerging solutions become stronger localized at the N-th node z_N with increasing s since it scales as $z_N \sim \lambda^{N-1}$. For $|\lambda| < 1$, the localization takes place at $z_1(t)$ for the same reason.

3.3.1. Case I: small perturbation. In this section we consider s to be small. Our aim is to determine a formal asymptotic expansion for the frequencies (3.3.5) and the profiles (3.3.4) of the periodic solutions and to derive evaluable approximate conditions for their stability. In particular, we are interested in the deformation of the Eckhaus stabilization line (3.2.11). In order to obtain asymptotic expressions for the profiles in case that $s, \varepsilon > 0$, we linearize the vector field in $\varepsilon = s = 0$. For a periodic solution (3.3.2), we introduce rescaled, rotating coordinates $u_j(t) \in \mathbb{C}$, $j = 1, ..., N$ according to

$$z_j = \sqrt{\varepsilon} e^{i\omega t} v_j u_j, \tag{3.3.7}$$

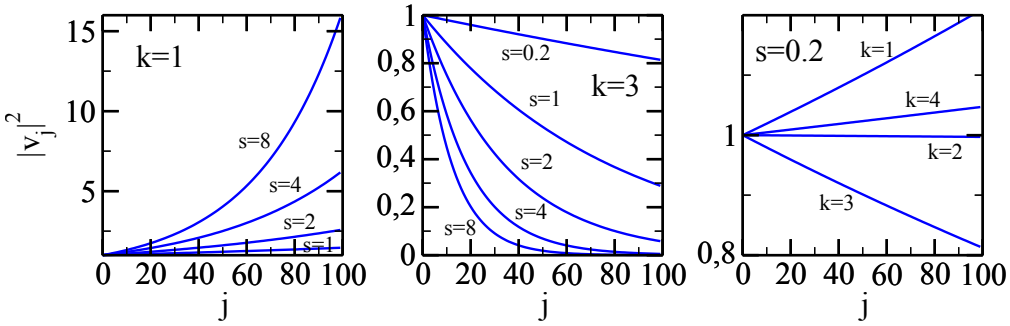

FIGURE 3.3.1. Moduli of the components of the initial profiles $\boldsymbol{V}(0,s)=\boldsymbol{b}(s)$ of emerging periodic solutions (see 3.3.4) and (3.3.6) for different wave numbers k (i.e., different eigenvalues $\lambda_k(s)$ of $\boldsymbol{G}_s$) and coupling strengths s as indicated in the figure. For all panels: $N=100$ and $\ell=26$.

with $\omega=\omega(\varepsilon,s)$ and $v_j=v_j(\varepsilon,s)$. Then (3.1.1) becomes

$$\dot{u}_j=\left(\alpha+i(\beta-\omega)-\varepsilon|v_ju_j|^2\right)u_j+\frac{v_{j+1}}{v_j}u_{j+1}, \tag{3.3.8}$$

$$\dot{u}_N=\left(\alpha+i(\beta-\omega)-\varepsilon|v_Nu_N|^2\right)u_N+\frac{v_1}{v_N}u_1+s\frac{v_\ell}{v_N}u_\ell, \tag{3.3.9}$$

In rotating coordinates, the equilibrium solution

$$u_j\equiv 1,\ j=1,...,N, \tag{3.3.10}$$

corresponds to the periodic solution (3.3.2) of (3.1.1) and the stability of (3.3.2) and (3.3.10) is the same. In Appendix B we show that for each eigenvalue $\lambda_k(s)=\gamma_{N,k}+\frac{s}{N}\gamma^\ell_{N,k}+\mathcal{O}\left(s^2\right)$ of $\boldsymbol{G}_s$, the corresponding branch of periodic solutions has frequencies

$$\omega_k(\varepsilon,s)=\beta+\Im(\gamma_{N,k})+\frac{s}{N}\Im\left(\gamma^\ell_{N,k}\right)+\mathcal{O}\left((|\varepsilon|+|s|)^2\right), \tag{3.3.11}$$

and profiles

$$v_j(\varepsilon,s)=\gamma^{j-1}_{N,k}\left(1+s\frac{j-1}{N}\gamma^{\ell-1}_{N,k}\right)+\mathcal{O}\left((|\varepsilon|+|s|)^2\right). \tag{3.3.12}$$

3.3.2. Case II: large perturbation. In this section we consider s to be large. To treat (3.1.1) as a weakly perturbed system we perform a change of variables

$$y_j(t)=\varsigma^j z_j\left(\varsigma^{2N}t\right), \tag{3.3.13}$$

with a small parameter $\varsigma=s^{-1/N-\ell+1}$, which is the inverse radius of the outer spectral circle of eigenvalues (3.2.8). This transformation normalizes the emerging profiles (3.3.6) corresponding to the eigenvalues (3.2.8). The transformed

variables (3.3.13) satisfy

$$\begin{aligned}(3.3.14)\ \dot{y}_j(t) &= \left(\varsigma^{2N}\mu - \varsigma^{2(N-j)}|y_j(t)|^2\right) y_j(t) \\ &\quad +\varsigma^{2N-1} y_j(t),\ j=1,...,N-1, \\ \dot{y}_N(t) &= \left(\varsigma^{2N}\mu - |y_N(t)|^2\right) y_N(t) + \varsigma^{3N-1} y_1 + \varsigma^{2N-1} y_\ell(t).\end{aligned}$$

Since $\varsigma^{3N-1}y_1 = \varsigma^N\left(\varsigma^{2N-1}y_1\right)$ and ς^N is small, we consider system (3.3.14) as a small perturbation of

$$\begin{aligned}(3.3.15)\qquad \dot{y}_j(t) &= \left(\varsigma^{2N}\mu - \varsigma^{2(N-j)}|y_j(t)|^2\right) y_j(t) \\ &\quad +\varsigma^{2N-1} y_j(t),\ j=1,...,N-1, \\ \dot{y}_N(t) &= \left(\varsigma^{2N}\mu - |y_N(t)|^2\right) y_N(t) + \varsigma^{2N-1} y_\ell(t).\end{aligned}$$

Although we cannot show that results for the persistence of hyperbolic invariant manifolds **[58]** apply and assure that (3.3.15) possesses the same hyperbolic invariant manifolds as does (3.3.14), the truncated system (3.3.15) is a natural approximation to (3.3.14). Note that in (3.3.15) the components y_1, ..., $y_{\ell-1}$ do not couple back to the rest of the system since the weak link from y_1 to y_N was taken out. Therefore, the dynamics of the subsystem y_ℓ, ..., y_N is independent and, apart from the zero solution, acts as a periodic force on the attached subsystem y_1, ..., $y_{\ell-1}$. In original variables (3.3.15) reads

$$\begin{aligned}(3.3.16)\qquad \dot{z}_j(t) &= \left(\mu - |z_j(t)|^2\right) z_j + z_{j+1}(t),\ j=1,...,N-1, \\ \dot{z}_N(t) &= \left(\mu - |z_N(t)|^2\right) z_N + s z_\ell(t).\end{aligned}$$

The linearization of (3.3.16) at the zero solution has eigenvalues

$$\mu+\nu,\ \text{ and }\ \bar{\mu}+\nu$$

where ν is a root of the characteristic equation

$$\left(\nu^{N-\ell+1} - s\right)\nu^{\ell-1} = 0$$

of the reduced coupling matrix H_s, which is obtained by erasing the link from z_1 to z_N from $\boldsymbol{G}_s$. It has eigenvalues

$$(3.3.17)\qquad \nu = 0 \text{ and } \nu = s^{1/N-\ell+1}\gamma_{N-\ell+1,k},\ k=1,...,N-\ell+1.$$

Periodic orbits which correspond to the algebraically $(\ell-1)$-fold eigenvalue $\nu=0$ are localized on the nodes z_1, ..., $z_{\ell-1}$.

3.4. Stability of the periodic orbits

3.4.1. Case I: small perturbation. The variational equation for system (3.3.8)–(3.3.9) at the stationary solution (3.3.10) is

$$\begin{aligned}\dot{u}_j &= \left(\alpha+\varepsilon+i\left(\beta-\omega\right)-2\varepsilon\left|v_j\right|^2\right)u_j+\frac{v_{j+1}}{v_j}u_{j+1},\\ \dot{u}_N &= \left(\alpha+\varepsilon+i\left(\beta-\omega\right)-2\varepsilon\left|v_N\right|^2\right)u_N+\frac{v_1}{v_N}u_1+s\frac{v_\ell}{v_N}u_\ell.\end{aligned}$$

We transform the system into $\mathbb{R}^{2N}$ ($\boldsymbol{x}_j = (\Re(u_j), \Im(u_j))^T$) and insert the expansions (3.3.11) and (3.3.12) to obtain

$$\begin{aligned}\dot{\boldsymbol{x}}_j &= -\left[\boldsymbol{M}_{\tilde{\lambda}}+2\varepsilon\boldsymbol{\delta}_{11}\right]\boldsymbol{x}_j+\boldsymbol{M}_{\tilde{\lambda}}\boldsymbol{x}_{j+1}+\mathcal{O}\left(\left(|\varepsilon|+|s|\right)^2\right)\\ \dot{\boldsymbol{x}}_N &= -\left[\boldsymbol{M}_{\tilde{\lambda}}+2\varepsilon\boldsymbol{\delta}_{11}\right]\dot{\boldsymbol{x}}_N+\boldsymbol{M}_{\tilde{\lambda}}\dot{\boldsymbol{x}}_1\\ &\quad +s\boldsymbol{M}_{\lambda_0^\ell}\left[\dot{\boldsymbol{x}}_\ell-\dot{\boldsymbol{x}}_1\right]+\mathcal{O}\left(\left(|\varepsilon|+|s|\right)^2\right)\end{aligned} \tag{3.4.1}$$

with $\lambda_0 = \gamma_{N,k}$, $\tilde{\lambda}(s) = \lambda_0 + \frac{s}{N}\lambda_0^\ell$, the matrix representation $\boldsymbol{M}: \mathbb{C} \to \mathbb{R}^{2\times 2}$ (as in (3.2.1)) and $\boldsymbol{\delta}_{mn} = (\delta_{jm}\delta_{kn})_{j,k}$ is the matrix which has the entry 1 at position (j,k) and zeros everywhere else. We drop the higher order terms in (3.4.1) and write the system in the form

$$\dot{\boldsymbol{X}} = A(\varepsilon, s)\,\boldsymbol{X} = \left[-\boldsymbol{I}_N\otimes\left(\boldsymbol{M}_{\tilde{\lambda}}+2\varepsilon\boldsymbol{\delta}_{11}\right)+\boldsymbol{G}_0\otimes\boldsymbol{M}_{\tilde{\lambda}}+\left(\boldsymbol{\delta}_{N1}-\boldsymbol{\delta}_{N\ell}\right)\otimes s\boldsymbol{M}_{\lambda_0^\ell}\right]\boldsymbol{X}. \tag{3.4.2}$$

Clearly, an MSF approach as in section 3.2 is not feasible any more. However, we have reduced the dynamical problem to an algebraic one. The eigenvalues of system (3.4.2) can be computed by standard numerical procedures to determine approximately the stability of the periodic solutions in the vicinity of a bifurcation point. The eigenvalues of (3.4.2) approximate the eigenvalues of the exact system (3.3.8)–(3.3.9) at the steady state (3.3.10) up to first order in ε and s. Anyway, this first order approximation leads to good predictions even for moderate values of the parameters, in particular for ε (see Fig. 3.4.1).

3.4.2. Resonances. An important observation for the perturbed system is that in comparison to the unperturbed case $s = 0$, for small $s > 0$ the point of stabilization of a periodic solution may be altered or not. It remains nearly the same if the corresponding eigenvalue $\lambda_k = \gamma_{N,k} + \mathcal{O}(s)$ fulfils

$$\arg\left(\gamma_{N,k}\right) \approx \arg\left(\gamma_{N,k}^\ell\right), \tag{3.4.3}$$

or equivalently, $\frac{k(l-1)}{N} \in \mathbb{Z}$. This corresponds to a situation where both components of the input $z_1(t) + sz_\ell(t)$ to node $z_N(t)$ possess approximately the same phase. At the same time it is a condition for maximizing the modulus $|\lambda_k| \approx \left|\gamma_{N,k} + \frac{s}{N}\gamma_{N,k}^\ell\right|$ and for $\gamma_{N,k}$ to span an eigenmode of both, the unperturbed cycle of length N and of a cycle which has the same length $N-\ell-1$ as the newly created cycle $\ell \to N \to (N-1) \to ... \to \ell$, i.e. to be an N-th

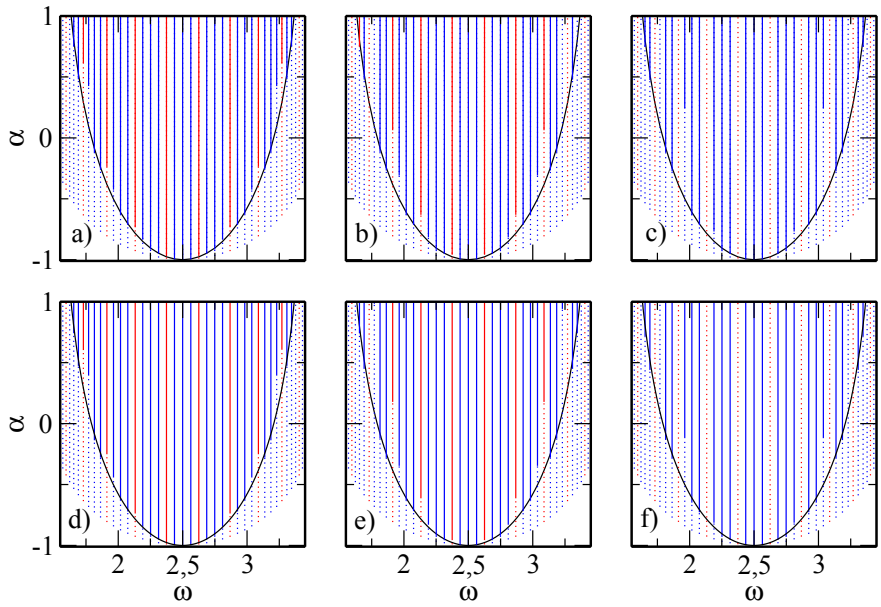

FIGURE 3.4.1. Bifurcation diagrams for different strengths s of the shortcut in a ring of $N = 100$ oscillators with a shortcut from node $\ell = 26$ to node $N = 100$; $\beta = 2.5$. Dashed lines indicate unstable periodic orbits and solid lines stable periodic orbits. The stabilization line for $s = 0$ is shown in black. The frequency of the solutions is plotted against the bifurcation parameter α. The perturbation strength s increases from left to right: a), d) $s = 0.05$; b), e) $s = 0.1$; c), f) $s = 0.2$. The upper panels a), b), c) show the approximated diagram obtained from (3.4.2). The lower panels d), e), f) show results of numerical bifurcation analysis of the full system for comparison. These calculations were carried out with the program AUTO **[46]**.

and an $(N - \ell + 1)$-th root of unity. On the contrary, the antiphase condition

$$\arg(\gamma_{N,k}) \approx \arg\left(\gamma_{N,k}^{\ell}\right) + \pi \tag{3.4.4}$$

causes the point of stabilization to grow rapidly with increasing s, i.e., it destabilizes the corresponding periodic orbit. The more precisely the equality (3.4.4) holds, the more pronounced is the destabilizing effect of the additional link (see Fig. 3.4.1).

3.4.3. Case II: Large s. For large s both systems, the original (3.1.1) and the truncated (3.3.16), admit two types of periodic solutions emerging in bifurcations corresponding to eigenvalues of scale $|\lambda| \approx 0$ or $|\lambda| \approx s^{1/N-\ell+1}$, respectively (see Eq. (3.2.7), (3.2.8), and (3.3.17)). In case of system (3.1.1) all these periodic solutions emerge in form of rotating eigenvectors (3.3.2)–(3.3.6)

of the coupling matrix G_s which leads to a locally pronounced activity in $z_1(t)$ for a corresponding eigenvalue $|\lambda| \approx 0$, and in $z_N(t)$ for $|\lambda| \approx s^{1/N-\ell+1}$ (see fig. 3.3.1). The same picture applies for bifurcations of (3.3.16) corresponding to the simple eigenvalues ($|\nu| \approx s^{1/N-\ell+1}$) of H_s, while the $\ell-1$-fold bifurcation at $\alpha = 0$ corresponding to $\nu = 0$ simultaneously creates several solutions which are completely localized in the attached subsystem $(z_1, ..., z_{\ell-1})$ where only the oscillators z_1, ..., z_k, $k = 1, ..., \ell-1$, are active and all others silent. For each of these solutions the first active element $z_k(t) = \sqrt{\alpha}e^{i\beta t}$ is located on the limit cycle of an isolated Stuart-Landau oscillator and all other z_j, $j < k$, lock either in phase or antiphase to their input signal z_{j+1}. However, these solutions can never stabilize, since the zero solution of the subsystem z_ℓ, ..., z_N is unstable after the first bifurcation corresponding to $|\nu| \approx s^{1/n}$. Therefore, it suffices to study the inhomogeneous ring

$$\begin{aligned} \dot{z}_j(t) &= \left(\mu - |z_j(t)|^2\right) z_j + z_{j+1}(t), \ j = 1, ..., n-1, \\ \dot{z}_n(t) &= \left(\mu - |z_n(t)|^2\right) z_n + s z_1(t), \ n = N - \ell + 1, \end{aligned} \tag{3.4.5}$$

to understand the possibly stable dynamics of (3.3.16). To approximate the stability of the emerging periodic solutions one can proceed as for the case of small s: write the system in scaled rotating coordinates (3.3.7), linearize around the equilibrium solution (3.3.10), expand the variational equations in powers of ε and truncate terms of order higher than $\mathcal{O}(\varepsilon)$.We obtain the following approximate variational equation (see Appendix B):

$$\begin{aligned} \dot{\boldsymbol{x}}_j &= -\left[s^{\frac{1}{n}}\boldsymbol{M}_{\gamma_{n,k}} + \varepsilon\left(\left|v_j^0(s)\right|^2 \begin{pmatrix} 3 & 0 \\ 0 & 1 \end{pmatrix} - \begin{pmatrix} 1 & 0 \\ 0 & 1 \end{pmatrix}\right)\right]\boldsymbol{x}_j \\ &\quad + \left[s^{\frac{1}{n}}\boldsymbol{M}_{\gamma_{n,k}} + \varepsilon\left(\left|v_j^0(s)\right|^2 - 1\right)\begin{pmatrix} 1 & 0 \\ 0 & 1 \end{pmatrix}\right]\boldsymbol{x}_{j+1}, \end{aligned} \tag{3.4.6}$$

where $\left|v_j^0(s)\right|^2 = n s^{\frac{2(j-1)}{n}} \frac{s^{\frac{2}{n}}-1}{s^2-1}$. Although the loss of symmetry prevents us from applying an MSF approach, (3.4.6) enables us to approximate the Floquet exponents by solving numerically the characteristic equation of (3.4.6).

3.5. Discussion

We have investigated how the introduction of a shortcut alters the dynamics in a unidirectional ring of Stuart-Landau oscillators. In absence of a shortcut, the system exhibits a bifurcation scenario similar to the Eckhaus instability observed in dissipative media. For small shortcut strengths s we have found that the Eckhaus stabilization line is modulated in the following manner: The destabilizing impact on periodic solutions is stronger for non-resonant modes than for resonant ones. The latter correspond to wavenumbers that are compatible with the lengths of both cycles which exist in the perturbed system, i.e. for the cycle of length $N-\ell+1$ which contains the shortcut, as well as for

the full cycle of length N. In contrary to the non-resonant solutions, the stabilization of the resonant periodic solutions occurs for similar parameter values as in the case without shortcut. As a result, one can control the destabilization of a specific set of wavenumbers via the link position ℓ and its strength s. In the case of a large shortcut strength s we have provided an argument that the cycle of length $N - \ell + 1$ dominates the dynamics and stable solutions can be treated as solutions of a single unidirectional inhomogeneous ring which has coupling strength s at only one link.

Further investigations will be dedicated to how small perturbations may be used to select solutions with a specific wavenumber by adding a corresponding set of resonant links. More generally, our findings may help to understand how perturbations with a more complicated structure, consisting of several shortcuts, can influence the dynamics of a unidirectional ring. Moreover, our observations might even help to locate an unknown shortcut when one is only allowed to vary a bifurcation parameter and observe the dynamics, since the modulated Eckhaus line can be used to identify the shortcut. A strong shortcut can be used in arbitrary networks in order to localize the activity on the cycles in which they are contained and amplify the activity in particular on their targets.

Another point which was not investigated here but deserves a closer study is the development of profiles far from the bifurcation point. The simplest, most important phenomenon is that, for increasing α, the exponential tails of the profiles develop into plateaus, where the profile amplitude is locally constant as a function of the component index. By taking the limit $N \to \infty$ one can argue that solutions may consist of several, sharply separated plateaus where each plateau can possess a different wavenumber. This complies with numerical observations, although all observed solutions with more than one plateau lie on the unstable branches which correspond to the inner spectral circle for large s. For sufficiently large values of s, those branches begin to curl with increasing α and seem to be unstable for arbitrary large values of α (see Fig. 3.5.1).

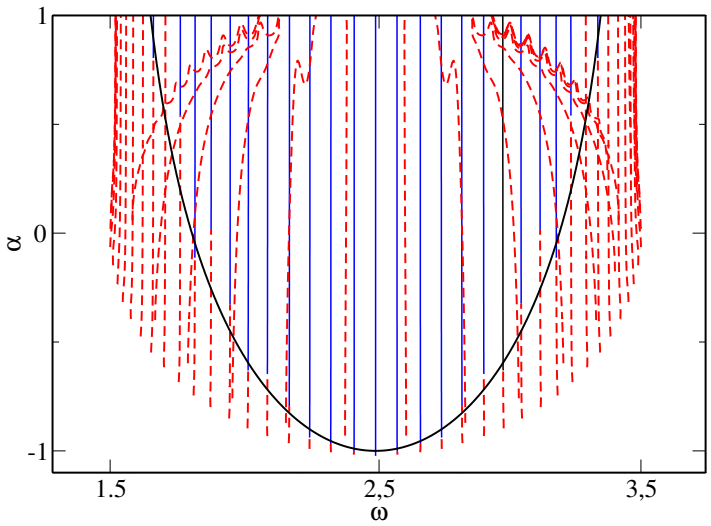

FIGURE 3.5.1. Bifurcation diagram for intermediate strength $s = 5$ of the shortcut. Fixed parameters are $N = 100$, $\ell = 26$, $\beta = 2.5$. Branches of unstable periodic orbits are indicated by dashed lines and stable branches by solid lines. Along the black line (3.2.11) the stabilization takes place for $s = 0$. The frequency of the solutions is plotted against the bifurcation parameter α. The calculations were carried out with the program AUTO [**46**].

CHAPTER 4

Synchronous Motion in Rings of Delay Coupled Phase Oscillators and Applications to Pattern Recognition

"The wheel is come full circle."
W. Shakespeare, King Lear

4.1. Introduction

In the previous chapter we have investigated the effect of a simple modification of a ring network, i.e. the introduction of an additional link. Here, we consider phase oscillators coupled in a ring scheme as well, but this time with a different type of modification. Namely, we add time delays in the couplings. This has fundamental consequences for the exhibited dynamics, amongst others increasing multistability of synchronous states for higher values of the delays. Provided with a global coupling structure coupled phase oscillators are well known as Kuramoto model [**102**]. A lot of research has been done on the synchronization properties of Kuramoto oscillators with instantaneous coupling and related bifurcation scenarios since the 1980s [**3**]. Similarly, Kuramoto oscillators with delayed couplings are well investigated [**193, 109**], whereas there are fewer results on networks of phase oscillators with a local coupling structure [**150**]. The first stability criterion for systems with delayed couplings was given in [**49**], however, it does not contain a description of the multistability and corresponding bifurcations. Here, we will investigate the existence, stability and bifurcations of synchronous states in a ring. Furthermore, we will show how to use these states in order to store and recognize patterns. For the reader not familiar with pattern recognition we give a short introduction.

The ability to recognize encoded patterns is a very general and omnipresent skill in humans and animals. Here, the term pattern can refer to a structure of any nature activating a sensory perception. Developing artificial pattern recognition systems as well as investigating actual natural mechanisms of pattern recognition in humans and animals has been a scientific challenge for decades. Until a couple of years ago, the state of the art was a model developed by Hopfield in 1982 [**80**]. It is a recurrent artificial neural network consisting of coupled discrete elements. In contrast to feedforward networks the underlying

graph might have loops leading to more complex dynamics and multistability, which in turn is used to store several patterns at once in the network.

Up to now, the Hopfield model and its variations have been extensively studied. The majority of the work was focused on stability analysis of the underlying dynamical system. For some recent results, see [**160, 186, 184**] and references therein. However, from the point of view of pattern recognition, all these models still share the idea of the original Hopfield model, i.e, storing patterns in stable fixed points of dynamical systems. On the other hand, experimental evidence strongly suggests that patterns are stored as objects with time resolution, i.e. as periodic orbits. For instance, experiments of the group of W.J. Freeman showed complex behaviour in the EEG tracings of olfactory bulbs in rabbits [**161**]. The spatial activity patterns indicated by EEG potentials differ for different odours, indicating that a partial pattern of receptor activity may result in a spatial pattern of neural activity in the bulb, which might in turn transmit odour-specific information to the olfactory cortex. Limit cycle activities occur for perceptible odors and chaotic activities occur for novel odors. These factors indicate that it is necessary to develop neural network models which use periodic solutions as memory. Up to now, there are few results in this direction. One approach developed in [**5**] constructs a piecewise linear map with a stable periodic solution for each stored pattern. Since each pattern is stored in only one map (one neuron), it loses the distributive and parallel processing property presented in both biological and artificial neural networks. Another approach developed in [**180**] studies the existence and stability of stable periodic solutions in discrete-time bidirectional associative memory neural networks. However, it does not show how the periodic solutions can be used as associative memory. In this chapter, we close this gap by presenting a system of coupled phase oscillators with time delay as associative memory, where the patterns are stored as stable periodic orbits. In this way, the model possesses distributive and parallel processing in the space of coupled neurons, as well as preserving the natural order of the elements in each pattern by the time order of each periodic orbit. Indeed, there is an increasing evidence that the brain's memory and retrieval functions are closely connected to spike timing [**76**].

To be more precise, we employ an idea developed in [**142, 190**] where it is shown how the tuning of delays in a ring of phase oscillators can transform stable synchronous spiking patterns into arbitrary stable spiking patterns. We will use these spiking patterns to represent encoded patterns. The recognition consists then in simulating the system with an initial condition associated to the pattern in question. The higher the convergence rate to the encoded pattern, the more probable is a recognition. Although this idea can be generalized to delayed networks with arbitrary coupling topology, as shown in chapter 5, the simple structure makes the ring accessible to analytic investigations.

The chapter is structured as follows. In section 4.2 we analyse the model equations with homogeneous delays. In particular, we study coexisting periodic solutions in such a system together with their number and stability. Section 4.3 introduces the pattern recognition mechanism. In section 4.4 we apply the model to various signals ranging from simple artificial ones to speech and present numerical results. Section 4.5 concludes this chapter.

4.2. Synchronous motions in rings of phase oscillators

In this section we introduce the dynamical system used as a pattern recognition device, determine the number of coexisting solutions and present a detailed bifurcation analysis.

4.2.1. The model equations. In the previous chapter we have investigated a unidirectional ring of elements where the local dynamics were given by Stuart-Landau oscillators. These are two-dimensional limit cycle oscillators characterized by a phase and an amplitude. However, when such elements are weakly coupled, the phases evolve on a slower timescale than the amplitudes and one can restrict to an equation for the phases only [**90**]. In this spirit we consider the delayed, unidirectional ring of phase oscillators.

$$\dot{x}_j(t) = \omega + \kappa \sin\left(x_{j+1}(t-\tau) - x_j(t)\right) \quad 1 \le j \le N. \tag{4.2.1}$$

Here $x_j \in 2\pi\mathbb{R}/\mathbb{Z}$ and all the oscillators have the same individual frequency ω. The coupling between the oscillators is of strength $\kappa > 0$ and delayed by a time delay $\tau > 0$. As our aim is to construct/memorize and recognize patterns by means of synchronous states, we first assure the existence of the synchronous solutions. We remark that by introducing new variables $y_j = x_j - \omega$ and rescaling the time $t \mapsto \kappa t$ system (4.2.1) transforms to $\dot{y}_j(t) = \sin\left(y_{j+1}(t-\tilde{\tau}) - y_j(t)\right)$. However, we will consider (4.2.1), since it does not make the analysis more complicated and still keeps the coupling strength and frequency explicitly.

4.2.2. Existence of synchronous periodic solutions . Synchronous periodic solutions of (4.2.1) are of the form

$$x_j(t) = x_s(t) = \Omega t \tag{4.2.2}$$

for some mean frequency $\Omega \in \mathbb{R}$. Substituting this solution in system (4.2.1) yields the transcendental equation for Ω

$$\Omega = \omega - \kappa \sin(\Omega\tau). \tag{4.2.3}$$

Now, introducing the variable $z = \Omega\tau$ Eq. (4.2.3) transforms to

$$\frac{z}{\kappa\tau} = \frac{\omega}{\kappa} - \sin(z). \tag{4.2.4}$$

That is, we look for intersections of a straight line through the origin with slope $\frac{1}{\kappa\tau}$ and a shifted sine, see Fig. 4.2.1(a).

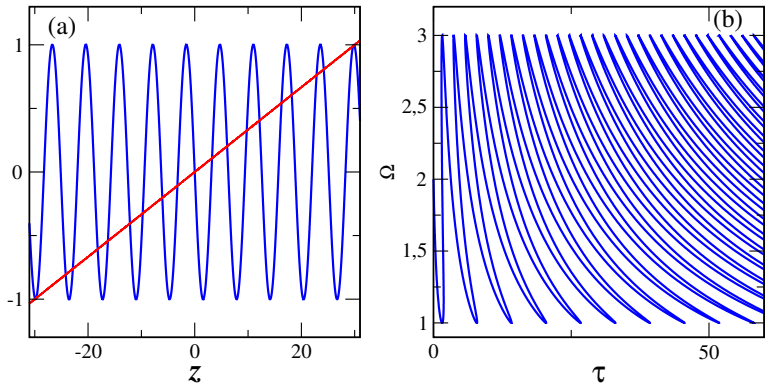

FIGURE 4.2.1. (a) Graphical representation of solutions to Eq. (4.2.4). The intersection points determine frequencies of synchronous solutions Ω, $z = \Omega\tau$. Parameters: $\omega = 0$, $\tau = 10$, and $\kappa = 3$. (b) Frequency of synchronous solutions versus delay τ, given by Eq. (4.2.5). Parameters: $\omega = 2$ and $\kappa = 1$.

In order to visualize how multiple synchronous solutions (4.2.2) with different frequencies appear for different delay times τ, let us represent the solutions of (4.2.3) in the following parametric form

$$\tau(s) = \frac{s}{\omega + \kappa \sin(-s)} \quad , \quad \Omega(s) = \frac{s}{\tau(s)}. \tag{4.2.5}$$

So the same branch of periodic solutions reappears slightly inclined for larger values of τ, see Fig. 4.2.1 (b). Both figures show that indeed, either increasing τ or κ leads to an increase of solutions of the form (4.2.2). Actually, it is known that the number of coexisting periodic solutions in systems with time delay τ grows at least linearly with τ **[189]**. In our case, using simple geometrical arguments, one can show that the number of such solutions is approximately $2\kappa\tau/\pi$. A proof together with the stability analysis is given in the following section.

4.2.3. Stability of synchronous solutions. The main result of this section is, that half of the above mentioned $2\kappa\tau/\pi$ synchronous solutions are linearly stable, whereas the other half is unstable. To determine the linear stability consider the linearization of Eq. (4.2.1) along a synchronous solution of the form (4.2.2)

$$\dot{\boldsymbol{\xi}}(t) = -K\boldsymbol{\xi}(t) + K\boldsymbol{G}\boldsymbol{\xi}(t-\tau),$$

where

$$K = \kappa \cos(\Omega\tau) \tag{4.2.6}$$

and $\boldsymbol{G} = \{g_{ij}\}$ is the adjacency matrix of the unidirectional ring coupling, i.e. $g_{ij} = 1$ if $j = i + 1 \bmod N$ and $g_{ij} = 0$ otherwise. Here N is the number of oscillators in the ring. Thus the linear stability is given by the distribution of

zeros $\mu \in \mathbb{C}$ of the following characteristic equation

$$\begin{aligned} F(\mu) &= \det\left(-\mu \boldsymbol{I}_N - K\boldsymbol{I}_N + Ke^{-\mu\tau}\boldsymbol{G}\right) \\ &= -(\mu + K)^N + K^N e^{-N\mu\tau}. \end{aligned}$$

The solutions μ of this equation are the characteristic exponents (eigenvalues) whose real parts determine the stability. The obtained characteristic equation can be factorized to the set of N simpler equations:

$$0 = \mu + K - Ke^{-\mu\tau}e_n, \quad n = 0, \ldots, N-1, \tag{4.2.7}$$

where $e_n = \exp[i2\pi n/N]$ are N-th roots of unity. Now we can prove the following lemma.

LEMMA 22. *Let $\boldsymbol{x}(t) = \Omega t \mathbf{1}_N$ be a synchronous solution of (4.2.1). The solution is linearly stable iff the following condition holds*

$$\cos(\Omega\tau) > 0.$$

Furthermore, if $\cos(\Omega\tau) < 0$, the following upper bound for the real parts of the characteristic exponents μ holds true

$$\Re(\mu) \leq -2\kappa\cos(\Omega\tau).$$

PROOF. Splitting Eq. (4.2.7) into real and imaginary parts ($\mu = \alpha + i\beta$) yields

$$\begin{aligned} 0 &= \alpha + K\left(1 - e^{-\alpha\tau}\cos\left(\frac{2\pi n}{N} - \beta\tau\right)\right), \\ 0 &= \beta - Ke^{-\alpha\tau}\sin\left(\frac{2\pi n}{N} - \beta\tau\right). \end{aligned} \tag{4.2.8}$$

Consider the two cases $K > 0$ and $K < 0$
i) Case $K > 0$. For $\alpha > 0$ we have $\alpha + K\left(1 - e^{-\alpha\tau}\cos\left(\frac{2\pi n}{N} - \beta\tau\right)\right) > 0$ which contradicts Eq. (4.2.8). Consequently, Eq. (4.2.8) can only be fulfilled for $\alpha < 0$. It is shown in [**49**] that $K > 0$ is also a necessary condition for stability which concludes the proof of the first part of the lemma.
ii) Case $K < 0$. If we have $\alpha \leq 0$ the upper bound is automatically valid. So suppose we have a solution (α, β) with $\alpha > 0$. Then, Eq. (4.2.8) implies

$$0 < -K\left(1 - e^{-\alpha\tau}\cos\left(\frac{2\pi n}{N} - \beta\tau\right)\right) < -2K,$$

so for $\alpha > -2K$ we would have $\alpha + K\left(1 - e^{-\alpha\tau}\cos\left(\frac{2\pi n}{N} - \beta\tau\right)\right) > 0$ which means that indeed, the real part α of μ can be bounded as follows

$$\alpha \leq -2K = -2\kappa\cos(\Omega\tau).$$

□

Using the condition for stability from lemma 22 we obtain estimations for the number of coexistent stable and unstable periodic orbits.

LEMMA 23. *Let $2\tau\kappa > \pi$. Then there are at least $\frac{\kappa\tau}{\pi} - \frac{1}{2}$ stable and unstable periodic synchronous solutions of Eq. (4.2.1), respectively.*

PROOF. Finding periodic solutions is equivalent to finding zeros of the function $f(\Omega) = \Omega - \omega + \kappa \sin(\Omega\tau)$. We have seen in the last lemma, that a solution with frequency Ω is stable if $\cos(\Omega\tau) > 0$. This is the case for $\Omega\tau \in \left(-\frac{\pi}{2}, \frac{\pi}{2}\right) + 2\pi l$. Motivated by this we define the disjoint intervals

$$\begin{aligned} I_l &= \left(-\frac{\pi}{2\tau}, \frac{\pi}{2\tau}\right) + \frac{2\pi l}{\tau} \qquad l \in \mathbb{Z}, \\ J_l &= \left(\frac{\pi}{2\tau}, \frac{3\pi}{2\tau}\right) + \frac{2\pi l}{\tau} \qquad l \in \mathbb{Z}, \end{aligned}$$

for which $\cos(\Omega\tau) > 0$ and $\cos(\Omega\tau) < 0$, respectively. We first remark that we have to fulfil $\Omega \in (\omega - \kappa, \omega + \kappa)$ (see Eq. (4.2.3)). A straightforward calculation shows that the number M of intervals I_l lying in $(\omega - \kappa, \omega + \kappa)$ satisfies

$$\frac{\kappa\tau}{\pi} - \frac{1}{2} \leq M \leq \frac{\kappa\tau}{\pi} + \frac{1}{2}.$$

Now in I_l we have

$$f'(\Omega) = 1 + \kappa\tau \cos(\Omega\tau) > 0$$

and further $f\left(-\frac{\pi}{2\tau} + \frac{2\pi l}{\tau}\right) \leq 0 \leq f\left(\frac{\pi}{2\tau} + \frac{2\pi l}{\tau}\right)$ for all $I_l \subset (\omega - \kappa, \omega + \kappa)$. So f has exactly one zero in each I_l by the strict monotonicity. By the same argument there has to be an odd number of zeros in each J_l. By the shape of f we conclude that it has one zero in each J_l as well. So the total number of zeros m in intervals J_l has the same bounds as M. □

4.2.4. Bifurcations of synchronous solutions. In subsection 4.2.2 we have seen that synchronous solutions undergo bifurcations as either the delay time τ or the coupling strength κ is varied. In this section we give some insight into these bifurcations. A solution (4.2.2) can change its stability when one of its characteristic exponents crosses the imaginary axis $\mu = i\beta$, $\beta \in \mathbb{R}$. Substituting $\mu = i\beta$ into (4.2.7) and splitting the obtained equation into real and imaginary parts yields

$$\begin{aligned} 0 &= K\left(1 - \cos\left(\frac{2\pi n}{N} - \beta\tau\right)\right), \\ 0 &= \beta - K \sin\left(\frac{2\pi n}{N} - \beta\tau\right). \end{aligned} \tag{4.2.9}$$

The first equation in (4.2.9) is fulfilled if either $K = 0$ or $\frac{2\pi n}{N} - \beta\tau = 2\pi l$ for some $l \in \mathbb{Z}$. Plugged into the second equation both conditions yield $\beta = 0$. Thus, Hopf bifurcations with $\beta \neq 0$ cannot occur in the model. The only possible destabilization corresponds to eigenvalues crossing the imaginary axis with vanishing imaginary part β. On the other hand, every periodic solution has a trivial characteristic exponent $\mu = 0$ corresponding to perturbations

in the direction of the periodic motion. So in order to look for a change of stability we have to find non-simple zeros of the characteristic function. Such non-simple zeros are possible if $F'(0) = -NK^{N-1}(K\tau + 1) = 0$. This is fulfilled if either one of the following conditions holds

$$K = 0 \quad , \quad \tau K = -1. \tag{4.2.10}$$

The following lemma describes the type of bifurcations taking place if the conditions (4.2.10) hold, see also Fig. 4.2.2. We remind that $K = \kappa\cos(\Omega\tau)$.

LEMMA 24. *Let $\boldsymbol{x}_\tau(t) = \Omega(\tau)\, t\mathbf{1}_N$ be a branch of synchronous solutions of Eq. (4.2.1) with $\kappa \neq 0$. Varying τ it undergoes a transcritical bifurcation at $K = 0$ with K from Eq. (4.2.6). If $\omega \neq \pi l\kappa$ for any $l \in 2\mathbb{Z}+1$ it undergoes a saddle-node bifurcation at $K = -1/\tau$ with K defined as above.*

PROOF. As it was mentioned above, under conditions (4.2.10) an eigenvalue crosses the imaginary axis with vanishing imaginary part. So the observed bifurcations can either be transcritical or fold. In a saddle-node bifurcation two new solutions emerge. This happens exactly when the right hand side in (4.2.3) crosses the identity (see Fig. 4.2.1 (a)), which is equivalent to

$$\begin{aligned} 1 &= \frac{\partial}{\partial\Omega}\left[\omega - \kappa\sin(\Omega\tau)\right] \\ &= -\tau\kappa\cos(\Omega\tau) = -\tau K. \end{aligned}$$

This condition also shows that at $K = 0$ no other solution emerges. Therefore, the bifurcation at $K = 0$ is transcritical. A straightforward calculation shows that the eigenvalues cross the imaginary axis with nonzero speed indeed. □

Fig. 4.2.2 shows the obtained bifurcation diagram for synchronous solutions, including the stability of the corresponding solutions. Here we used that for $\tau = 0$ we have $K = \kappa > 0$, so the synchronous state is stable. For the other solutions on the branch the stability can then be inferred by the order of the bifurcations. A remarkable feature is that with increasing τ, the two bifurcations, transcritical and fold, are converging towards each other.

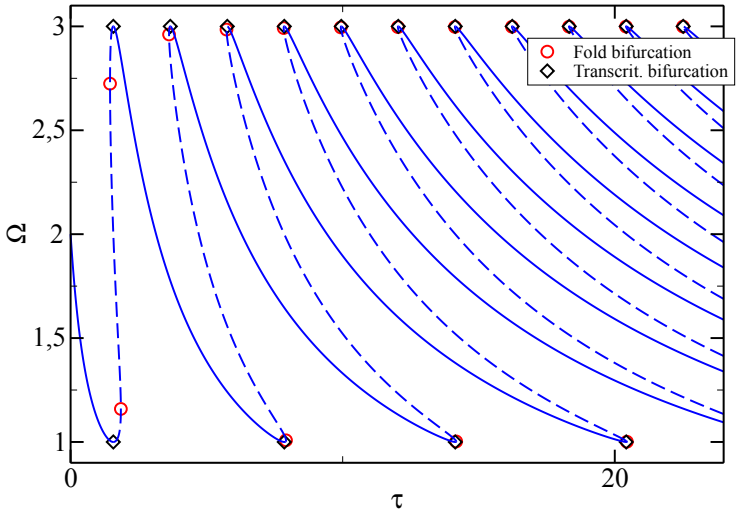

FIGURE 4.2.2. Bifurcation diagram for synchronous solutions (4.2.2). The frequency Ω is plotted versus the time delay τ. Dotted lines represent unstable and plain lines stable solutions. The parameters are $\omega = 2$ and $\kappa = 1$.

4.3. Pattern recognition

In this section we present the idea of how pattern recognition can be realized with the ring of delay coupled oscillators. We have seen in the previous section that system (4.2.1) admits coexisting synchronous solutions $x_j^i(t) = \Omega_i t$ with frequencies $\{\Omega_i\}_{i\in I} \subset (\omega - \kappa, \omega + \kappa)$ given by Eq. (4.2.3). In analogy with the firing times of neuronal systems **[64, 30]** we pay special attention to the moments when an oscillator $x_j^i(t)$ reaches the boundary of the periodic domain $[0, 2\pi]$, i.e. $x_j(t_j) = 2\pi$. This choice of phase is arbitrary, and any other phase φ_* instead of 2π can be chosen **[143]**. In what follows, we will use the obtained crossing time sequences t_j to represent patterns. In section 4.3.1 we explain how a given pattern can be encoded in a ring of phase oscillators, see Fig. 4.3.1. Afterwards, in section 4.3.2 we explain the dynamic recognition process.

4.3.1. Encoding. The idea for encoding a pattern in a ring of delay coupled oscillators is based on a time shift transformation **[190, 142]**. We shortly describe it here and refer to chapter 5 for a detailed description. We assume that a pattern $\boldsymbol{P}$ is represented by some N-dimensional vector $\boldsymbol{P} = (p_1, p_2, ..., p_N) \in \mathbb{R}^N$. First, let us choose an Ω_i that corresponds to a stable synchronous solution of (4.2.1). The timeshift transformation

$$y_j(t) = x_j(t - p_j) \tag{4.3.1}$$

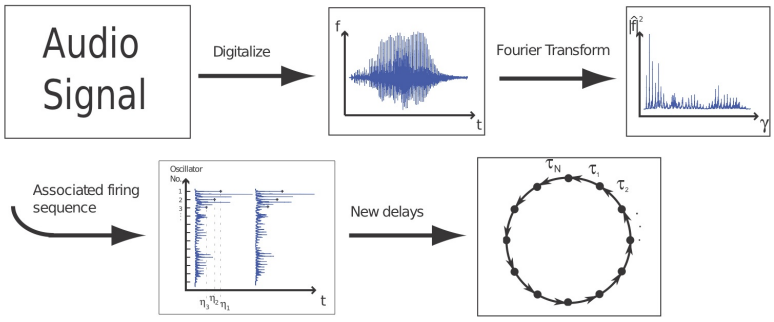

FIGURE 4.3.1. The process chart visualizes the encoding mechanism. Step one is the recording and digitalization of a given stimulus. The second step is not mandatory for pattern encoding. However, we employ it in this section as it yields better results. It consists of a fast Fourier transformation (FFT) of the recorded stimulus. Then, a firing sequence P is associated to the Fourier transform such that each value of the FFT's square modulus is identified with the firing time of an element of the ring. The last step is calculating the coupling delays in the ring according to (4.3.3), so the resulting dynamical system admits the firing sequence P as a stable solution.

converts (4.2.1) to the system

$$\dot{y}_j(t) = \omega + \kappa \sin\left(y_{j+1}(t-\tau_j) - y_j(t)\right), \tag{4.3.2}$$

which has the same form as (4.2.1) except that the new delays

$$\tau_j := \tau - (p_{j+1} - p_j) \tag{4.3.3}$$

are non-identical. Here we assume that $\tau_j \geq 0$, which is always possible by taking τ sufficiently large. Under the transformation (4.3.1), the synchronous state $x_j(t) = \Omega_i t$ transforms into the solution

$$y_j(t) = \Omega_i \cdot (t - p_j)$$

of system (4.3.2). The stability properties of this solution are also preserved as will be shown in chapter 5. Thus, in the system with non-homogeneous delays (4.3.2), an oscillator j crosses the phase 2π at times $p_j, p_j + \frac{2\pi}{\Omega_i}, \ldots$. Consequently, changing the delays $\tau \mapsto \tau_j$ yields the new system (4.3.2) which exhibits exactly the required crossing sequence $\boldsymbol{P}$ as a stable periodic solution. In particular, the encoding is not a dynamic process but simply consists of the calculation of the N delays τ_j.

4.3.2. Recognition. Now suppose $\boldsymbol{P}$ is encoded as described above. Let

$$\boldsymbol{Q} = \boldsymbol{P} + (\delta_1, \delta_2, ..., \delta_N)$$

be a perturbed version of pattern $\boldsymbol{P}$ that is to be recognized. We associate an initial function for system (4.3.2) in a natural manner

$$\boldsymbol{y}^0(t) = \Omega_i \cdot (t - q_1, t - q_2, ..., t - q_N).$$

So for $\delta_i = 0$ it corresponds to the synchronous state $\Omega_i t$ itself in transformed coordinates. Then, the recognition task consists of deciding whether $\boldsymbol{Q}$ is recognized as the previously encoded pattern $\boldsymbol{P}$. In order to do so we start system (4.3.2) with the initial function y^0 associated to $\boldsymbol{Q}$ and stop after a fixed time T. Then some measure of similarity between $\Phi_T(\boldsymbol{Q})$, which is $\boldsymbol{Q}$ evolved under the flow of (4.3.2), and $\boldsymbol{P}$ is considered to decide whether $\boldsymbol{Q}$ should be recognized as $\boldsymbol{P}$. To specify the measure of similarity employed here, consider the following straightforward calculation. Transformed back in original coordinates the initial function $\boldsymbol{y}^0$ reads

$$\begin{aligned} x_j^0(t) &= y_j^0(t + p_j) \\ &= \Omega_i(t + p_j - q_j) \\ &= \Omega_i(t - \delta_j). \end{aligned}$$

This means that solving system (4.3.2) with initial function y^0 (corresponding to $\boldsymbol{Q}$) is equivalent to solving the original system (4.2.1) with initial function $x_j^0(t)$ (corresponding to $\boldsymbol{\Delta} = (\delta_1, \delta_2, ..., \delta_N)$). In other words, pattern $\boldsymbol{Q}$ is recognized as version of $\boldsymbol{P}$ if the orbit with initial function $x_j^0(t)$ corresponding to $\boldsymbol{Q}$ converges fast enough to the synchronous state with frequency Ω_i (where "fast enough" has to be quantified in a specific situation). Consequently, we can use the order parameter $r(t) = \sum_{j=1}^{N} \left| e^{i\Phi_t(x^0)} \right|$ as measure of similarity (see Def.2).

The computation of the delays as described above is comparable to the computation of the weights in the learning phase of the Hopfield model. It constitutes the main step of the learning phase. Furthermore, the time T after which we stop simulation of the differential equations and a threshold for the order parameter that lets us decide whether the flow after time T is close enough to the synchronous state, that is whether the pattern is recognized or not are important parameters which can be chosen in the learning phase as well. They compare to the number of iterations and the threshold θ in the Hopfield model. We remark that the capacity of this method is of order $\mathcal{O}(N)$, in comparison to the order $\mathcal{O}(N/\log(N))$ of the Hopfield's model. Another advantage is that, unlike in the Hopfield model, patterns which are not corrupted by noise are recognized immediately, because synchronous motions in Eq. (4.2.1) and their transformed counterparts in (4.3.2) are invariant.

4.4. Numerical results

In this section we present numerical results for pattern recognition. An important quantity for the mechanism is the size and shape of the basin of attraction of the stable periodic solution representing the encoded pattern,

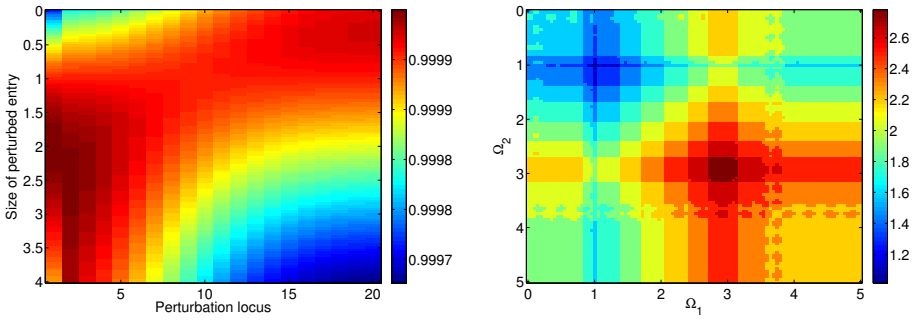

FIGURE 4.4.1. (a) Encoded pattern $(2, 1, ..., 1)$. Initial values are $\boldsymbol{P} + \boldsymbol{Q}_j$ with $\boldsymbol{Q}_j = (0, ..., 0, \varepsilon, 0, ..., 0)$, where j determines the location and ε the size of the perturbation. Colour codes the order parameter measured after time $T = 900$. Parameters are $\tau = 3$, $\omega = 1$, $\kappa = 1$. (b) Visualization of attractor basins for two oscillators. The axis correspond to initial functions $(\Omega_1 t\mathbf{1}, \Omega_2 t\mathbf{1})$. Colour codes the frequency of synchronous motion at time $T = 50000$. Parameters are $\omega = 2$, $\kappa = 1$ and $\tau = 20$. For this value of τ we observe thirteen coexisting synchronous states of which seven are stable (see Fig. 4.2.2).

as the basin contains initial conditions (patterns) that are possibly identified with the encoded pattern (see Fig. 4.4.1 (b)). Obviously, we can not present a complete picture of the basins of attraction as the phase space of Eq. (4.2.1) is infinite dimensional. However, we will address some aspects of this question numerically in the following section. All simulations in this section are performed using an Euler method with step width 0.001 to solve the delay differential equations.

4.4.1. Recognition of artificial patterns. We start with a simple pattern $\boldsymbol{P} = (2, 1, ..., 1)$. Fig. 4.4.1 shows the order parameter after time $T = 90$ for initial values $\boldsymbol{P} + \boldsymbol{Q}_j$, where $\boldsymbol{Q}_j = (0, ..., 0, \varepsilon, 0, ..., 0)$. Here j determines the location and ε the size of the perturbation. We observe that, from a certain index j on, initial values $\boldsymbol{P} + \boldsymbol{Q}_j$ converge to the pattern with the same speed.

As a preparation for more complex audio signals we next investigate recognition of simple sine waves. The task is the following: Suppose two sine waves of different frequencies are encoded as two patterns $\boldsymbol{P}_1$ and $\boldsymbol{P}_2$. It is to decide whether a given third wave $\boldsymbol{Q}$ is recognized as either one of the two encoded sines. Here, we proceed as described in the flow chart Fig. 4.3.1. According to our scheme, the corresponding (fast) Fourier transforms $\boldsymbol{P}_1$ and $\boldsymbol{P}_2$ are the patterns associated with the signals. The use of Fourier transform has the following advantages: one can cut off the transformed signal above a certain frequency which can be seen as a simple denoising process and at the same time it accelerates the recognition process. Furthermore, for short

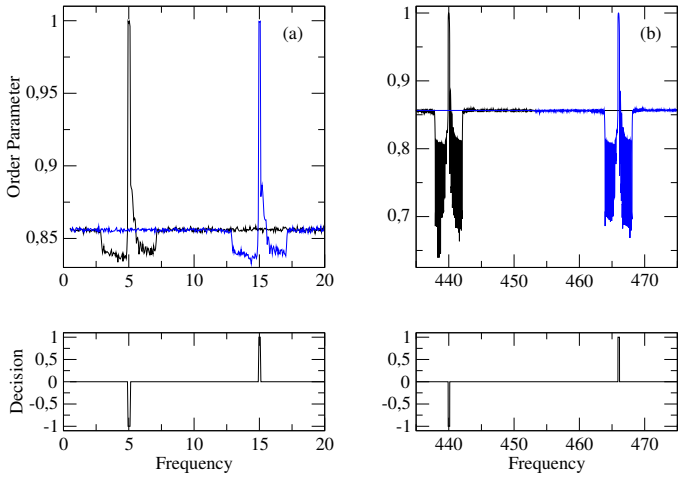

FIGURE 4.4.2. Pattern recognition with two encoded sine waves of frequencies 5Hz and 15Hz (a) and 440Hz and 466Hz (b). A third wave which is to be recognized is used as initial value for the system transformed according to the 5Hz and 15Hz patterns respectively (see flow chart 4.3.1). Upper plots show order parameters after time $T = 50$ for the different recognition processes. Parameters are $\tau = 3$, $\omega = 1$, $\kappa = 1$. Lower plots show decision of the PR device. -1 stands for "Pattern 1 is chosen", 1 for "Pattern 2 is chosen" and 0 for none.

enough time windows the time course of the signal is not important and the Fourier transform contains the main information independent of the signal's exact timing. The pattern associated to a sine wave of a fixed frequency f is a delta peak δ_f (in an ideal case without noise). It is evident that the error tolerance does not depend on the absolute value of the frequency f but rather on the frequency difference of the perturbation and the pattern to be identified.

Fig. 4.4.2 shows the results of two different recognition processes. In the first recognition (a) two sine waves of 5Hz and 15Hz are encoded. Again, the recognition process consists of deciding whether a third given sine wave is recognized as either one. It can be seen in the lower left plot that the 5Hz and the 15Hz wave are recognized with an error tolerance of ± 0.1Hz. The same results hold for recognition of the standard pitch A (440Hz) and one semitone higher ($\sim$466Hz) (Fig. 4.4.2 (b)). In both cases the order parameter is measured after time $T = 50$ which corresponds to $\sim$17 times the delay time $\tau = 3$. So the recognition is still relatively fast.

4.4.2. Speech Recognition. In this section, we use the model for speech recognition. As in the previous section for sine waves, the original audio recording is first transformed with the fast Fourier transform (This is done to circumvent that two identical signals with different timing are not recognized

as the same). The modulus vector is then taken as pattern which can be encoded by computing the delays as described in section 4.3. The original audio signals are the numbers from one to ten, recorded in German and spoken by two different voices (male and female), each in three takes. So in total, it is a set of 60 audio tracks. We emphasize that the audio tracks are recorded with a simple audio interface. Consequently, they are corrupted with noise yielding a SNR around 20dB. In the training phase we calculated the delays and set the parameters to $\omega = 1$, $\kappa = 1$, $\tau = 3$, and $T = 25$. In this setting, the system admits one stable synchronous orbit. This means all initial conditions eventually converge to this solution, so the recognition process depends on the rate of convergence towards the synchronous orbit: the faster the converge is, the more probable it is, that it is recognized as being this pattern. After the training phase we performed random recognition runs in the following way. First we encoded two recordings of two randomly chosen different numbers between one and ten. For the recognition we randomly chose one of the four remaining recordings that coincide with one of the two encoded numbers. Of these random runs we performed one thousand with a success rate of around $75\backslash\%$. The relatively low success rate partially has its origin in the very similar frequency spectrum of the German numbers 1,2 and 3. Excluding two of these yields success rates of around $85\backslash\%$.

4.5. Discussion

In this chapter, we have presented a detailed analysis of the synchronous solutions in a ring of coupled phase oscillators. We have shown that the introduction of time delays in the coupling leads to coexistence of multiple periodic synchronous solutions with different frequencies. Particularly, the number of stable periodic orbits can be controlled and chosen arbitrarily high by increasing the delay. Their frequencies, bounded from below and above by $\omega - \kappa$ and $\omega + \kappa$ respectively, can be easily determined numerically by solving the transcendent Eq. (4.2.3). Furthermore, we have found a simple stability criterion and described the bifurcations when increasing the delay. More precisely, we have seen that a branch of synchronous solutions alternately undergoes transcritical and saddle-node bifurcations. For future investigations it would certainly be interesting to look for modulated wave solutions which are known to bifurcate from rotating waves in systems with rotational symmetry [**156, 157**].

The subsequent sections were dedicated to give an evidence that a ring of delay coupled oscillators can be used for information processing purposes. Here, in contrast to other models, the encoding of patterns is computationally efficient. For a signal of length N it just consists of N point operations, the calculation of the new delays, in contrast to the Hopfield model which requires the computation of N^2 coupling weights. This results in the higher capacity N in comparison to a capacity of order $\mathcal{O}(N/\log(N))$ in the Hopfield model.

Furthermore, not only boolean patterns but arbitrary patterns can be encoded. Using the results from section 4.2, the model can be controlled easily and parameters can be tuned suited to the application on hand.

Results from section 4.4 show that the model can be used as a reliable device for simple artificial pattern recognition as well as for single word speech recognition. We remark that a downside of the model consists in the infinite dimensional phase space which makes both, analytic investigations and numerical simulations more demanding than for iterations in finite dimensional spaces as in the case of the Hopfield model.

The aim of sections 4.3 and 4.4 was to introduce the main ideas for a new approach to pattern recognition to show the model's potential capability for information processing. Consequently, there are still open questions and paths for future research. For example, in section 4.2 it was shown that for larger values of the delay τ the model possesses a large number of coexisting stable periodic orbits. This fact could possibly be exploited further. Furthermore, one could even think of coupling different rings representing different classes to yield a single object representing a composite of classes. Also, as in standard recognition models such as the Hopfield model, the basins of attractions play an essential role for the functioning of the method. We have explored the basins of synchronous solutions in the DDE numerically. We believe that it is not only a mathematically interesting problem, but also the model would greatly benefit from a more detailed description of the basins of attraction.

CHAPTER 5

Parameter Space Reduction in Networks of Delay Coupled Elements

"Delay is preferable to error."
T. Jefferson

5.1. Introduction

In the previous chapter we introduced a transformation which shifts the time individually for each node of a network with delayed couplings. Here, we will investigate properties and invariants of this transformation in a very general setting. In general, differential equations with time delays have been subject of intensive mathematical research in the last decades. Recently, major impulses for theoretical investigations came from the challenge of understanding and modelling the human brain [**91, 69, 42**]. Here, time delays appear due to the finite speed of action potentials propagating through axons [**118, 185, 27**]. It was observed that the qualitative behaviour of brain networks is closely related to their heterogeneous delay distributions. These were shown to play important roles in phenomena such as coherence in the resting state activity [**42, 69**], nonstationary bifurcations of equilibria [**8**] and enhanced synchronizability [**55, 43**]. Further examples of delay-coupled systems are interacting lasers where delays appear due to the finite speed of light travelling through optical fibres [**187, 54, 164**]. In population dynamics, delays correspond to maturing and gesturing times [**100**], and in gene regulatory networks, delays represent the time the system needs to produce a protein [**111, 40**]. Thus, delays are often included in order to account for the time a signal needs to propagate from one node of the network to another or for the processing time that it takes to emit a response to some input. An inevitable property of real networks of interacting systems with delays is that, generically, each delay time is different from any other.

Nevertheless, there exist comparatively few attempts to study systems with several different delays analytically. An important reason for this is that their analysis is usually much harder than for identical delays and techniques available for systems with one delay are in general not applicable in the case of multiple delays. In particular, the analysis of spectra of solutions becomes more complicated since the characteristic quasi-polynomials involve several

exponential terms [**15, 72**]. At least for coupled systems with two different delays some analytical results are available. For instance, Nussbaum [**131**] proved the existence of periodic solutions in a system with two commensurable delays. Moreover some detailed studies on bifurcations in coupled systems with two different delay times were conducted [**14, 29, 159, 28, 71**]. In particular, we mention Shayer et al. [**159**], where the investigation initially assumes three different delays. In the course of the investigation, the authors discover that the stability of a steady state depends only on two values combined from these delays. This finding is a special case of the more general result that we present in this chapter. Higher order scalar systems with two delays are considered, e.g., by Gu et al. [**70**], who study stability crossing curves for this system. For the same system, Ruan and Wei [**154**] refine techniques for the determination of the roots of characteristic quasi-polynomials of single delay equations to treat the case of two delays. Yanchuk and Giacomelli [**188**] consider a scalar system with two large delays and show that this system can be described by a complex Ginzburg-Landau equation in the neighbourhood of an equilibrium. Finally, we want to mention studies of Hopfield neural networks with delayed connections where many different delays are taken into account [**68, 192, 174, 113**]. Here, the primary object of investigation is sufficient conditions for global convergence of the system towards a single steady state in order to obtain a well-defined method of input classification.

In this chapter, the focus of our interest is a componentwise timeshift transformation (CTT) which allows to change the interaction delays while the dynamical properties of the system remain the same. Apart of providing an intuition about the functionality of delays, the transformation proves to be particularly useful in cases where it is possible to achieve a smaller or in some sense preferable set of delays in the transformed system. This is especially apparent for the case when the nodes are coupled in a single unidirectional ring as in the previous chapter. The corresponding special case of the CTT was also utilized more or less explicitly in [**9, 117, 138, 142**]. Therefore, let us illustrate the CTT for this example. In a general form, a ring of N unidirectionally delay-coupled systems can be written as

$$\frac{\mathrm{d}}{\mathrm{dt}}x_j(t) = f_j\left(x_j(t), x_{j-1}(t-\tau_{j-1})\right),\ j = 1, ..., N, \tag{5.1.1}$$

where j is considered modulo N and $\tau_j \geq 0$ are N possibly different delays. Given a solution $x_j(t)$, $j = 1, ..., N$, we introduce new variables

$$y_j\left(t\right) := x_j\left(t + \eta_j\right), \tag{5.1.2}$$

by shifting the nodes independently in time by certain amounts $\eta_j \geq 0$. Formally, we find that the dynamics of the variables $y_j(t)$ obey

$$\frac{\mathrm{d}}{\mathrm{dt}}y_j(t) = f_j\left(y_j(t), y_{j-1}(t-\tilde{\tau}_{j-1})\right),\ j = 1, ..., N, \tag{5.1.3}$$

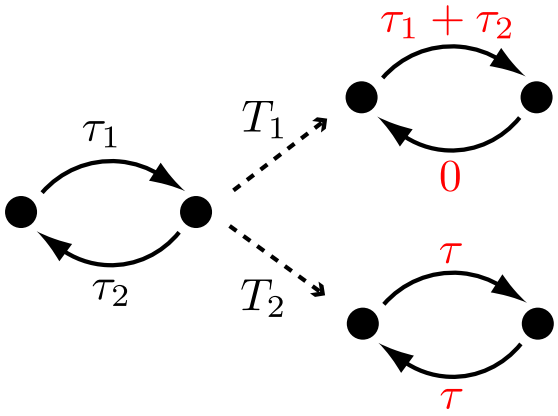

FIGURE 5.1.1. Two simple examples of CT-Transformations for a ring of two delay-coupled systems. The transformation T_1 reduces the number of delays from two to one and T_2 reveals a hidden symmetry in the system by adjusting the two delays to the same value $\tau = (\tau_1 + \tau_2)/2$.

with new delays $\tilde{\tau}_j = \tau_j + \eta_j - \eta_{j+1}$. In other words, finding timeshifts η_j for given delays $\tilde{\tau}_j$ is equivalent to solving a system of linear equations.

For the case of a ring with only two nodes, which is depicted in Fig. 5.1.1, we illustrate the possible effect of the timeshift (5.1.2) in Fig. 5.1.2. The plots (a)–(c) show an initial piece of a solution and its change under the CTT (two delay-coupled Mackey-Glass systems **[116]** were used to create this example). The process of transformation is indicated by the symbols T and $\tilde{T}$, which are given a precise meaning in section 5.4. Each transformation corresponds to a particular choice of the timeshifts in (5.1.2). Here, T converts (5.1.1) to (5.1.3) and $\tilde{T}$ describes the reverse transformation from (5.1.3) to (5.1.1). In (a) and (c), the arrows between the timetraces of both components indicate the delayed dependence of $\dot{x}_1(t)$ on $x_2(t-\tau_2)$ and $\dot{x}_1(t)$ on $x_2(t-\tau_2)$, similar in (b) for y_1 and y_2 for the transformed delays $\tilde{\tau}_1$ and $\tilde{\tau}_2$. From (5.1.2) it follows that the timetraces of the single components have exactly the same form in both systems. Both solutions only differ in the relative timeshifts between their components.

Baldi and Atiya **[9]** discovered that by choosing timeshifts $\eta_j = \sum_{k=1}^{j-1} \tau_k$ one obtains the transformed delays

$$\tilde{\tau}_j = \begin{cases} 0, & \text{for } 1 \le j \le N-1, \\ \sum_{k=1}^{N} \tau_k, & \text{for } j = N. \end{cases} \tag{5.1.4}$$

They used this simplified form to predict oscillatory behaviour and bifurcations for a neural circuit exhibiting delayed excitatory and inhibitory connections. Mallet-Paret **[117]** utilized the same transformation to prove a Poincaré-Bendixson Theorem for monotone cyclic feedback systems with delays. A

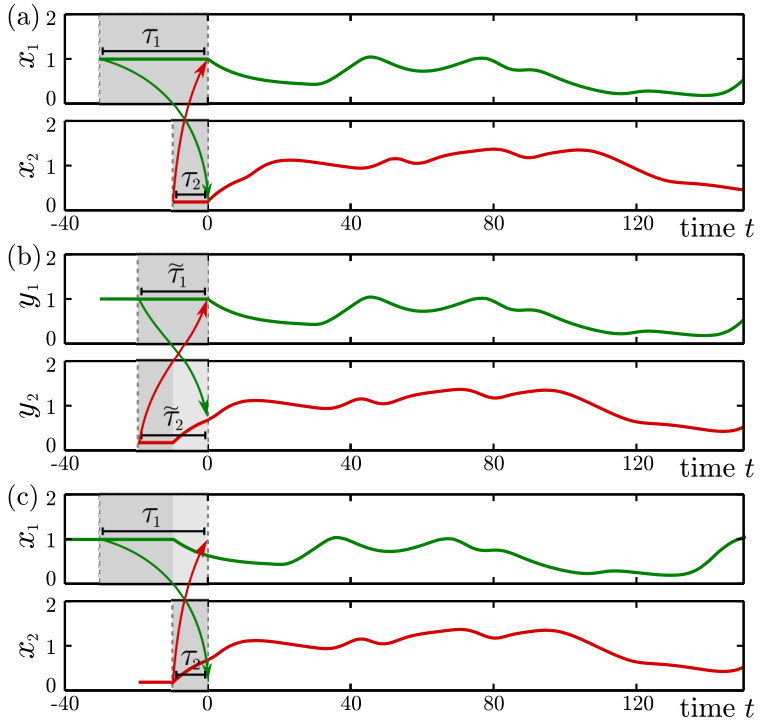

FIGURE 5.1.2. CT-Transformation for a pair of bidirectionally coupled Mackey-Glass systems **[116]**, cf. Fig.5.1.1. Plot (a) shows the original solution $\boldsymbol{x}(t) = (x_1(t), x_2(t))$ of (5.2.1). Plot (b) shows the transformed solution $\boldsymbol{y}(t) = (y_1(t), y_2(t))$ of (5.2.2}), which is shifted to the left by amounts $\eta_1 = 0$ and $\eta_2 = 10$. Plot (c) shows the solution $\boldsymbol{x}(t + \eta_1)$ obtained after a reverse transformation of $\boldsymbol{y}(t)$ (see section 5.4 for details).

slightly different set of timeshifts can be found in **[138]** and **[142]**, where the choice $\eta_j = (N - j)\bar{\tau} + \sum_{k=1}^{j} \tau_k$, with the mean delay $\bar{\tau} = \frac{1}{N}\sum_k \tau_k$, was proposed. This leads to identical transformed delays

$$\tilde{\tau}_j \equiv \bar{\tau}. \tag{5.1.5}$$

For a ring of identical nodes, i.e. $f_j \equiv f$ for all j, it turns out that the obtained system is much more tractable due to its rotational symmetry. One may say that this hitherto hidden symmetry was revealed by the CTT. See also Fig.5.1.1 for an illustration of the two above mentioned timeshifts in a ring of two nodes.

For both variants, (5.1.4) and (5.1.5), it is evident that if one is interested in the changes of dynamic behaviour with respect to the different delays τ_j it suffices to vary a single parameter, i.e. the mean delay $\bar{\tau} = \frac{1}{N}\sum_k \tau_k$, instead of the N different parameters τ_j, $j = 1, ..., N$. In other words, the parameter space dimension is much smaller than it might have appeared at first glance.

Similar as for a ring, the CTT allows to identify a canonical set of delay parameters in a general network as we explain in section 5.5.

Before doing so let us pose a question. What does the knowledge about dynamical features of the transformed system (5.1.3) really tell us about the dynamical features of the original system (5.1.1)? It might seem intuitive that they are the same since the timeshift $y_j(t) \mapsto y_j(t-\eta_j)$ inverses (5.1.2). This is true for the particular solution (5.1.2) but, in general, the expression $y_j(t-\eta_j)$ (with $\eta_j > 0$) may not be defined at all. This is because, in general, solutions of delay differential equations (DDEs) cannot be continued backwards. Another subtlety arises if one considers timeshifts η_j leading to anticipating arguments, that is negative delays. In this case (5.1.3) has fundamentally different properties from an ordinary DDE with positive delays. For instance, initial value problems are ill-posed in general **[72]**. Even though we will restrict ourselves to the situation where transformed delays are positive, a proper treatment of the above question should introduce state spaces and flows to formulate and compare the dynamical properties of the original and the transformed system. Such a rigorous treatment of the CTT was not given in any of the above mentioned works **[9, 117, 138, 142]**. We will do this in a quite general setting using semidynamical systems in section5.4 where we also give a rigorous definition of the CTT. In particular, the structural similarity of the state spaces and the stability of invariant sets is studied. In section 5.2 we introduce notations to describe general networks of delay coupled dynamical systems and in section 5.3 we study the special cases of equilibria and periodic orbits of DDEs in which case the equivalence of the dynamics of the original and the transformed system is relatively easy to show.

5.2. Networks of delay coupled dynamical systems

To describe a general network of N coupled systems we choose a framework which enables us to account for multiple links between two nodes holding different delays. That is, the coupling structure of the network is assumed to be represented by a multidigraph. This is a set of node indices, $\mathcal{N} = \{1, ..., N\}$, and a set $\mathcal{E}$ of directed links. Throughout the whole chapter we assume that $(\mathcal{N}, \mathcal{E})$ is weakly connected (see 4). We recall that this means that each node can be reached from any other node by traversing a sequence of links, where each link may be traversed in arbitrary direction. For networks with several connected components our results can be applied separately to each component. For each link $\ell \in \mathcal{E}$ the functions $s, t : \mathcal{E} \to \mathcal{N}$ assign its source $s(\ell)$ and its target $t(\ell)$. This means that the link ℓ connects the node $x_{s(\ell)}$ to the node $x_{t(\ell)}$. The delay time of ℓ is denoted by $\tau(\ell)$. Note that there may indeed exist two links ℓ_1 and ℓ_2 in $\mathcal{E}$ with $s(\ell_1) = s(\ell_2)$ and $t(\ell_1) = t(\ell_2)$ but $\tau(\ell_1) \neq \tau(\ell_2)$. For node x_j, we introduce the set of its incoming links as

$$I_j = \{\ell \in \mathcal{E} : t(\ell) = j\}.$$

Then, the dynamics of x_j can be written as

$$\frac{\mathrm{d}}{\mathrm{dt}}x_j(t) = f_j\left(\left(x_{s(\ell)}\left(t-\tau\left(\ell\right)\right)\right)_{\ell\in I_j}\right) \in \mathbb{R},\ j=1,...,N, \tag{5.2.1}$$

where we assume $x_j(t) \in \mathbb{R}$ without loss of generality. This notation allows to include a self-dependency of $x_j(t)$ via a link ℓ with $s(\ell) = t(\ell) = j$. It is also possible to have an instantaneous dependence by setting $\tau(\ell) = 0$. For (5.2.1), the introduction of new variables $y_j(t)$ as in (5.1.2) leads to the transformed system

$$\frac{\mathrm{d}}{\mathrm{dt}}y_j(t) = f_j\left(\left(y_{s(\ell)}\left(t-\tilde{\tau}\left(\ell\right)\right)\right)_{\ell\in I_j}\right),\ j=1,...,N, \tag{5.2.2}$$

with modified delays

$$\tilde{\tau}\left(\ell\right) = \tau\left(\ell\right) - \eta_{t(\ell)} + \eta_{s(\ell)}. \tag{5.2.3}$$

5.3. Spectrum of equilibria and periodic orbits

An equilibrium point $\bar{\boldsymbol{x}} = (\bar{x}_1,...,\bar{x}_N) \in \mathbb{R}^N$ of (5.2.1) is a point which satisfies

$$f_j\left(\left(\bar{x}_{s(\ell)}\right)_{\ell\in I_j}\right) = 0,\ j=1,...,N. \tag{5.3.1}$$

Obviously $\bar{\boldsymbol{x}}$ is also an equilibrium of (5.2.2). In the following we assume that $f_j \in C^1$. Then a characteristic exponent λ of $\bar{\boldsymbol{x}}$ in (5.2.1) corresponds to an exponential solution $\boldsymbol{\xi}\left(t\right) = e^{\lambda t}\boldsymbol{\xi}_0 \in \mathbb{C}^N$ of the variational equation

$$\frac{\mathrm{d}}{\mathrm{dt}}\xi_j\left(t\right) = \sum_{\ell\in I_j}\partial_{s(\ell)}f_j\left(\left(\bar{x}_{s(\ell')}\right)_{\ell'\in I_j}\right)\xi_{s(\ell)}\left(t-\tau\left(\ell\right)\right). \tag{5.3.2}$$

If all of the characteristic exponents of $\bar{\boldsymbol{x}}$ possess negative real parts this assures that $\bar{\boldsymbol{x}}$ is stable, if at least one has positive real part then $\bar{\boldsymbol{x}}$ is unstable [**72**]. In the transformed system (5.2.2) the timeshifted variation $\boldsymbol{\chi}\left(t\right)$, given by $\chi_j\left(t\right) = \xi_j\left(t+\eta_j\right)$, is a solution of the corresponding variational equation of $\bar{\boldsymbol{x}}$

$$\frac{\mathrm{d}}{\mathrm{dt}}\chi_j\left(t\right) = \sum_{\ell\in I_j}\partial_{s(\ell)}f_j\left(\left(\bar{x}_{s(\ell')}\right)_{\ell'\in I_j}\right)\chi_{s(\ell)}\left(t-\tilde{\tau}\left(\ell\right)\right). \tag{5.3.3}$$

Hence, the characteristic exponents of $\bar{\boldsymbol{x}}$ are the same in (5.2.1) and (5.2.2).

Similarly, the stability of a periodic solution $\bar{\boldsymbol{x}}\left(t\right) = \bar{\boldsymbol{x}}\left(t+T\right)$ is determined by its Floquet exponents if their real parts are different from zero. Each exponent λ corresponds to a solution $\boldsymbol{\xi}\left(t\right)$ of the variational equation

$$\frac{\mathrm{d}}{\mathrm{dt}}\xi_j\left(t\right) = \sum_{\ell\in I_j}\partial_{s(\ell)}f_j\left(\left(\bar{x}_{s(\ell')}\left(t-\tau\left(\ell'\right)\right)\right)_{\ell'\in I_j}\right)\xi_{s(\ell)}\left(t-\tau\left(\ell\right)\right) \tag{5.3.4}$$

which has the form $\boldsymbol{\xi}(t) = e^{\lambda t}\boldsymbol{p}(t)$ with a periodic function $\boldsymbol{p}(t) = \boldsymbol{p}(t+T)$. Again, the timeshifted solution $\boldsymbol{\chi}(t)$ with $\chi_j(t) = \xi_j(t+\eta_j)$ fulfils the variational equation

$$\frac{\mathrm{d}}{\mathrm{dt}}\chi_j(t) = \sum_{\ell\in I_j} \partial_{s(\ell)} f_j\left(\left(\bar{y}_{s(\ell')}\left(t-\tilde{\tau}\left(\ell'\right)\right)\right)_{\ell'\in I_j}\right)\chi_{s(\ell)}\left(t-\tilde{\tau}(\ell)\right) \tag{5.3.5}$$

of the corresponding periodic solution $\bar{y}_j(t) = \bar{x}_j(t+\eta_j)$ in the transformed system. Let us summarize this section in a theorem:

THEOREM 25. *The following statements hold true:*
(i) A fixed point $\bar{\boldsymbol{x}}$ possesses the same characteristic exponents in Eq. (5.2.1) and Eq. (5.2.2).
(ii) A periodic solution $\bar{\boldsymbol{x}}(t)$ possesses the same Floquet exponents in Eq. (5.2.1) as the corresponding transformed solution $\bar{\boldsymbol{y}}(t)$ of Eq. (5.2.2).

5.4. The componentwise timeshift transformation

5.4.1. Definitions. In this section we introduce a rigorous formulation of the idea which underlies the change of variables (5.1.2). We define the CTT in terms of the underlying infinite dimensional phase spaces of (5.2.1) and (5.2.2).

First recall that a semidynamical system (or a semiflow) is a mapping

$$\begin{aligned}\Phi : [0,\infty)\times X &\to X,\\ (t,\boldsymbol{x}) &\mapsto \Phi_t(\boldsymbol{x}),\end{aligned}$$

on a Banach space X which fulfils:

(i) $\Phi_0 = Id$
(ii) $\Phi_{t+s} = \Phi_t \circ \Phi_s$, $\forall t, s \geq 0$
(iii) $\Phi_t : X \to X$ is continuous for all $t \geq 0$.

The state spaces for DDEs contain segments of functions, which represent the history of the solution curve $\boldsymbol{x}(t)$. For instance, in Fig.5.1.2 the shaded part of the timetrace in (a) corresponds to the initial segment of the depicted solution. For the original system (5.2.1), we choose the state space to be

$$\mathcal{C} = \prod_{j=1}^{N} C\left([-r_j, 0]\,;\,\mathbb{R}\right),\ r_j = \max_{\ell\in O_j}\tau(\ell),$$

where $O_j = \{\ell \in \mathcal{E} :\ s(\ell) = j\}$ is the set of all outgoing links from the j-th node. Hence, the value r_j is the largest delay time on outgoing links of the node j. This definition ensures, that the history for the j-th component is available for all delayed arguments appearing on the right hand side of (5.2.1). Similarly, we choose

$$\tilde{\mathcal{C}} = \prod_{j=1}^{N} C\left([-\tilde{r}_j, 0]\,;\,\mathbb{R}\right),\ \tilde{r}_j = \max_{\ell\in O_j}\tilde{\tau}(\ell)$$

as state space for the transformed system (5.2.2). Assuming that solutions exist for all future times (e.g. if f_j are Lipschitz continuous), there exist semiflows

$$\Phi : [0,\infty) \times \mathcal{C} \to \mathcal{C}, \qquad (t, \boldsymbol{x}) \mapsto \Phi_t(\boldsymbol{x}),$$
$$\Psi : [0,\infty) \times \tilde{\mathcal{C}} \to \tilde{\mathcal{C}}, \qquad (t, \boldsymbol{y}) \mapsto \Psi_t(\boldsymbol{y}),$$

for (5.2.1) and (5.2.2). Now let us formulate (5.1.2) as a state space transformation $T : \mathcal{C} \to \tilde{\mathcal{C}}$. We define T componentwise for $j = 1, ..., N$, and pointwise for $\boldsymbol{x}_0 \in \mathcal{C}$ and $t \in [-\tilde{r}_j, 0]$, as

$$T_j[\boldsymbol{x}_0](t) = \begin{cases} [\boldsymbol{x}_0(t+\eta_j)]_j, & \text{for } t \in [-\tilde{r}_j, -\eta_j], \\ \left[\Phi_{t+\eta_j}(\boldsymbol{x}_0)\right]_j(0), & \text{for } t \in [-\min\{\eta_j, \tilde{r}_j\}, 0]. \end{cases} \tag{5.4.1}$$

For illustration see Fig.5.1.2(b), where the shading marks the segment $\boldsymbol{y}_0 = T[\boldsymbol{x}_0]$ for the initial segment $\boldsymbol{x}_0$ indicated in (a). The lighter shading indicates the part defined by the second case of (5.4.1). Let us show that (5.4.1) is well-defined. For this we need to assure that $\boldsymbol{y}_0 = T[\boldsymbol{x}_0] \in \tilde{\mathcal{C}}$. This only requires that the term $[\boldsymbol{x}_0(t-\eta_j)]_j$ appearing in (5.4.1) is defined for all $t + \eta_j$ with $t \in [-\tilde{r}_j, -\eta_j]$. For the case in which $[-\tilde{r}_j, -\eta_j]$ is non-empty, this is equivalent to $t+\eta_j \geq -r_j$ for all $t \in [-\tilde{r}_j, -\eta_j]$. In order to show this, choose a link $\ell \in O_j$ with maximal delay $\tilde{\tau}(\ell) = \tilde{r}_j$. Then,

$$r_j - \tilde{r}_j \geq \tau(\ell) - \tilde{\tau}(\ell) = \tau(\ell') - \left(\tau(\ell') - \eta_{t(\ell')} + \eta_j\right) \geq -\eta_j.$$

Therefore, $t+\eta_j \geq -\tilde{r}_j+\eta_j \geq -r_j$ for $t \in [-\tilde{r}_j, -\eta_j]$ and (5.4.1) is well-defined.

Furthermore, one easily checks that

$$T \circ \Phi_t = \Psi_t \circ T, \text{ for all } t \geq 0. \tag{5.4.2}$$

That is, T transforms solutions of (5.2.1) into solutions of (5.2.2). As inherited from the semiflow Φ, the transformation T is neither injective nor surjective in general. Therefore, one cannot expect a dynamical equivalence of (5.2.1) and (5.2.2) in the strict form of topological conjugacy, i.e. $\Psi = h \circ \Phi \circ h^{-1}$ for some homeomorphism h. Moreover, since T is not surjective, (5.4.2) does not even signify that Ψ is properly semiconjugate to Φ. However, this "weak semiconjugacy" is mutual as we show in the following, and this fact implies a strong equivalence as well.

5.4.2. CT-equivalence. Let us find a reverse transformation from (5.2.2) to (5.2.1). It should transform $\tilde{\tau}(\ell)$ back to $\tau(\ell)$ which leads to the natural definition of reverse timeshifts

$$\tilde{\eta}_j = \bar{\eta} - \eta_j \geq 0, \text{ with } \bar{\eta} = \max_{1 \leq j \leq N} \eta_j.$$

Then, the reverse transformation $\tilde{T} : \tilde{\mathcal{C}} \to \mathcal{C}$ is given as

$$\tilde{T}_j[\boldsymbol{y}_0](t) = \begin{cases} \left(\Psi_{t+\tilde{\eta}_j}(\boldsymbol{y}_0)\right)_j(0), & t \in [-\min\{\tilde{\eta}_j, r_j\}, 0], \\ \left(\boldsymbol{y}_0(t+\tilde{\eta}_j)\right)_j(0), & t \in [-r_j, -\tilde{\eta}_j]. \end{cases} \tag{5.4.3}$$

Analogously to (5.4.2), we have

$$\tilde{T} \circ \Psi = \Phi \circ \tilde{T}, \tag{5.4.4}$$

and additionally T and $\tilde{T}$ are reverse in the sense that

$$\tilde{T} \circ T = \Phi_{\bar{\eta}} \quad \text{and} \quad T \circ \tilde{T} = \Psi_{\bar{\eta}}. \tag{5.4.5}$$

See, for example, Fig.5.1.2(c), where the shaded region indicates the initial segment $(\tilde{T} \circ T)[\boldsymbol{x}_0]$ of the solution $(\tilde{T} \circ T)[\boldsymbol{x}](t) = \boldsymbol{x}(t + \bar{\eta})$, with $\bar{\eta} = 10$. The lighter shaded region indicates where the second case of (5.4.3) takes effect.

The equations (5.4.2), (5.4.4) and (5.4.5) constitute a notion of equivalence which can be applied not only to semidynamical systems which stem from systems of DDEs, but as well to systems such as delay coupled PDEs or more generally to abstract evolution equations. Therefore we define in a more abstract fashion:

Definition 26. Two semidynamical systems $\Phi : [0, \infty) \times X \to X$ and $\Psi : [0, \infty) \times Y \to Y$ are called CT-equivalent if there exist mappings $T : X \to Y$, $\tilde{T} : Y \to X$ and $\bar{\eta} \geq 0$ such that

$$T \circ \tilde{T} = \Psi_{\bar{\eta}},\ T \circ \Phi_t = \Psi_t \circ T,$$
$$\tilde{T} \circ T = \Phi_{\bar{\eta}},\ \tilde{T} \circ \Psi_t = \Phi_t \circ \tilde{T}.$$

In the following, the analysis is carried out in the general setting on Banach spaces X and Y but we keep in mind that the results apply to the case of DDEs on the spaces $X = \mathcal{C}$ and $Y = \tilde{\mathcal{C}}$ as introduced above. We still use the term CT-equivalence for the general formulation though, since most probably the equivalent systems Φ and Ψ will in practice be connected by a transformation, which resembles (5.4.1).

5.4.3. Dynamical invariants of CT-equivalent semidynamical systems. In this section, we derive some properties of CT-equivalent systems in the sense of Definition 26. We show that their state spaces hold a structure of corresponding strongly invariant sets. Then, assuming that the CTTs T and $\tilde{T}$ are Lipschitz continuous, we prove that stability properties are preserved as well. For the DDE systems (5.2.1) and (5.2.2) this is the case if all f_j are Lipschitz continuous. Throughout, we assume that X and Y are Banach spaces. Before stating the main results of this section (Theorems 27 and 29), we give some definitions:

A set $A \subseteq X$ is called positively invariant under Φ if for any $t \geq 0$:

$$\Phi_t(A) \subseteq A.$$

$A \subseteq X$ is called invariant under Φ if for any $t \geq 0$:

$$\Phi_t(A) = A.$$

For any set $A \subseteq X$, we define its strongly invariant hull $H_\Phi(A)$ as the set

$$H_\Phi(A) := \{\boldsymbol{x} \in X \mid \exists t_1, t_2 \geq 0,\ \hat{\boldsymbol{x}} \in A :\ \Phi_{t_1}(\hat{\boldsymbol{x}}) = \Phi_{t_2}(\boldsymbol{x})\}.$$

A strongly invariant set $A \subseteq X$ is a set that coincides with its strongly invariant hull, i.e.

$$H_\Phi(A) = A.$$

The class of strongly invariant sets is denoted by

$$\operatorname{sis}(\Phi) = \{A \subseteq X \mid A = H_\Phi(A)\}.$$

Note that positive invariance is implied by both, invariance and strong invariance. But between invariance and strong invariance there holds no implication. Of course a strongly invariant set always contains a maximal invariant set which might be empty.

THEOREM 27. *Let $\Phi : [0,\infty) \times X \to X$ and $\Psi : [0,\infty) \times Y \to Y$ be CT-equivalent. Then,*
(i) for each (positively) Φ-invariant set $A \in X$, the set $T[A] \in Y$ is (positively) Ψ-invariant,
(ii) there is a one-to-one correspondence between (strongly) invariant sets of Φ and Ψ.

PROOF. Ad (i): Let A be positively invariant, $\boldsymbol{x} \in A$ and $\boldsymbol{y} = T[\boldsymbol{x}]$. Then, $\Psi_t(\boldsymbol{y}) = T[\Phi_t(\boldsymbol{x})] \in T[A]$. Hence $T[A]$ is positively invariant.
If A is invariant, then for each $\boldsymbol{x} \in A$ and each $t \in [0,\infty)$ there is an $\boldsymbol{x}_{-t} \in A$ such that $\Phi_t(\boldsymbol{x}_{-t}) = \boldsymbol{x}$ and correspondingly for each $\boldsymbol{y} = T[\boldsymbol{x}] \in T[A]$ there is $\boldsymbol{y}_{-t} = T[\boldsymbol{x}_{-t}]$ with

$$\Psi_t(\boldsymbol{y}_{-t}) = T[\Phi_t(\boldsymbol{x}_{-t})] = T[\boldsymbol{x}] = \boldsymbol{y}.$$

Ad (ii): Let $A \in \operatorname{sis}(\Phi)$. We define a corresponding set $\tilde{A} = H_\Psi(T[A]) \in \operatorname{sis}(\Psi)$. Correspondence for strongly invariant sets is proven via

$$(H_\Phi \circ \tilde{T}) \circ (H_\Psi \circ T) = \mathrm{id}_{\operatorname{sis}(\Phi)} \text{ and } (H_\Psi \circ T) \circ (H_\Phi \circ \tilde{T}) = \mathrm{id}_{\operatorname{sis}(\Psi)},$$

where, by symmetry, it suffices to show only one equality. Let $\boldsymbol{y} \in \tilde{A}$, then there exist $t_1, t_2 \geq 0$ and $\hat{\boldsymbol{y}} = T[\hat{\boldsymbol{x}}] \in T[A]$ such that $\Psi_{t_2}(\boldsymbol{y}) = \Psi_{t_1}(\hat{\boldsymbol{y}}) \in \tilde{A}$. Thus,

$$\begin{aligned}
\Phi_{t_2}\left(\tilde{T}[\boldsymbol{y}]\right) &= \tilde{T}[\Psi_{t_2}(\boldsymbol{y})] = \tilde{T}[\Psi_{t_1}(\hat{\boldsymbol{y}})] \\
&= \tilde{T}[\Psi_{t_1}(T[\hat{\boldsymbol{x}}])] = \tilde{T}[T[\Phi_{t_1}(\hat{\boldsymbol{x}})]] \\
&= \Phi_{t_1+\bar{\eta}}(\hat{\boldsymbol{x}}) \in H_\Phi(A) = A.
\end{aligned}$$

Hence, $\tilde{T}[\boldsymbol{y}] \in A$. That is, $\tilde{T}\left[\tilde{A}\right] \subseteq A$ and $H_\Phi\left(\tilde{T}\left[\tilde{A}\right]\right) \subseteq A$. We have also shown that for $\hat{\boldsymbol{x}} \in A$, $\Phi_{t_1+\bar{\eta}}(\hat{\boldsymbol{x}}) \in \tilde{T}\left[\tilde{A}\right]$ and therefore $\hat{\boldsymbol{x}} \in H_\Phi\left(\tilde{T}\left[\tilde{A}\right]\right)$. This yields $A \subseteq H_\Phi\left(\tilde{T}\left[\tilde{A}\right]\right) \subseteq A$, i.e. $A = H_\Phi\left(\tilde{T}\left[\tilde{A}\right]\right)$ and $\left(H_\Phi \circ \tilde{T}\right) \circ (H_\Psi \circ T) = \mathrm{id}_{\operatorname{sis}(\Phi)}$.
For invariant sets, the one-to-one correspondence is mediated directly via T and $\tilde{T}$. □

DEFINITION 28. The maximal Lyapunov exponent (MLE) of a point $\boldsymbol{x} \in X$ with respect to a semidynamical system $\Phi : [0,\infty) \times X \to X$ on a Banach space X is defined as

$$\lambda(\boldsymbol{x}) := \limsup_{t\to\infty} \limsup_{|\xi|\searrow 0} \frac{1}{t} \ln\left(\frac{|\Phi_t(\boldsymbol{x}+\xi) - \Phi_t(\boldsymbol{x})|}{|\xi|}\right) \in [-\infty,\infty].$$

The MLE of $\boldsymbol{x} \in A \subseteq X$ with respect to the set A is defined as

$$\begin{aligned}\lambda(x,A) &:= \limsup_{t\to\infty} \limsup_{|\xi|\searrow 0} \min_{a\in A} \frac{1}{t} \ln\left(\frac{|\Phi_t(\boldsymbol{x}+\xi) - a|}{|\xi|}\right) \\ &= \limsup_{t\to\infty} \limsup_{|\xi|\searrow 0} \frac{1}{t} \ln\left(\frac{\operatorname{dist}(\Phi_t(\boldsymbol{x}+\xi), A)}{|\xi|}\right).\end{aligned}$$

The MLE of a set $A \in X$ is defined as $\lambda(A) = \sup_{\boldsymbol{x}\in A} \lambda(\boldsymbol{x}, A)$.

THEOREM 29. *Let the CT-transformations T and $\tilde{T}$ be Lipschitz-continuous and let X, Y be Banach spaces. Then,*
(i) corresponding (strongly) invariant sets of Φ and Ψ possess the same maximal Lyapunov exponents (MLEs),
(ii) for each positively invariant set $A \in X$, the set $T[A] \in Y$ has the same type of stability.

Claim (i) is a direct consequence of the following Lemma.

LEMMA 30. *Let X, Y be Banach spaces and let T and $\tilde{T}$ be Lipschitz-continuous with constants L_T and $L_{\tilde{T}}$. Then, we have $\lambda(\boldsymbol{x}) \le \lambda(T[\boldsymbol{x}]) \le \lambda(\Phi_{\bar{\eta}}(\boldsymbol{x}))$ for all $\boldsymbol{x} \in X$.*

PROOF. For each $\boldsymbol{x}, \boldsymbol{\chi} \in \mathcal{C}$, $t \ge \bar{\eta}$:

$$\begin{aligned}&\frac{1}{t} \ln\left(\frac{|\Phi_t(\boldsymbol{x}) - \Phi_t(\boldsymbol{x}+\boldsymbol{\chi})|}{|\boldsymbol{\chi}|}\right) \\ = \;& \frac{1}{t} \ln\left(\frac{\left|\Phi_{t-\bar{\eta}}\left(\tilde{T}\circ T[\boldsymbol{x}]\right) - \Phi_{t-\bar{\eta}}\left(\tilde{T}\circ T[\boldsymbol{x}+\boldsymbol{\chi}]\right)\right|}{|\boldsymbol{\chi}|}\right) \\ = \;& \frac{1}{t} \ln\left(\frac{\left|\tilde{T}\circ \Psi_{t-\bar{\eta}}(T[\boldsymbol{x}]) - \tilde{T}\circ \Psi_{t-\bar{\eta}}(T[\boldsymbol{x}]+\boldsymbol{\xi})\right|}{|\boldsymbol{\chi}|}\right),\end{aligned}$$

with $|\boldsymbol{\xi}| = |T[\boldsymbol{x}+\boldsymbol{\chi}] - T[\boldsymbol{x}]| \le L_T|\boldsymbol{\chi}|$,

$$\begin{aligned}\ldots \;\le\; & \frac{1}{t} \ln\left(\frac{L_{\tilde{T}}\,|\Psi_{t-\bar{\eta}}(T[\boldsymbol{x}]) - \Psi_{t-\bar{\eta}}(T[\boldsymbol{x}]+\boldsymbol{\xi})|}{(|\boldsymbol{\xi}|/L_T)}\right) \\ = \;& \frac{1}{t} \ln\left(\frac{|\Psi_{t-\bar{\eta}}(T[\boldsymbol{x}]) - \Psi_{t-\bar{\eta}}(T[\boldsymbol{x}]+\boldsymbol{\xi})|}{|\boldsymbol{\xi}|}\right) + \frac{1}{t}\ln\left(L_T L_{\tilde{T}}\right)\end{aligned}$$

Therefore,

$$\frac{1}{t} \ln\left(\frac{|\Phi_t(\boldsymbol{x}) - \Phi_t(\boldsymbol{x}+\boldsymbol{\chi})|}{|\boldsymbol{\chi}|}\right) \le \frac{1}{t} \ln\left(\frac{|\Psi_{t-\bar{\eta}}(T[\boldsymbol{x}]) - \Psi_{t-\bar{\eta}}(T[\boldsymbol{x}]+\boldsymbol{\xi})|}{|\boldsymbol{\xi}|}\right),$$

and, thus,

$$\lambda(\boldsymbol{x}) \leq \lambda(T[\boldsymbol{x}]).$$

The same reasoning for $\boldsymbol{y} = T[\boldsymbol{x}]$ gives

$$\lambda(\boldsymbol{x}) \leq \lambda(T[\boldsymbol{x}]) \leq \lambda(\Phi_{\bar{\eta}}(\boldsymbol{x})).$$

□

Now we can prove Theorem 29

PROOF. Lemma 30 implies claim (i). To see that consider two corresponding sets $A \in \operatorname{sis}(\Phi)$ and $\tilde{A} \in \operatorname{sis}(\Psi)$. Then it is impossible that $\lambda(A) > \lambda(\tilde{A})$ since for any $\boldsymbol{x} \in A$ there exists $\boldsymbol{y} = T[\boldsymbol{x}] \in \tilde{A}$ such that $\lambda(\boldsymbol{x}) \leq \lambda(\boldsymbol{y})$. The same holds vice versa and therefore $\lambda(A) = \lambda(\tilde{A})$. Similarly, one shows this for the case of invariant sets.
Ad (ii): Let $A \in \mathcal{C}$ be an (asymptotically) stable positively invariant set. We show that if A is (asymptotically) stable so is $T[A]$. Let $\varepsilon > 0$, $\boldsymbol{y}_0 = T[\boldsymbol{x}_0] \in T[A]$ and $\boldsymbol{\xi}_0 \in \tilde{\mathcal{C}}$ a small initial perturbation, i.e. $|\boldsymbol{\xi}_0| \leq \delta$ with $\delta = \delta(\varepsilon) > 0$ to be specified later. Define the perturbed solution

$$\tilde{\boldsymbol{y}}_t = \Psi_t(\boldsymbol{y}_0 + \boldsymbol{\xi}_0) = \boldsymbol{y}_t + \boldsymbol{\xi}_t,$$

where $\boldsymbol{y}_t = \Psi_t(\boldsymbol{y}_0)$ is the unperturbed solution. Consider

$$\begin{aligned}
\tilde{\boldsymbol{x}}_t : &= \tilde{T}[\tilde{\boldsymbol{y}}_t] = \tilde{T}[\Psi_t(\boldsymbol{y}_0 + \boldsymbol{\xi}_0)] \\
&= \Phi_t\left(\tilde{T}[\boldsymbol{y}_0 + \boldsymbol{\xi}_0]\right) \\
&= \Phi_t\left(\tilde{T} \circ T[\boldsymbol{x}_0] + \left(\tilde{T}[\boldsymbol{y}_0 + \boldsymbol{\xi}_0] - \tilde{T}[\boldsymbol{y}_0]\right)\right) \\
&= \Phi_t(\boldsymbol{x}_{\bar{\eta}} + \boldsymbol{\chi}_{\bar{\eta}}),
\end{aligned}$$

with

$$\begin{aligned}
|\boldsymbol{\chi}_{\bar{\eta}}| &= \left|T[\boldsymbol{y}_0 + \boldsymbol{\xi}_0] - \tilde{T}[\boldsymbol{y}_0]\right| \\
&\leq L_{\tilde{T}} \cdot \delta,
\end{aligned}$$

where $L_{\tilde{T}}$ is the Lipschitz constant of $\tilde{T}$. Since $\boldsymbol{x}_{\bar{\eta}} \in A$ and A is (asymptotically) stable, we can find a $\delta = \delta(\varepsilon)$ such that

$$\mathrm{d}(\tilde{\boldsymbol{x}}_t, A) \leq \frac{\varepsilon}{L_T},$$

and, in case of asymptotic stability, such that

$$\tilde{\boldsymbol{x}}_t \to A.$$

This means, we can represent $\tilde{\boldsymbol{x}}_t$ as $\tilde{\boldsymbol{x}}_t = \boldsymbol{a}_t + \boldsymbol{\chi}_t$ with $\boldsymbol{a}_t \in A$, $|\boldsymbol{\chi}_t| \leq \frac{\varepsilon}{L_T}$ and, in case of asymptotic stability, $|\boldsymbol{\chi}_t| \to 0$, for $t \to \infty$. Note that $t \mapsto \boldsymbol{a}_t$ has not

to be a solution. Define $\boldsymbol{b}_t = T[\boldsymbol{a}_t] \in T[A]$. Then,

$$\begin{aligned} |\tilde{\boldsymbol{y}}_{t+\bar{\eta}} - \boldsymbol{b}_t| &= \left| T \circ \tilde{T}[\tilde{\boldsymbol{y}}_t] - T[\boldsymbol{a}_t] \right| \\ &= |T[\boldsymbol{a}_t + \boldsymbol{\chi}_t] - T[\boldsymbol{a}_t]| \\ &\leq L_T |\boldsymbol{\chi}_t| \leq \varepsilon \end{aligned}$$

and $|\tilde{\boldsymbol{y}}_{t+\bar{\eta}} - \boldsymbol{b}_t| \to 0$, if A is asymptotically stable. This completes the proof. □

5.5. Reduction of delay-parameters

The Theorems 27 and 29 show that CT-equivalence is indeed a very strong equivalence. For virtually all cases one is best advised to study the system which possesses the most convenient distribution of delays within the concerned equivalence class. However, it is difficult give a general identification of the appropriate distribution, since it strongly depends on the problem at hand. We can acknowledge two possible guiding principles, which correspond to the transformations of delays in a ring that were mentioned in the introduction (cf. (5.1.4) and (5.1.5)). Firstly, a homogenization of delays can sometimes lead to a higher degree of symmetry and thereby allow for simplifications. In other cases a "concentration" of the delays on selected links may be useful.

In section 5.5.1 we show, that it is always possible to find timeshifts η_j, $j = 1, ..., N$, such that the number of different delays in system (5.2.1) reduces to the cycle space dimension $C = L - N + 1$ of the network, where $L = \#\mathcal{E}$ is the number of links and $N = \#\mathcal{N}$ is the number of nodes in the network. Effectively, this means that no more than C delay-parameters have to be taken into account during investigation (see Fig. 5.1.1). For a connected network this number cannot be reduced further as we show in section 5.5.2.

5.5.1. Construction of an instantaneous spanning tree. In this section we construct a set of links, called a "spanning tree" (see Def. 32), on which all connection delays can be eliminated by componentwise timeshifts. Let us firstly introduce the necessary notions:

Definition 31. A semicycle $c = (\ell_1, ..., \ell_k)$ is a closed path in the undirected graph which is obtained by dropping the orientation from all links from the multigraph $(\mathcal{N}, \mathcal{E})$.

Now we define a spanning tree

Definition 32. A spanning tree of $(\mathcal{N}, \mathcal{E})$ is a set of links $S \subseteq \mathcal{E}$ which contains no semicycles but all nodes, that is $\{s(\ell), t(\ell)\}_{\ell \in S} = \mathcal{N}$.

A spanning tree can be thought of as a "skeleton" of the graph. Following its links one can visit each node in the graph exactly once. For instance, the solid, red links in Figs. 5.5.2(c) form spanning trees. A spanning tree can also be characterized as a maximal cycle-free set of links. Consequently,

adding another link which is not contained in the spanning tree creates a semicycle. For instance, if in Figs. 5.5.2(a) the link with delay τ_1 is added to the spanning tree the semicycle c_1 is created. A spanning tree of a connected network necessarily contains $N-1$ links, therefore the cycle space dimension C coincides with the number of links not contained in a spanning tree. In the context of the CTT, an important quantity for a semicycle is its delay sum.

DEFINITION 33. The delay sum of a semicycle $c=(\ell_1,...,\ell_k)$ with respect to a delay distribution and an orienting link ℓ_1 is

$$\Sigma(c) := \sum_{j=1}^{k} \sigma_j \tau(\ell_j),$$

where $\sigma_j \in \{\pm 1\}$ indicates whether the link ℓ_j points in the same direction as ℓ_1 ($\sigma_j = 1$) or not ($\sigma_j = -1$). The roundtrip of c is the modulus of its delay sum

$$\mathrm{rt}(c) := |\Sigma(c)|. \tag{5.5.1}$$

The following Lemma gives a characterization of timeshift-transformed delay distributions and describes their relation to the underlying graph structure. More specifically, it shows that the delay sums of semicycles are invariant under timeshifts.

LEMMA 34. *Let $\tau, \tilde{\tau} : \mathcal{E} \to [0,\infty)$ be two delay distributions in a connected network. Then, the following statements are equivalent:*
(i) There exist $\eta_j \geq 0$, $j=1,...,N$, such that $\tilde{\tau}(\ell) = \tau(\ell) - \eta_{t(\ell)} + \eta_{s(\ell)}$.
(ii) For all semicycles c of the network holds:

$$\Sigma_\tau(c) = \Sigma_{\tilde{\tau}}(c).$$

PROOF. (i) $\Rightarrow$ (ii) Indeed, for any cycle $c=(\ell_1,...,\ell_k)$ we have

$$\begin{aligned}\Sigma_{\tilde{\tau}}(c) &= \sum_{j=1}^{k} \sigma_j \tilde{\tau}(\ell_j) = \sum_{j=1}^{k} \sigma_j \left(\tau(\ell_j) - \eta_{t(\ell_j)} + \eta_{s(\ell_j)}\right) \\ &= \Sigma_\tau(c) + \sum_{j=1}^{k} \sigma_j \left(\eta_{s(\ell_j)} - \eta_{t(\ell_j)}\right) = \Sigma_\tau(c).\end{aligned}$$

(ii) $\Rightarrow$ (i) Select an arbitrary spanning tree $S=(\ell_1,...,\ell_{N-1})$. Select $\xi = (\xi_1,...,\xi_N)$ and $\chi=(\chi_1,...,\chi_N)$ such that $\tau(\ell_j) = \xi_{t(\ell_j)} - \xi_{s(\ell_j)}$ and $\tilde{\tau}(\ell_j) = \chi_{t(\ell_j)} - \chi_{s(\ell_j)}$ for $j=1,...,N-1$. (Note that both defining sets of equations are inhomogeneous linear systems of type $\mathbb{R}^{N\times(N-1)}$ and of rank $N-1$. Therefore they possess solutions.) The shifts ξ and χ define distributions (with possibly negative values)

$$\begin{aligned}\hat{\tau}_1(\ell) &= \tau(\ell) - \xi_{t(\ell)} + \xi_{s(\ell)}, \\ \hat{\tau}_2(\ell) &= \tilde{\tau}(\ell) - \chi_{t(\ell)} + \chi_{s(\ell)}.\end{aligned}$$

Both, $\hat{\tau}_1$ and $\hat{\tau}_2$, are instantaneous along S, i.e., $\hat{\tau}_1(\ell) = \hat{\tau}_2(\ell) = 0$ for $\ell \in S$. Each link ℓ which is not in S corresponds to a unique fundamental semicycle $c = c(S, \ell)$ which is created by adding ℓ to S. It is the only link in c which may hold a non-zero value $\hat{\tau}_1(\ell)$ or $\hat{\tau}_2(\ell)$, respectively. By the part (i) $\Rightarrow$ (ii) we have

$$\hat{\tau}_1(\ell) = \Sigma_\tau(c) = \Sigma_{\tilde{\tau}}(c) = \hat{\tau}_2(\ell).$$

Hence $\hat{\tau}_1 = \hat{\tau}_2$. With $\eta_j := \xi_j - \chi_j$ this gives

$$\tilde{\tau}(\ell) \quad = \quad \tau(\ell) - \eta_{t(\ell)} + \eta_{s(\ell)}.$$

Note that η_j can always be chosen to be non-negative since a simultaneous shift $\eta_j \mapsto \eta_j + \bar{\eta}$ by some amount $\bar{\eta} \in \mathbb{R}$ does not change the resulting transformed distribution $\tilde{\tau}$. □

Often, this lemma makes it straightforward to determine possible transformations, since it circumvents the explicit determination of timeshifts. For instance, in the case of the two coupled systems depicted in Fig. 5.1.1, it follows immediately that $\tau = (\tau_1 + \tau_2)/2$.

Now we can state the main result of this section, which is the construction of a transformation (5.1.2) such that the number of delays is minimized.

THEOREM 35. *For every connected network with dynamics given by Eq. (5.2.1), there exists a spanning tree S and timeshifts η_j such that in the transformed system (5.2.2) all links $\ell \in S$ are instantaneous,*

$$\tilde{\tau}(\ell) = 0, \text{ for } \ell \in S,$$

and for each link ℓ outside the spanning tree the delay $\tilde{\tau}(\ell)$ equals the roundtrip $rt(c(\ell))$ (Eq. (5.5.1)) along the corresponding fundamental cycle $c(\ell)$,

$$\tilde{\tau}(\ell) = T(c(\ell)), \text{ for } \ell \notin S.$$

PROOF. The following algorithm describes the general procedure to find a reduced set of delays. For a more definite example see Fig. 5.5.2 and its description following this proof. The main idea of the algorithm is as follows. We construct spanning trees and timeshifts iteratively such that after each step the number of non-zero delays on the spanning tree has decreased by at least one. Therefore the algorithm finishes after at most $N-1$ iterations. Each step consists of two stages.

Stage (i). Construction of a spanning tree:

Select a spanning tree $S = \{\ell_1, ..., \ell_{N-1}\}$ in the following way. First, pick a link ℓ_1 with minimal delay, i.e. $\tau(\ell_1) = \min_{\ell \in \mathcal{L}} \{\tau(\ell)\} \in [0, \infty)$. Proceed picking links $\ell_2, ..., \ell_j$ with minimal delays (under all links except the ones already picked) as long as the set $S_j = \{\ell_1, ..., \ell_j\}$ contains no semicycles. If at the j-th step the chosen link would create a semicycle when added to S_{j-1}, do not add it but ignore it for the rest of this stage. Following this procedure, called Kruskal's algorithm **[99]**, yields a spanning tree $S = \{\ell_1, ..., \ell_{N-1}\}$.

Stage (ii). Construction of timeshifts:

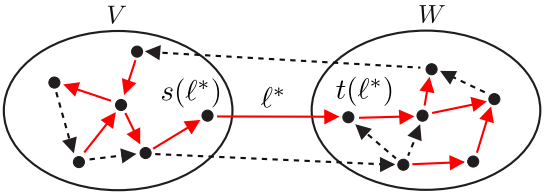

FIGURE 5.5.1. Illustration of the fundamental cut corresponding to the link ℓ^* in the spanning tree S (solid red links), $s(\ell^*)$ and $t(\ell^*)$ denote the source and target of ℓ^*. Links which are not contained in S are indicated by dashed lines.

Now consider the link $\ell^* \in S$ with minimal positive delay (in the very first step of the construction it equals ℓ_1 if $\tau(\ell_1) > 0$). The link induces a fundamental cut **[45]**, i.e. it partitions the spanning tree S in two connected components: the source component V of ℓ^* and the target component W of ℓ^*, see Fig. 5.5.1.

Since S is spanning, this is a partition of all nodes. Now let us define the timeshifts by $\eta_j = 0$ for $j \in V$ and $\eta_j = \tau(\ell^*)$ for all $j \in W$.
From the shifts η_j we obtain the new delay distribution $\tilde{\tau}(\ell) = \tau(\ell) + \eta_{s(\ell)} - \eta_{t(\ell)}$. For a link $\ell \neq \ell^*$ which connects nodes within one set of the partition, i.e. $s(\ell), t(\ell) \in V$ or $s(\ell), t(\ell) \in W$, we have $\eta_{s(\ell)} = \eta_{t(\ell)}$. This implies $\tilde{\tau}(\ell) = \tau(\ell)$. In particular this is the case for all links in $S \setminus \{\ell^*\}$ and therefore $\tau(\ell) = 0 = \tilde{\tau}(\ell)$ for all instantaneous links in S. For ℓ^* we have $\tilde{\tau}(\ell^*) = 0$ because $s(\ell^*) \in V$ and $t(\ell^*) \in W$, which means $\eta_{s(\ell^*)} - \eta_{t(\ell^*)} = -\tau(\ell^*)$.
Hence, the delay distribution $\tilde{\tau}$ reduced the number of delays on the spanning tree S by one compared to the distribution τ. We remind that $\tau(\ell^*)$ is the smallest positive delay not only on the spanning tree but over all the links which connect V and W. Therefore, $\tau(\ell) \geq 0$ for all $\ell \in \mathcal{L}$. Indeed, if there were a link between V and W with a smaller delay we must have included it in the spanning tree in step (i)

If a link ℓ exists in S with $\tilde{\tau}(\ell) \neq 0$ we repeat stage (i) starting from an initial set S_j which contains all j instantaneous links from the spanning tree constructed in the previous step. Then stage (ii) yields a spanning tree with a strictly larger number of instantaneous links. In this way we arrive at an instantaneous spanning tree S in at most $N-1$ iterations. The statement that $\tilde{\tau}(\ell) = T(c(\ell))$ for $\ell \notin S$ follows from Lemma 34. □

Fig. 5.5.2 illustrates how the algorithm described in the proof of Theorem 35 determines a delay reduction in the depicted network of $N = 7$ coupled systems with cycle space dimension $C = 3$. We assume an initial delay-distribution as given in the first row of the table in Fig. 5.5.2(b). Then, the spanning tree in (a), indicated by solid, red links, is selected by the algorithm as a successive cycle-free collection of links with smallest delays. Let us denote the links of the example by ℓ_j with $\tau_j = \tau(\ell_j)$, $j = 1, ..., 7$. Note that in (a) ℓ_1

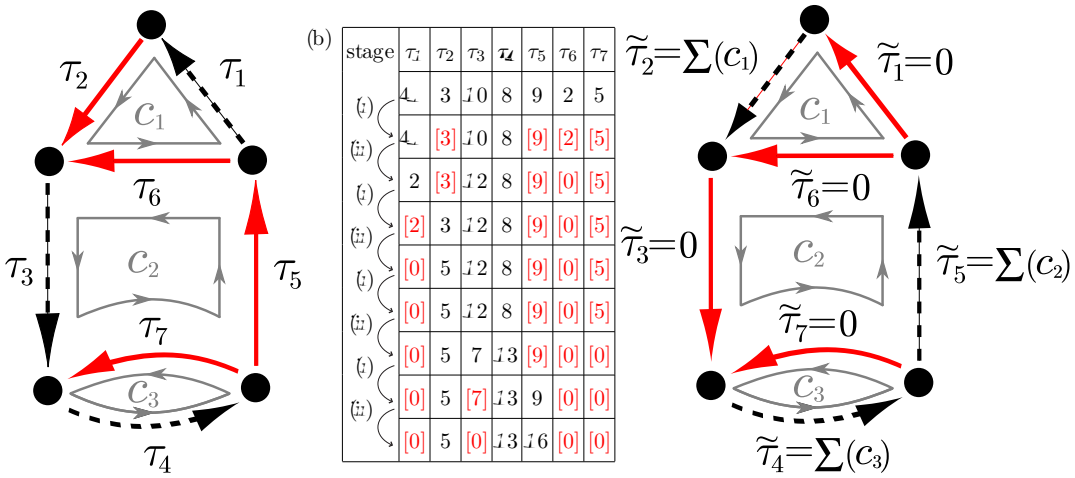

stage	τ_1	τ_2	τ_3	τ_4	τ_5	τ_6	τ_7
(i)	4	3	10	8	9	2	5
(ii)	4	[3]	10	8	[9]	[2]	[5]
(i)	2	[3]	12	8	[9]	[0]	[5]
(ii)	[2]	3	12	8	[9]	[0]	[5]
(i)	[0]	5	12	8	[9]	[0]	[5]
(ii)	[0]	5	12	8	[9]	[0]	[5]
(i)	[0]	5	7	13	[9]	[0]	[0]
(ii)	[0]	5	[7]	13	9	[0]	[0]
	[0]	5	[0]	13	16	[0]	[0]

FIGURE 5.5.2. Illustration of the delay reduction in a network of $N = 7$ delay-coupled systems with cycle space dimension $C = 3$ (cf. proof of Theorem. 35). In (a) the initially selected spanning tree with original delays τ_j, $j = 1, ..., 7$, is indicated by red, solid links, Three semicycles c_1, c_2, and c_3 are indicated by the grey curves following the contained links; in (c) the final spanning tree with transformed delays $\tilde{\tau}_j$ is indicated. The table (b) shows the steps taken by the reduction algorithm. Bracketed, red values indicate the delay times on the currently selected spanning tree at each step.

is not contained in the spanning tree although $\tau_1 < \tau_5$ and $\tau_1 < \tau_7$, and ℓ_5 and ℓ_7 are both contained. This is because if the links ℓ_2 and ℓ_6 with $\tau_2, \tau_6 < \tau_1$ are already selected, then an addition of ℓ_1 would lead to the inclusion of the semicycle c_1, which is not allowed. Each row of table (b) corresponds to a step of the algorithm, where the bracketed, red values correspond to the delay times of the currently selected spanning tree. Two stages are repeated alternately: In stage (i) a spanning tree with minimal delay sum is determined and in stage (ii) the minimal delay in this spanning tree is eliminated by a componentwise timeshift. In (c) the spanning tree is shown which is selected at the final stage. It contains only instantaneous links when the algorithm is completed. The remaining delays on links not contained in the final spanning tree, correspond to the delay sums of the corresponding semicycles (c_1, c_2, c_3), oriented as indicated in the figure, i.e., $\tilde{\tau}_2 = \Sigma(c_1) = \tau_1 + \tau_2 - \tau_6$; $\tilde{\tau}_5 = \Sigma(c_2) = \tau_3 + \tau_5 + \tau_6 - \tau_7$; and $\tilde{\tau}_4 = \Sigma(c_3) = \tau_4 + \tau_7$.

5.5.2. Genericity of the dimension of the delay parameter space. We call C the essential number of delays since it is the minimal number to which the number of different delays in a network can be reduced generically. Here "generically" means that the conditions which allow for further reduction

of delays form a null set in the parameter space of delays $\mathbb{R}^L_{\geq 0} = \{(\tau(\ell))_{\ell\in\mathcal{E}} : \tau(\ell) \geq 0\}$ of the original system. The reducibility condition to m different delays is described by the L linear equations

$$\eta_{t(\ell)} - \eta_{s(\ell)} + \tilde{\tau}(\ell) = \tau(\ell), \ \ell \in I_j, \tag{5.5.2}$$

with the restriction for $\tilde{\tau}(\ell)$ to take one of m different values $\{\theta_1, ..., \theta_m\}$. System (5.5.2) can be equivalently written in the vector form $G_q\mathbf{v} = \boldsymbol{\tau}$, where $\mathbf{v}$ is the $(N+m)$-dimensional vector of unknowns $\mathbf{v} = (\eta_1, \ldots, \eta_N, \theta_1, \ldots \theta_m)$ and $\boldsymbol{\tau}$ is the L-dimensional vector of delays $\tau(\ell)$. For any fixed assignment $\tilde{\tau}(\ell) = \theta_{q(\ell)}$, $\ell \in I_j$, with $q : I_j \to \{0, ..., m\}$, and $\theta_0 := 0$, one obtains a different matrix $G_q \in \mathbb{R}^{L\times(N+m)}$. It can further be shown that the rank of the matrix G_q is smaller than $N - 1 + m$. This implies for $m < C = L - (N-1)$ that $N - 1 + m < L$. Hence, the number of equations in (5.5.2) is larger than the number of unknowns. Such equation cannot be solved generically, unless the given delays $\tau(\ell)$ satisfy some special condition of positive codimension.

5.6. Discussion

In this chapter we have studied a componentwise timeshift transformation (CTT) for a general class of coupled differential equations with constant coupling delays. We have defined appropriate phase spaces such that the CTT conveys an equivalence for the semiflows of the original and the transformed system which is reminiscent to, but weaker than topological conjugacy. We have shown several dynamical invariants for the equivalent flows. Firstly, for delay differential equations, the characteristic exponents of equilibria and the Floquet exponents of periodic orbits are invariant under the CTT. More generally, for CT-equivalent semidynamical systems, we have shown that there exists a one-to-one correspondence between invariant and strongly invariant sets, respectively. As a main stability result we have shown that corresponding positively invariant sets have the same kind of stability, and invariant and strongly invariant corresponding sets possess the same maximal Lyapunov exponents. To sum up, the observable dynamics of the coupled units might change its relative timing in the transformed system, but qualitatively it remains the same. In particular attractors and their stability are invariant.

We have presented a constructive proof that there is always a CTT which reduces the delays to at most $C = L - N + 1$ different delays, where L is the number of links in the network and N is the number of nodes. The number of different delays C coincides with the cycle space dimension of the underlying graph. Furthermore, we have shown that the sum of delays along semicycles in the network is invariant under CTTs. This reveals a strong link between a coupled delay differential equation and the topology of the underlying graph. Although a CTT which reduces the number of different delays to a minimum is usually not unique, we have shown that the minimal number of different delays itself cannot be reduced in general.

We believe that our results have a relevance for several applied areas (see also [**114**]). For example, in theoretical neuroscience it is an accepted fact that in the case of two mutually delay coupled units [**133**] (as in Fig. 5.1.1) or more generally, in unidirectionally coupled rings [**138**], the delays can always be chosen identical for theoretical investigations. Moreover, in view of our results, the observations about the role of the greatest common divisor of loop-lengths in networks of delay coupled excitable systems with homogeneous delays [**96, 152**] can be formulated more generally in terms of the delay sums along the network's cycles. The CTT is an important tool for investigators working with delayed dynamical systems since it clarifies one aspect of the way in which different interaction delays in a coupled system work together.

Furthermore, the CTT can speed up the numerical simulation of a system by reducing the number of different delays or by reducing the maximal delay time. The computational advantages of the transformed system might be of interest especially in the field of delayed neural networks, where large scale simulations of networks with many different delay times are conducted.

CHAPTER 6

Routes to Synchrony in Large Networks with Delayed Coupling

"It is all that introduces order,
all that gives unity, that permits us
to see clearly and to comprehend
at once both the ensemble and the details."
Henri Poincare

6.1. Introduction

So far, we have considered networks with a deterministic coupling structure. However, many networks in applications are known to form their structure in a random fashion. A broad class of these random networks is given by the so called scale-free networks which were (re-)discovered[1] in 1999 [**11**]. Since then, large networks such as the world-wide-web, populations of brain cells or citation networks have been found to have this property [**56**]. Here, the term scale-free refers to the distribution of node degrees which follows a power-law. To put it in simple terms, many nodes have low degrees and very few nodes have high degrees. Subsequently to their discovery, the dynamics on these structures have attracted much attention [**108**]. However, it turned out that the dynamics on scale-free networks are qualitatively close to the dynamics in globally coupled networks, at least when restricted to the investigation of synchronicity. More precisely, for phase oscillators, scale-free networks exhibit a second-order transition to synchrony as in the Kuramoto system of globally coupled oscillators, i.e. increasing the global coupling yields a gradual increase of the order parameter (see Definition 2) [**67**]. A couple of years ago, a model was introduced where the individual phase oscillator's frequencies are positively correlated to their respective degrees. In [**67**] the case of a linear correlation was discussed where nodes with higher degree have a higher frequency. A surprising effect of this correlation is the so-called explosive synchronization: increasing the global coupling strength does not lead to a gradual increase of the order parameter, but one can observe a sudden

[1]In fact, it was discovered by D. de Solla Price as early as 1965 that the network of citations between scientific articles is scale-free even though he did not use this term [**41**]. It is remarkable that the number of citations of this article exploded in the last ten years.

jump in the order parameter corresponding to a first order transition from an incoherent state to an almost synchronous state. Thereafter, T.K. Peron and F.A. Rodrigues [**140**] investigated the same system with transmission delays in the couplings. Based on numerical simulations of scale-free networks and analytic results for simple star graphs they hypothesized that delay can improve the synchronization properties in the case of explosive synchronization. Furthermore, they numerically found two distinct routes to synchrony, depending on the size of the coupling delay: For certain values, the transition is of second order, i.e. the order parameter increases gradually when increasing the global coupling. Whereas for other delay values the transition seems to be of first order with a characteristic jump in the order parameter and the emergence of hysteresis. The specific mechanism of bifurcation of the incoherent solution and the nature of the different routes to synchrony remained in the dark. So far, most of the results are of numerical origin and there exist few attempts to understand this phenomenon analytically. One attempt to simplify the analysis of dynamics in large random networks was introduced in 2008 by E. Ott and T.M. Antonsen [**132**] and was extended last year [**147**]. The authors were able to characterize the synchronization manifold analytically and thereby reduce the dimension of the associated problem.

In this chapter, we generalize these ideas to the case of delayed couplings in order to investigate the effect of delay on explosive synchronization. We obtain an infinite system of delay differential equations which describes the dynamics on a random network of phase oscillators in the limit of a large number of elements. Using these equations, we reduce the problem of finding (partially) synchronous states to a complex algebraic equation. We show that for these states, the bifurcations are all of first order, independent of the value of the time delay. Also, we can confirm the hypothesis that the transitions occur through saddle-node bifurcations. Consequently, we believe that the solutions found in [**140**] which constitute the second order transitions are more complex than the solutions we investigate here, i.e. rotating wave solutions. Furthermore, we show that larger delays yield better synchronizability for this class of solutions.

We remark that we will not state rigorous results about the possible convergence of solutions of the finite network model towards those of the infinite dimensional system here. Obtaining such results proved to be a very hard problem. For instance, in the rather simple case of global undelayed coupling a first proof of the bifurcations in the thermodynamic limit and its relation to the finite dimensional dynamics was only done a few years ago (forty years after the formulation of the hypothesis by Kuramoto) and involved deep functional analytic theorems [**33, 32**]. However, we show that our findings are in good agreement with numerical simulations. Furthermore we remark, that as in [**147**], the reasoning can be done for directed networks similarly and the choice of undirected networks is for the sake of clarity.

This chapter is structured as follows. In section 6.2 we introduce the main equations for a network of finite size N with arbitrary random coupling topology and deduce an infinite system of delay differential equations for the case $N \to \infty$. In section 6.3 we apply the obtained results to the case of scale-free networks with frequency-degree correlations and state the resulting equations. In the subsequent section 6.4 we investigate the existence of incoherent and partially synchronized solutions. Then follows an investigation of bifurcations for both, the finite network model and its thermodynamic limit in section 6.5. We conclude with a discussion of the results and an outlook on open questions in section 6.6.

6.2. Phase oscillators with delayed coupling in the thermodynamic limit

Consider the following model of phase oscillators coupled with delay

$$\dot{\theta}_i(t) = \omega_i + \lambda \sum_{j=1}^{N} a_{ij} \sin\left(\theta_j(t-\tau) - \theta_i(t)\right) \tag{6.2.1}$$

We assume that the global coupling λ and the delay τ are nonnegative real numbers. Let the adjacency matrix $\mathbf{A} = \{a_{ij}\}$ with $a_{ij} \in \{0, 1\}$ be symmetric, so the network is undirected. With zero global coupling λ, oscillator i rotates with frequency ω_i and the oscillators will not synchronize unless all the ω_i are identical. However, increasing the coupling strength, the nodes will begin to interact and might end up being synchronized for large enough couplings, although their individual speeds are different. Indeed, in [**67**] it was shown that for $\tau = 0$ and unimodal distributions of the frequencies ω_i the system undergoes a second order bifurcation, i.e. the coherence increases gradually and the whole network ends up synchronized when increasing the coupling strength. However, if the frequencies are chosen to be positively correlated to the node's degrees, say for simplicity $\omega_i = \sum_j a_{ij}$, the bifurcation scenario changes qualitatively. A sudden jump in the coherence, leading from an incoherent state to an almost synchronous state, can be observed for a critical coupling strength. Subsequently, in [**140**] a numerical analysis was carried out which led to the hypothesis that for certain values of τ there is a first order transition from an incoherent state to a coherent state. For the other values of τ the transition seems to be of second order, i.e. the order parameter increases gradually when increasing the coupling strength. In this chapter, using a new approach introduced in [**147**] we want to investigate the kinds and locations of bifurcation from the incoherent state in dependence of the delay value τ. The approach is based on choosing an appropriate thermodynamic limit for Eq. (6.2.1). Once these equations are obtained we can restrict the dynamics to the synchronous manifold. On the synchronous manifold we use a characterization introduced by Ott and Antonsen [**132**]. We remark that a system similar to (6.2.1) was

investigated in [**49**], only that here the coupling strength is scaled by the in-degree of the respective node and the individual frequencies are assumed to be identical, so

$$\dot{\phi}_i(t) = \omega + \frac{\lambda}{\sum_{j=1}^{N} a_{ij}} \sum_{j=1}^{N} a_{ij} \sin\left(\phi_j(t-\tau) - \phi_i(t)\right).$$

An important consequence of this scaling is the existence of globally synchronized solutions $\phi(t) = \Omega t$, obtained by solving the equation $\Omega = \omega - \lambda \sin(\Omega\tau)$. Equations of this kind often arise when dealing with this type of equation. We remind that we encountered the same equation in chapter 4 when investigating synchronous motions in rings of phase oscillators. For these solutions, the simple stability criterion $\cos(\Omega\tau) > 0$ can be shown ([**49**] and Lemma 22). For Eq. (6.2.1) these solutions do not exist in general, which makes matters more complicated.

6.2.1. The local order parameter and its thermodynamic limit. In order to perform a thermodynamic limit of system (6.2.1) let us present some preparatory thoughts. The main step will be the derivation of a quantity which represents the thermodynamic limit of the local order parameter r_i as defined below in Eq. (6.2.4). Let us first rewrite the velocity fields v_i on the right hand side as

$$v_i(t) = \omega_i + \lambda \Im\left(e^{-i\theta_i(t)} \sum_{j=1}^{N} a_{ij} e^{i\theta_j(t-\tau)}\right). \tag{6.2.2}$$

Suppose we are given a finite random network with a degree distribution $P(d)$ where d is the node degree. Let $a(d \to k)$ be the probability that there is a link from a node of degree d to a node of degree k. Then the number of links from any node of degree d to a given node of degree k is given by

$$P(d)\, a(d \to k).$$

Equivalently, the number of links between all nodes of degree d and all nodes of degree k is given by

$$P(d)\, a(d \to k)\, P(k).$$

Summing over all d, k we must get the total number of expected links in the network. Now, let $\langle k \rangle$ denote the average degree in the network. Then the expected value for the total number of links in the network is $N\langle k \rangle$. So we have the following condition for a

$$\sum_{d} \sum_{k} P(d)\, a(d \to k)\, P(k) = N\langle k \rangle. \tag{6.2.3}$$

Equivalently to the order parameter in globally coupled phase oscillators we define the local order parameter r_i for solutions of Eq. (6.2.1) as

$$r_l(t) = \sum_{j=1}^{N} a_{lj} e^{i\theta_j(t)} \tag{6.2.4}$$

and which can be thought of the net input of node l. Now we want to find a quantity that represents this variable for $N \to \infty$. First, we assume that in the limit, there is a smooth density function $f(\theta, \omega|d, t)$, such that $\frac{1}{2\pi} f(\theta', \omega'|d, t)\, d\theta' d\omega'$ is the probability that a node with degree d at time t has its phase and its frequency in the interval $[\theta', \theta' + d\theta']$ and $[\omega', \omega' + d\omega']$ respectively. Then, the number of nodes with these properties is given by $P(d) \frac{1}{2\pi} f(\theta', \omega'|d, t)\, d\theta' d\omega'$. Let us call $L_{\{d\}\to k}$ the set of links from all nodes of degree d with these properties to a given node of degree k. The number of links in this set is given by multiplying with the connection probability a. So

$$\#L_{\{d\}\to k} = P(d)\, a(d \to k) \frac{1}{2\pi} f\left(\theta', \omega'|d, t\right) d\theta' d\omega'.$$

Consequently, the number of links from all nodes of degree d to all nodes of degree k is obtained by multiplying with the number $P(d)$ of nodes of degree k. Calling this set of links $L_{\{d\}\to\{k\}}$ we have

$$\#L_{\{d\}\to\{k\}} = P(d)\, a(d \to k)\, P(k) \frac{1}{2\pi} f\left(\theta', \omega'|d, t\right) d\theta' d\omega'.$$

Summing up over all (incoming) degrees $1 \le d < \infty$ and integrating over θ' and ω' we finally get the net input into a node of degree k

$$R(k, t) = \sum_d P(d)\, a(d \to k) \left(\frac{1}{2\pi} \int_0^{2\pi} e^{i\theta'} \int_0^{\infty} f\left(\theta', \omega'|d, t\right) d\omega' d\theta' \right). \tag{6.2.5}$$

6.2.2. The continuity equation. Using the quantity R we now deduce the thermodynamic limit of Eq. (6.2.1). First, rewriting the velocity field (6.2.2) as

$$v_i(t) = \omega_i + \lambda \Im\left(e^{-i\theta_i(t)} r_i(t - \tau) \right)$$

and using the results from the previous section we can define the equivalent for the thermodynamic limit by

$$v(\omega|k, t) = \omega + \lambda \Im\left(e^{-i\theta} R(k, t - \tau) \right).$$

Using that the total mass must be conserved, we have the continuity equation $\frac{\partial}{\partial t} f = -\frac{\partial}{\partial \theta}(vf)$ and thus we obtain the following delay differential equation for the density f

$$\frac{\partial}{\partial t} f(\theta, \omega|k, t) = -\frac{\partial}{\partial \theta} \left(\left[\omega + \lambda \Im\left(e^{-i\theta} R(k, t - \tau) \right) \right] f(\theta, \omega|k, t) \right). \tag{6.2.6}$$

Now, following Ott and Restrepo [**147**], we make the following Ansatz for the density f

$$f(\theta,\omega|k,t) = \left[1+\left(\sum_{n=1}^{\infty} b(\omega,k,t)^n e^{-in\theta}+c.c.\right)\right] g(\omega|k). \tag{6.2.7}$$

Remarkably, this Ansatz describes the whole synchronization manifold [**132**]. It is crucial for the following analysis as it reduces the dimension of the problem. More precisely, instead of infinitely many equations for the Fourier coefficients for each k, we will be left with only one equation for each k. And indeed, plugging this Ansatz into Eq. (6.2.6) yields the infinite system of integral delay differential equations (see Appendix A)

$$\frac{\partial b}{\partial t}(k,t) = i\omega b(k,t) - \frac{\lambda}{2}\left(R^*(k,t-\tau)\, b^2(k,t) - R(k,t-\tau)\right) \tag{6.2.8}$$

$$R(k,t) = \sum_d P(d)\, a(d\to k)\, \frac{1}{2\pi}\int_0^{2\pi} e^{i\theta'}\int_0^{\infty} f\left(\theta',\omega'|d,t\right) d\omega' d\theta'. \tag{6.2.9}$$

Admittedly, these equations do not look much simpler than the finite network (6.2.1), and in a certain sense they aren't. However, a huge advantage is that we got rid of the randomness of the couplings a_{ij}, which are now incorporated in the probability a. This will enable us to infer results valid for any realization of a large scale-free random network. Before we go on investigating scale-free structures, let us define the order parameter for this system.

Definition 36. We define the global order parameter for solutions of Eq. (6.2.8) as

$$r = \left|\sum_d \tilde{P}(d)\, \frac{1}{2\pi}\int_0^{\infty}\int_0^{2\pi} f\left(\theta',\omega'|d,t\right) e^{i\theta'} d\theta' d\omega'\right|.$$

6.3. Scale-free networks with frequency-degree correlations

The previous approach is a generalization of the ideas introduced in [**147**] and reduces to the case considered therein for $\tau = 0$. Let us now assume that we have a scale-free network, that is the degrees are distributed according to a power-law with degree probability

$$\tilde{P}(d) = \frac{1}{\zeta_\gamma} d^{-\gamma} \quad \gamma > 2$$

where

$$\zeta_\gamma = \sum_{d=1}^{\infty} d^{-\gamma}$$

is the normalization and the associated degree distribution P is given by $P = n\tilde{P}$. Let us furthermore assume that the natural frequencies ω_i are positively correlated to the node degrees d_i in the simplest way, that is $\omega_i = d_i$. In other

words, the (conditional) frequency distribution g is given by

$$g(\omega|d) = \delta(\omega - d) \tag{6.3.1}$$

where $\delta(x) = \begin{cases} 1 & x = 0 \\ 0 & \text{else} \end{cases}$ is the Dirac delta function. The main result of this section is the deduction of the main equations in the thermodynamic limit.

THEOREM 37. *For a scale-free network with the above degree and frequency distributions, the thermodynamic limit of Eq. (6.2.1) is given by the following infinite system of delay differential equations*

$$\begin{aligned} \frac{1}{k}\frac{\partial b}{\partial t}(k,t) &= ib(k,t) - \frac{\lambda}{2}\left(\tilde{R}^*(t-\tau)\, b^2(k,t) - \tilde{R}(t-\tau)\right) \\ \tilde{R}(t) &= \frac{1}{\zeta_{\gamma-1}}\sum_d d^{1-\gamma} b(d,t). \end{aligned} \tag{6.3.2}$$

PROOF. Let us first compute the quantity R given by Eq. (6.2.9). Plugging the Ansatz from Eq. (6.2.7) in the integral, all the terms with $e^{in\theta'}$ and $n \neq 0$ chancel out and we obtain

$$\begin{aligned} &\int_0^\infty \int_0^{2\pi} f\left(\theta', \omega'|d, t\right) e^{i\theta'} d\theta' d\omega' \\ = &\int_0^\infty \int_0^{2\pi} \left[1 + \left(\sum_{n=1}^\infty b\left(\omega', d, t\right)^n e^{-in\theta'} + c.c.\right)\right] g\left(\omega'|d\right) e^{i\theta'} d\theta' d\omega' \\ = &\, 2\pi \int_0^\infty g\left(\omega'|d\right) b\left(\omega', d, t\right) d\omega'. \end{aligned}$$

Now, using the form (6.3.1) of the distribution for the natural frequencies, we get

$$\begin{aligned} &\frac{1}{2\pi}\int_0^\infty \int_0^{2\pi} f\left(\theta', \omega'|k, t\right) e^{i\theta'} d\theta' d\omega' \\ = &\int_0^\infty g\left(\omega'|d\right) b\left(\omega', d, t\right) d\omega' \\ = &\int_0^\infty \delta\left(\omega' - d\right) b\left(\omega', d, t\right) d\omega' \\ = &\, b(d,t). \end{aligned}$$

At this step, evaluating the expression (6.2.5) for R we obtain

$$R(k,t) = \sum_d P(d)\, a(d \to k)\, b(d,t). \tag{6.3.3}$$

Now, the probability $a(d \to k)$ that two nodes of degree d and k are connected by a link is proportional to their respective degrees and thus, respecting the normalization given by 6.2.3, we obtain

$$a(d \to k) = \frac{dk}{N\langle k\rangle}.$$

Let us further simplify by using

$$\langle k\rangle \quad = \quad = \sum_d d\tilde{P}\left(d\right) = \frac{\zeta_{\gamma-1}}{\zeta_\gamma}$$

so we get

$$R\left(k,t\right) = \frac{k}{\zeta_{\gamma-1}} \sum_d d^{1-\gamma} b\left(d,t\right)$$

which is just scaled by k. Consequently, we define

$$\tilde{R}\left(t\right) \quad := \quad \frac{1}{\zeta_{\gamma-1}} \sum_d d^{1-\gamma} b_d\left(t\right). \tag{6.3.4}$$

and obtain the above system of DDEs. □

We remind that once we solve the Eqs. (6.3.2) the $b\left(k,t\right)$ yield the density function for the oscillator's phases by Eq. (6.2.7), in our case

$$f\left(\theta,k,t\right) = 1 + \left(\sum_{n=1}^{\infty} b\left(k,t\right)^n e^{-in\theta} + \sum_{n=1}^{\infty} \left(b\left(k,t\right)^n\right)^* e^{in\theta}\right). \tag{6.3.5}$$

As in **[132]** for the non-delayed case we can show the following

LEMMA 38. *Let b be a solution of Eq. (6.3.2) with initial functions $b_0\left(k,t\right)$ satisfying $\sup_{t\in[-\tau,0]} \left|b_0\left(k,t\right)\right| \leq 1$ for all $k \in \mathbb{N}$. Then we have $\left|b\left(k,t\right)\right| \leq 1$ for all $t \geq 0$.*

PROOF. Let us write $b\left(k,t\right) = \left|b\left(k,t\right)\right| e^{-i\psi(k,t)}$. Then the delay differential equation writes as

$$\frac{1}{k}\left(\frac{\partial}{\partial t}\left|b\right|\right) e^{-i\psi} - \frac{i}{k}\left|b\right|\dot{\psi} e^{-i\psi} \quad = \quad ik\left|b\right| e^{-i\psi} - \frac{\lambda}{2}\left(\tilde{R}^*\left|b\right|^2 e^{-2i\psi} - \tilde{R}\right)$$

where we omit the variables (k,t) for the sake of clarity and remind that only $\tilde{R}$ involves time delay. Now, multiplying with $e^{i\psi}$ we obtain

$$\frac{1}{k}\frac{\partial}{\partial t}\left|b\right| - \frac{i}{k}\left|b\right|\dot{\psi} = ik\left|b\right| - \frac{\lambda}{2}\left(\left|b\right|^2 \tilde{R}^* e^{-i\psi} - \tilde{R} e^{i\psi}\right)$$

and finally taking the real part yields

$$\frac{1}{k}\frac{\partial}{\partial t}\left|b\left(t\right)\right| = -\frac{\lambda}{2}\Re\left(\tilde{R}^*\left(t-\tau\right) e^{-i\psi(t)}\right)\left(\left|b\left(t\right)\right|^2 - 1\right).$$

As $\frac{\partial}{\partial t}\left|b\right|$ vanishes for $\left|b\right| = 1$, solutions with initial conditions in the unit circle must stay in the unit circle.

□

This lemma guarantees that the global order parameter r is reasonably defined. Indeed, using the above results we have

$$r = \left|\sum_d \tilde{P}\left(d\right) b\left(d,t\right)\right|. \tag{6.3.6}$$

Hence, the solution with $b(k,t) = 0 \quad \forall k$ corresponds to the incoherent solution and the solution with $b(k,t) = 1 \quad \forall k$ corresponds to the completely synchronous state.

6.4. Existence of rotating waves in scale-free networks

Let us begin to look for the simplest class of solutions, that is solutions which do not depend on time.

THEOREM 39. *The only stationary solution Eq. (6.3.2) admits is the incoherent state.*

PROOF. For a stationary solution we have $\frac{\partial}{\partial t} b(k,t) = 0$. As $b(k,t)$ is then time independent let us write $b(k,t) = b_k \in \mathbb{C}$. Furthermore $\tilde{R}$ is also time independent, so DDE (6.2.8) becomes

$$b_k = \frac{\lambda}{2i}\left(b_k^2 \tilde{R}^* - \tilde{R}\right).$$

As $\tilde{R}$ is a constant independent of k, these are simple quadratic equations

$$0 = b_k^2 - \frac{2i}{\lambda \tilde{R}^*} b_k - \frac{\tilde{R}}{\tilde{R}^*}$$

with solutions

$$b_k = \frac{1}{\lambda \tilde{R}^*}\left[i \pm \sqrt{\left(\lambda \left|\tilde{R}\right|\right)^2 - 1}\right].$$

Plugging these back into the equation for $\tilde{R}$, we obtain a self-consistency relation

$$\begin{aligned}
\tilde{R} &= \frac{1}{\zeta_{\gamma-1}} \sum_d d^{1-\gamma} b_d \\
\iff \zeta_{\gamma-1} \lambda \left|\tilde{R}\right|^2 &= \sum_d d^{1-\gamma}\left[i \pm \sqrt{\left(\lambda \left|\tilde{R}\right|\right)^2 - 1}\right] \\
\iff \lambda \left|\tilde{R}\right|^2 &= i \pm \sqrt{\left(\lambda \left|\tilde{R}\right|\right)^2 - 1}.
\end{aligned}$$

As the left hand side is real, in order to fulfil this equation we must have

$$\left|\tilde{R}\right| = 0$$

and choose the solution β_k with negative sign. But then $b_k = 0$ which corresponds to the incoherent state. □

After having seen that there is only the trivial stationary solution, we investigate simple nonstationary solutions in the model Eqs. (6.3.2). Motivated by the S^1-symmetry of these equations, we make the following Ansatz for rotating waves

$$b_k(t) = e^{i\Omega t} \beta_k$$

where the β_k do not depend on time. This corresponds to a density function f of the form $f(\theta,t,k) = \tilde{f}(\Omega t - \theta, k)$ which is a travelling wave with wave speed Ω. Especially, the waves have the same speed for all degrees k, so we consider phase-locked solutions, that is solutions for which the phase difference between nodes is constant. As in the finite network case, different degrees of coherence can be observed. Here, the size of $|\beta_k|$ determines the amount of coherence among the nodes of degree k whereas the argument of β_k determines their location on the unit sphere. To see this we compute the series from the Ansatz (6.3.5). As in **[132]** we obtain

$$f(\theta,t,k) = \frac{(1-|\beta_k|)(1+|\beta_k|)}{(1-|\beta_k|)^2 + 2|\beta_k|(1-\cos(\theta - \arg(\beta_k)))}.$$

It is easy to check that f has a single maximum at $\theta = \arg(\beta_k)$. Furthermore, the curvature in this point is given by

$$f''(\arg(\beta_k), t, k) = -2|\beta_k| \frac{1+|\beta_k|}{(1-|\beta_k|)^3}$$

and we have $f(\arg(\beta_k)) = \frac{1}{1-|\beta_k|}$. Hence, for $|\beta_k| \to 1$ both, the density and its curvature are unbounded. On the other hand, the integral over f is independent of $|\beta_k|$ and thus, f must approach a delta distribution concentrated in $\arg(\beta_k)$. Now we show that rotating wave solutions can be found by finding the roots of a complex nonlinear function.

THEOREM 40. *$b_k(t) = e^{i\Omega t}\beta_k$ is a solution of Eq. (6.3.2) if*

$$\begin{aligned} \lambda\zeta_{\gamma-1}e^{i\Omega\tau}|M|^2 &= i[\zeta_{\gamma-1} - \Omega\zeta_\gamma] \\ &\quad - \sum_d s\left(1-\frac{\Omega}{d}\right) d^{1-\gamma}\sqrt{\lambda^2|M|^2 - \left(1-\frac{\Omega}{d}\right)^2} \end{aligned} \tag{6.4.1}$$

where

$$M = \frac{e^{-i\Omega\tau}}{\zeta_{\gamma-1}} \sum_d d^{1-\gamma}\beta_d$$

and $s(x)$ designates the sign of the real number x.

PROOF. First, for the quantity $\tilde{R}$ we obtain

$$\tilde{R}(k,t) = \frac{1}{\zeta_{\gamma-1}} e^{i\Omega t} \sum_d d^{1-\gamma}\beta_d.$$

Plugging this into the DDE (6.3.2) yields

$$\frac{i\Omega}{k}\beta_k = i\beta_k - \frac{\lambda}{2}\left(\beta_k^2 \frac{e^{i\Omega\tau}}{\zeta_{\gamma-1}} \sum_d d^{1-\gamma}\beta_d^* - \frac{e^{-i\Omega\tau}}{\zeta_{\gamma-1}} \sum_d d^{1-\gamma}\beta_d\right) \tag{6.4.2}$$

Next set

$$M = \frac{e^{-i\Omega\tau}}{\zeta_{\gamma-1}} \sum_d d^{1-\gamma}\beta_d \tag{6.4.3}$$

to rewrite the last equation as

$$\frac{i\Omega}{k}\beta_k = i\beta_k - \frac{\lambda}{2}\left(\beta_k^2 M^* - M\right). \tag{6.4.4}$$

This is the quadratic equation

$$0 = \beta_k^2 + \frac{2i}{\lambda M^*}\left(\frac{\Omega}{k} - 1\right)\beta_k - \frac{M}{M^*}.$$

As M is independent of k we can solve this equation to obtain

$$\begin{aligned}\beta_k &= -\frac{i}{\lambda M^*}\left(\frac{\Omega}{k} - 1\right) \pm \sqrt{\frac{M}{M^*} - \frac{1}{\lambda^2 (M^*)^2}\left(1 - \frac{\Omega}{k}\right)^2} \\ &= \frac{1}{\lambda M^*}\left[i\left(1 - \frac{\Omega}{k}\right) \pm \sqrt{\lambda^2 |M|^2 - \left(1 - \frac{\Omega}{k}\right)^2}\right]. \qquad (6.4.5)\end{aligned}$$

Now we have to decide which solution to choose. Formally, functions $b(k,t) = e^{i\Omega t}\beta_k$ with arbitrary combinations of β_k constitute a solution of Eq. (6.3.5). However, suppose $\lambda = 0$. Then, by Eq. (6.4.4) we should have $\beta_k = 0$, which makes sense as this corresponds to the incoherent solution, which is to be expected in the case of uncoupled oscillators. So we reject the solution β_k of the quadratic equation which goes to infinity as λ goes to zero. Let us see to which branch this corresponds in Eq. (6.4.5). For $\lambda = 0$, multiplying the equation with λ it writes as

$$0 = i\left(1 - \frac{\Omega}{k}\right) \pm i\left|1 - \frac{\Omega}{k}\right|.$$

So we take the solution with sign $-s\left(1 - \frac{\Omega}{k}\right)$ in order to fulfil this equation, i.e.

$$\beta_k = \frac{1}{\lambda M^*}\left[i\left(1 - \frac{\Omega}{k}\right) - s\left(1 - \frac{\Omega}{k}\right)\sqrt{\lambda^2 |M|^2 - \left(1 - \frac{\Omega}{k}\right)^2}\right]. \tag{6.4.6}$$

Now, plugging these solutions for the β_k back into the Eq. (6.4.3) for M we obtain

$$\begin{aligned}\lambda\zeta_{\gamma-1}e^{i\Omega\tau}|M|^2 &= \sum_d d^{1-\gamma}\left[i\left(1 - \frac{\Omega}{d}\right) - s\left(1 - \frac{\Omega}{d}\right)\sqrt{\lambda^2 |M|^2 - \left(1 - \frac{\Omega}{d}\right)^2}\right] \\ &= i\left[\zeta_{\gamma-1} - \Omega\zeta_\gamma\right] - \sum_d s\left(1 - \frac{\Omega}{d}\right) d^{1-\gamma}\sqrt{\lambda^2 |M|^2 - \left(1 - \frac{\Omega}{d}\right)^2}.\end{aligned}$$

□

The price one has to pay for the non-global coupling is that the equation for $(\Omega, |M|^2)$ is rather involved as it is not possible to explicitly split the complex equation into real and imaginary parts. Even numerically it is very demanding

to solve this equation. However, instead of solving infinitely many DDEs we reduced the problem to finding the roots of a complex function. Also, using the representation for the β_k we can infer the following

LEMMA 41. *Let $b_k(t) = e^{i\Omega t}\beta_k$ be a solution of the system (6.3.2). If we have*

$$\lambda^2 |M|^2 \geq \left(1 - \frac{\Omega}{d}\right)^2$$

for some $d \in \mathbb{N}$, then the nodes of degree d are synchronized.

PROOF. Under this assumption, the square root is real and we can calculate the modulus of β_d as

$$\begin{aligned} |\beta_d|^2 &= \frac{1}{|\lambda M^*|^2}\left[\left(1 - \frac{\Omega}{d}\right)^2 + \lambda^2 |M|^2 - \left(1 - \frac{\Omega}{d}\right)^2\right] \\ &= 1. \end{aligned}$$

As mentioned above in the classification of partially synchronized states, this corresponds to the case where all the nodes of degree d are synchronized. □

A consequence of the last lemma is that for certain rotating wave solutions, there is a simple synchronization hierarchy.

COROLLARY 42. *Let $b_k(t) = e^{i\Omega t}\beta_k$ be a solution of the system (6.3.2) with $\Omega < 1$. Then, if the nodes of degree d are synchronized for some $d \in \mathbb{N}$, all the nodes of degree $k < d$ are synchronized as well. If the nodes of degree d are synchronized for all $d \in \mathbb{N}$ we must have $\lambda \geq 1$.*

PROOF. For the first statement, by assumption the nodes of degree d are synchronized, so $\lambda^2 |M|^2 \geq \left(1 - \frac{\Omega}{d}\right)^2$ by the previous lemma. By the assumption $\Omega < 1$ the function $\left(1 - \frac{\Omega}{d}\right)^2$ is strictly monotonous in d, so we must have $\lambda^2 |M|^2 \geq \left(1 - \frac{\Omega}{d}\right)^2 > \left(1 - \frac{\Omega}{k}\right)^2$ for any $k < d$ and we are done by the previous lemma again. For the second statement remark that by assumption we must have

$$\lambda |M| \geq 1 - \frac{\Omega}{k}$$

for all k. As $|M| \leq 1$ the statement follows. □

We remark that indeed, in the numerical results obtained in **[140]**, the onset of desynchronization is at values $\lambda > 1$ for all values of the delay τ. Also, as can be seen in the next section, in our numerical results the branches of solutions with highest coherence, i.e. largest order parameter indeed fulfil the condition $\Omega < 1$. Hence, led by these observations we hypothesize that the nodes synchronize hierarchically, beginning with degree-one nodes. This can also be observed in simulations of the finite network, as shown in the next section. The case $\Omega \geq 1$ is much more involved and will be treated in future investigations.

6.5. Bifurcations of rotating wave solutions

Having shown the existence of rotating waves in the previous section, we will now investigate their bifurcations numerically by solving Eq. (6.4.1) for $\left(\Omega, |M|^2\right)$. However, before we investigate the existence of rotating wave solutions in the infinite dimensional approximation, let us have a closer look at the dynamics in a finite scale-free network with a positive correlation between the node's degree and their individual frequency. These were investigated in [**140**], however, we want to shed light on the dynamics from a slightly different angle in order to compare the results to the dynamics in the infinite dimensional model.

6.5.1. Bifurcations of rotating wave solutions in finite scale-free networks. As pointed out in the first section, there is no easy way to find coherent solutions in Eq. (6.2.1) analytically, so we investigate the bifurcations numerically. We remark that the displayed bifurcation diagrams are for a fixed coupling structure. However, if the number of oscillators is large the variations between the dynamics for different realizations of the random coupling structure are only quantitative and of very small amount. We simulate Eq. (6.2.1) with a realization of an adjacency matrix A of the size $N = 1000$ representing a scale-free network with the parameter $\gamma = 2.5$. The delay time is chosen as $\tau = 0.5$ and the frequency ω_i equals the degree of node i. In Fig. 6.5.1 a) we plot the global coupling λ against the order parameter r after a transient time $T = 10000$. We observe a seemingly continuous transition from the incoherent to the synchronous state where no hysteresis is observed, i.e. independently of increasing or decreasing the parameter λ the same bifurcation diagrams are obtained. However, looking at it more detailed we see that there is another transition to synchrony.In Fig. 6.5.1 b)-d) we show the distribution of frequencies of the individual oscillators after a transient time together with their respective degrees. For a coupling $\lambda = 1.02$ all the oscillators rotate with the same speed $\Omega \approx 1.7178$ (Fig. 6.5.1 b) and inset). We can write these solutions as

$$\theta_i(t) = \Omega t + \varphi_i \tag{6.5.1}$$

and remark that, despite the fact that all the oscillators have the same frequency, the order parameter r is not equal to one. Consequently, the state must consist of at least two different clusters with constant phase difference $\varphi_j \neq \varphi_k$. Decreasing the coupling by 0.02 to $\lambda = 1$ yields a different picture (Fig. 6.5.1 c)). Oscillators with higher degrees and therefore highest individual frequencies separate from the phase locked cluster. They are not synchronized to the remaining oscillators any more, but they rather rotate with what is almost their individual frequency (see Corollary 42 and remark thereafter). Furthermore, the frequencies of nodes with smaller degrees are now spread around a mean frequency (see inset in Fig. 6.5.1 c)). Hence, what we observe

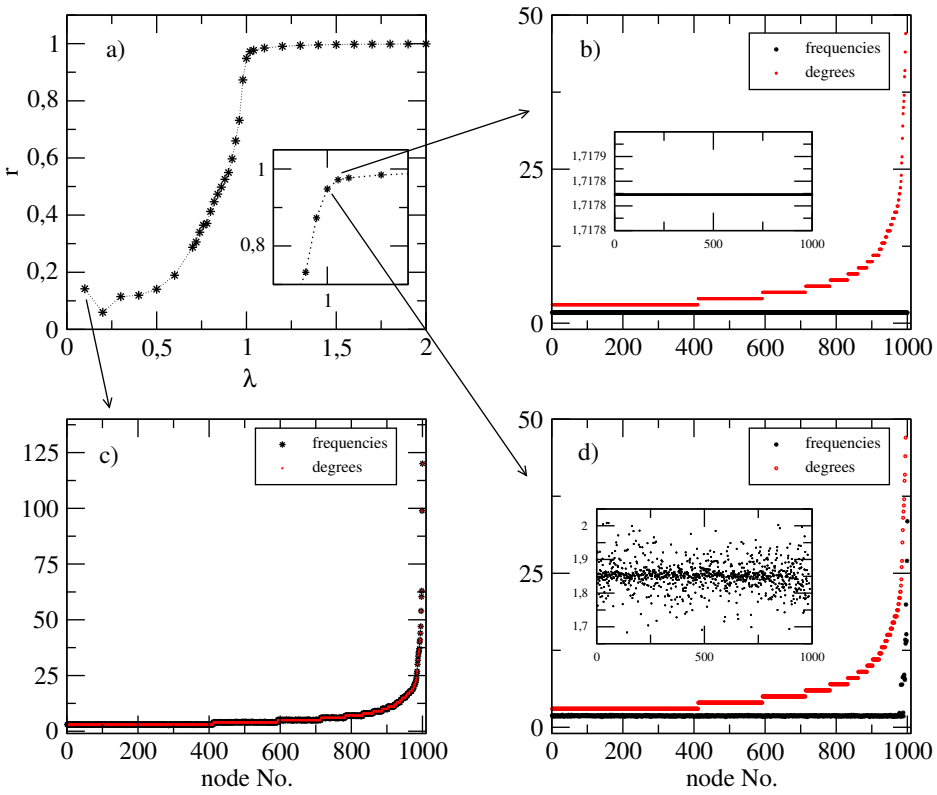

FIGURE 6.5.1. Bifurcations in Eq. (6.2.1) with $\tau = 0.5$ and network size $N = 1000$. In a) the order parameter r is plotted against the global coupling strength λ. The inset shows a magnification. Plots b), c) and d) show frequencies and corresponding degrees of the oscillators for $\lambda = 1.02$ (a), $\lambda = 1$ (b) and $\lambda = 0.1$ (c) after time $T = 10000$. The insets are magnifications of the frequencies.

here is a destabilization of a many-cluster state with constant rotation frequency Ω. Decreasing the coupling further from $\lambda = 1$ increases the variance of the oscillator's frequencies. Beginning with oscillators with higher degrees, more and more oscillators desynchronize until all of them regain their individual frequencies eventually for zero coupling, see Fig. 6.5.1 d) for $\lambda = 0.1$. What is important here is that the range of coupling strengths λ for which all the oscillators are phase-locked at the same frequency is rather small. Or in other words, only taking into account solutions which can be written as in equation (6.5.1) the bifurcation from Fig. 6.5.1 is of first order.

As observed in **[140]**, the bifurcation for $\tau = 1$ is qualitatively different. In Fig. 6.5.2 we show the bifurcation scenario for the same setting as before, so the size of the network is $N = 1000$ and the scaling of the network structure is $\gamma = 2.5$. In a) we plot the global coupling λ against the order parameter

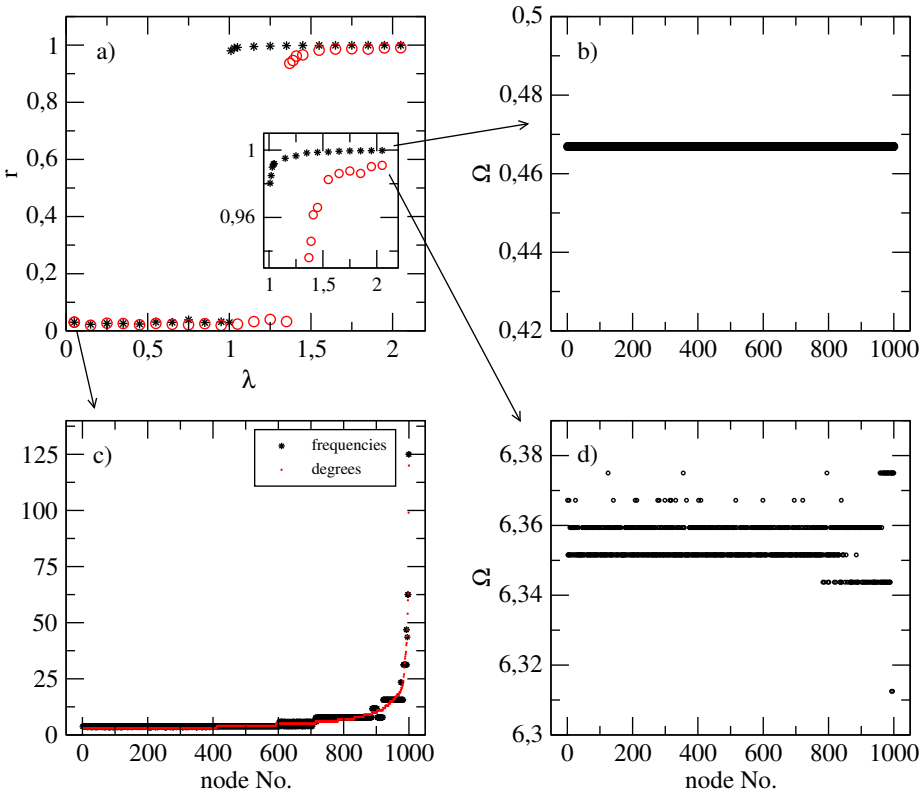

FIGURE 6.5.2. Bifurcations in Eq. (6.2.1) with $\tau = 1$ and network size $N = 1000$. In a) the order parameter r is plotted against the global coupling strength λ. The black stars correspond to values obtained by decreasing λ from 2 to 0 and the red circles to values obtained by increasing λ from 0 to 2. The inset shows a magnification. Plots b), c) and d) show frequencies and corresponding degrees (in c) of the oscillators for $\lambda = 2.05$ (a), $\lambda = 2.05$ (b) and $\lambda = 0.05$ (c) after time $T = 10000$.

r as in the previous figure. We see that in contrast to the previous case, the transition to synchrony does not occur through a gradual increase of the order parameter, but rather through a sudden jump from an incoherent state to an almost synchronous state. Furthermore, the system is now hysteretic: when we decrease the global coupling from $\lambda = 2$ (black stars), a synchronization loss is observed at $\lambda = 1.02$. However, increasing the coupling from $\lambda = 0$, the transition to synchrony appears only at $\lambda = 1.4$. A closer look on the frequencies of these solutions shows that this is indeed a hysteretic loop. Although the order parameters for $\lambda = 2.05$ are almost identical, the frequencies of the corresponding solutions differ essentially (see Fig. 6.5.2 b) and d)). While in b) all the oscillators seem to have the same rotation frequency $\Omega < 1$, the solution in d) has five clusters of considerably higher frequencies, all grouped

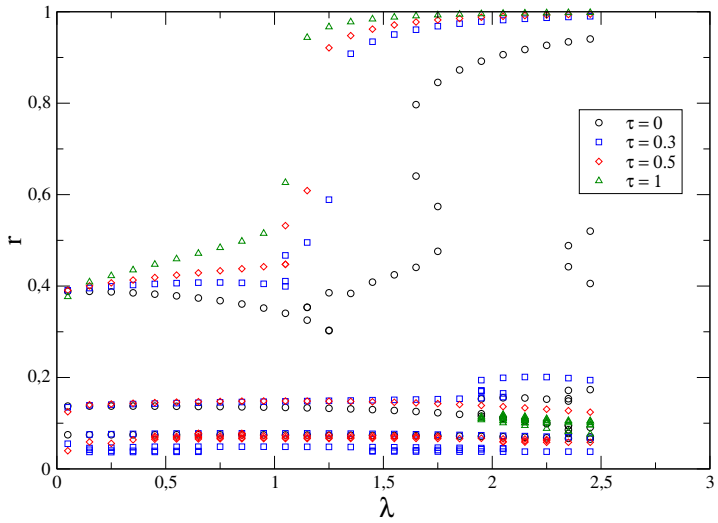

FIGURE 6.5.3. Bifurcation diagram for rotating wave solutions for different values of the time delay τ.

between $\Omega = 6.34$ and $\Omega = 6.38$. Hence, this solution will not be observed in our analysis of the infinite dimensional model in the next section. Another remarkable difference to the previous case is that for a rather small coupling strength of $\lambda = 0.05$, we do not observe the state in which all the oscillators rotate with their own frequency, but certain groups of intermediate-degree nodes are already synchronized.

6.5.2. Bifurcations of rotating waves in the thermodynamic limit. Rotating wave solutions in the thermodynamic limit model (6.3.2) are given by $b_k(t) = e^{i\Omega t}\beta_k$ where Ω and $|M|^2$ are solutions of the complex Eq. (6.4.1). In order to determine the β_k we would have to solve the full system 6.4.2 which consists of an infinite number of equations. Even if we only take into consideration a finite number of degrees, this is still a large computational amount. However, we can easily obtain the moduli $|\beta_k|$ through the obtained solution $(\Omega, |M|^2)$ from Eq. (6.4.1). In the following, we present solutions of Eq. (6.3.2) for degrees up to $k = 2000$. In Fig. 6.5.3 we show bifurcations of rotating waves for different values of the delay τ. First we remark that for delay values $\tau = 0$ and $\tau = 1$ first order transitions to synchrony are observed in the finite network model (see Fig. 6.5.2 and **[140]**). In Fig. 6.5.3 we can observe a large gap in the order parameter at $\lambda \approx 1.1$ for $\tau = 1$ and at $\lambda \approx 1.6$ for $\tau = 0$ and these are in very good agreement with the finite network case. Next we remark that for all four values of time delay τ, the upper branches with order parameter $r \geq 0.85$ correspond to solutions with $|\beta_k| = 1$ for all k. Hence, these are solutions where all the nodes of the same degree are phase synchronized, whereas the synchronized clusters of different degrees can have a constant phase difference, resulting in an order parameter $r < 1$. We remark

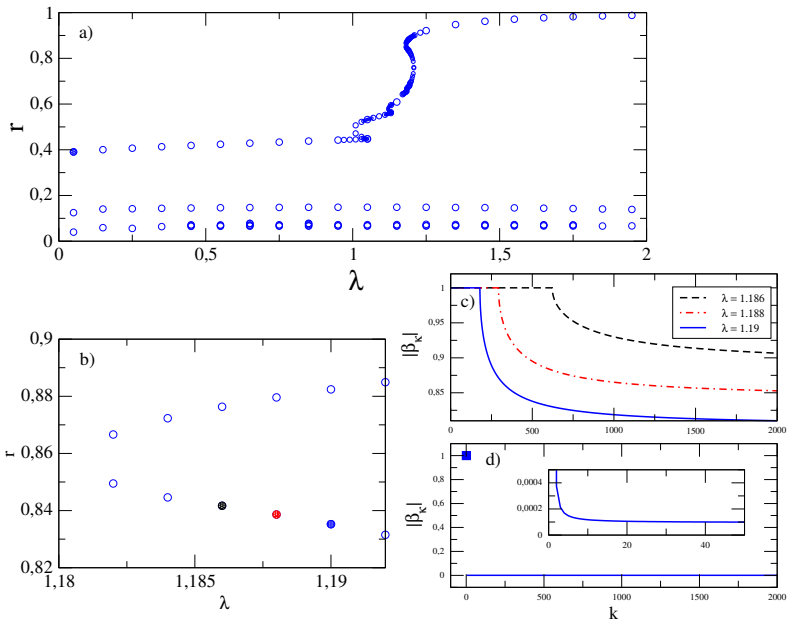

FIGURE 6.5.4. Bifurcations of rotating wave solutions for $\tau = 0.5$. In a) the order parameter r is plotted against the global coupling λ and b) shows a magnification. Plot c) shows the $|\beta_k|$ for different coupling strengths close to the saddle-node bifurcation from b). Plot d) shows the $|\beta_k|$ for a solution at $\lambda = 0.05$.

that the prediction from corollary 42 that $\lambda > 1$ for these states is confirmed by these examples. A striking feature of the bifurcation diagram is that the larger the delay τ, the earlier these solutions appear when increasing λ, and the higher their order parameter is. In other words, increasing the delay yields higher coherence in the dynamics. Of course, this statement does not refer to the stability of the corresponding states.

In Fig. 6.5.4 we show in more detail the bifurcation mechanism for $\tau = 0.5$. The first remarkable feature is that the synchronous state disappears through a saddle-node bifurcation at around $\lambda = 1.18$. As just described, the upper branch consists of solutions in which all nodes with the same degree are synchronized. In the lower branch, one can see that this state transforms into a state in which nodes with higher degrees desynchronize at around $\lambda = 1.185$. In Fig. 6.5.4 c) we show the values of $|\beta_k|$ for the solutions from Fig.6.5.4 b). At $\lambda = 1.186$ nodes up to degrees $k = 623$ are synchronized, resulting in $|\beta_k| = 1$ whereas the modulus of the β_k for nodes with higher degrees decreases gradually (black dashed line). The same picture is obtained for the values $\lambda = 1.188$ (red dash-dotted line) and $\lambda = 1.19$ (blue thick line), where the number of synchronized degrees decreases with λ. In Fig. 6.5.4 d) we show that when λ is decreased down to 0.05, only nodes with degree $k = 1$

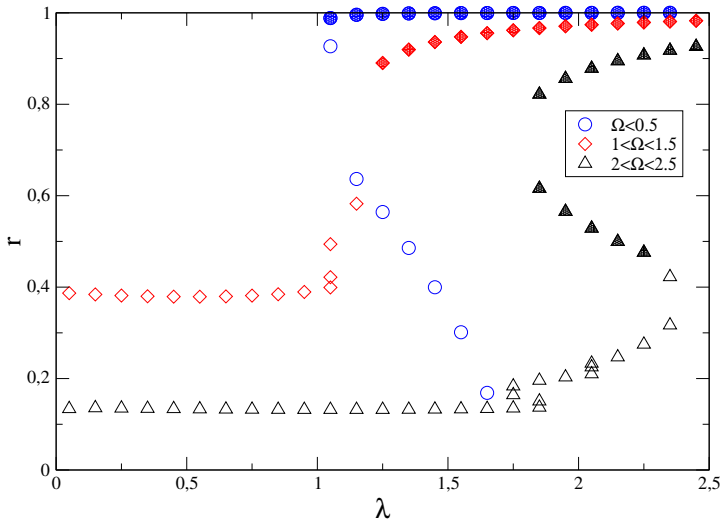

FIGURE 6.5.5. Bifurcations of rotating wave solutions for $\tau = 6$. The different shapes/colours correspond to different branches.

are synchronized, whereas all the other degrees have a $|\beta_k|$ close to zero (see magnification in the inset of d)).

As a last example we shortly want to discuss the case of larger delay times. In Fig. 6.5.5 we show a bifurcation diagram for $\tau = 6$. Again, for the solution of highest coherence we observe a characteristic jump in the order parameter for a coupling λ close to one. A new feature is the appearance of two more branches of high coherence. It is known that periodic solutions reappear when increasing the delay time. More precisely, if a system with delay τ admits a periodic solution of period T, the same solution will exist for $\tilde{\tau} = \tau + T$ [**189**]. Now the observed branch could be a branch of reappearing solutions. The filled circles designate solutions where all the β_k have modulus one. So apart from the appearance of new branches, it is remarkable that these lead to solutions with relatively low order parameter, while all the degree-groups are synchronized. In other words, these correspond to solutions $b_k(t) = e^{i\Omega t}e^{i\varphi_k}$ where the φ_k are the phase differences between the synchronized clusters.

6.5.3. Existence of saddle-node bifurcations. Motivated by the observation of the various saddles in the bifurcation diagrams, we now investigate the occurrence of saddles analytically. In a saddle point $(\lambda, |M|)$ given as solution of Eq. (6.4.1) we must have that $\frac{\partial |M|}{\partial \lambda}$ is unbounded. In order to see when this happens, we first rewrite equation (6.4.1) as

$$\begin{aligned} \Re F(\lambda, \Omega, m) &= 0 \\ \Im F(\lambda, \Omega, m) &= 0 \end{aligned}$$

with $m = |M|^2$ and

$$\begin{aligned} F(\lambda, \Omega, m) &= \lambda m \zeta_{\gamma-1} e^{i\Omega\tau} - i\left[\zeta_{\gamma-1} - \Omega\zeta_\gamma\right] \\ &\quad + \sum_d s\left(1 - \frac{\Omega}{d}\right) d^{1-\gamma} \sqrt{\lambda^2 m - \left(1 - \frac{\Omega}{d}\right)^2}. \end{aligned}$$

This function is differentiable for $\Omega \notin \mathbb{N}$. In this case, by the implicit function theorem we have

$$\frac{\partial(\Omega, m)}{\partial\lambda} = -\frac{\partial F}{\partial(\Omega, m)}^{-1} \frac{\partial F}{\partial\lambda}$$

for regular points (λ, Ω, m). In other words, a saddle appears when the main condition for the implicit function theorem is violated, i.e. $\det\left(\frac{\partial F}{\partial(\Omega,m)}\right) = 0$. Indeed, We obtain the slope of m as

$$m'(\lambda) = \det\left(\frac{\partial F}{\partial(\Omega, m)}\right)^{-1} \left[\Re\left(\frac{\partial F}{\partial\Omega}\right)\Im\left(\frac{\partial F}{\partial\lambda}\right) - \Im\left(\frac{\partial F}{\partial\Omega}\right)\Re\left(\frac{\partial F}{\partial\lambda}\right)\right].$$

So we compute

$$\begin{aligned} \frac{\partial F}{\partial m} &= \lambda\zeta_{\gamma-1} e^{i\Omega\tau} + \frac{\lambda^2}{2} \sum_d \frac{s\left(1 - \frac{\Omega}{d}\right) d^{1-\gamma}}{\sqrt{\lambda^2 m - \left(1 - \frac{\Omega}{d}\right)^2}} \\ \frac{\partial F}{\partial\Omega} &= i\lambda m\tau\zeta_{\gamma-1} e^{i\Omega\tau} + i\zeta_\gamma \\ &\quad - \sum_d \frac{\left|1 - \frac{\Omega}{d}\right| d^{-\gamma}}{\sqrt{\lambda^2 m - \left(1 - \frac{\Omega}{d}\right)^2}}. \end{aligned}$$

As the resulting condition is very involved, let us first restrict to a saddle-node bifurcation of states for which the nodes of degree d are synchronized for all d. Then we have $\lambda^2 m \geq \left(1 - \frac{\Omega}{d}\right)^2$, so

$$\begin{aligned} \det\left(\frac{\partial F}{\partial(\Omega, m)}\right) &= \Re\left(\frac{\partial F}{\partial\Omega}\right)\Im\left(\frac{\partial F}{\partial m}\right) - \Im\left(\frac{\partial F}{\partial\Omega}\right)\Re\left(\frac{\partial F}{\partial m}\right) \\ &= \left[-\lambda m\tau\zeta_{\gamma-1}\sin(\Omega\tau) - \sum_d \frac{\left|1 - \frac{\Omega}{d}\right| d^{-\gamma}}{\sqrt{\lambda^2 m - \left(1 - \frac{\Omega}{d}\right)^2}}\right] \cdot \\ &\quad \cdot \left[\lambda\zeta_{\gamma-1}\sin(\Omega\tau)\right] \\ &\quad - \left[\lambda m\tau\zeta_{\gamma-1}\cos(\Omega\tau) + \zeta_\gamma\right] \cdot \\ &\quad \cdot \left[\lambda\zeta_{\gamma-1}\cos(\Omega\tau) + \frac{\lambda^2}{2} \sum_d \frac{s\left(1 - \frac{\Omega}{d}\right) d^{1-\gamma}}{\sqrt{\lambda^2 m - \left(1 - \frac{\Omega}{d}\right)^2}}\right]. \end{aligned}$$

If we further restrict to $\tau = 0$ the condition for a saddle becomes

$$\begin{aligned} 0 &= \sum_d d^{1-\gamma} + \frac{\lambda}{2} \sum_d \frac{s\left(1-\frac{\Omega}{d}\right) d^{1-\gamma}}{\sqrt{\lambda^2 m - \left(1-\frac{\Omega}{d}\right)^2}} \\ &= \sum_d d^{1-\gamma} \left(1 + \frac{\lambda s \left(1-\frac{\Omega}{d}\right)}{2\sqrt{\lambda^2 m - \left(1-\frac{\Omega}{d}\right)^2}} \right). \end{aligned}$$

Under the above assumptions we can follow from the imaginary part of Eq. (6.4.1) that $\Omega = \frac{\zeta_{\gamma-1}}{\zeta_\gamma} \approx 1.91$. In the general case $\tau \neq 0$ the condition $\det\left(\frac{\partial F}{\partial(\Omega,m)}\right)$ can be used to numerically determine the saddle-node bifurcations.

6.6. Discussion

In this chapter, we have extended a new approach to study large random networks to the case of delayed couplings. This enabled us to study in more detail the dynamics exhibited by a network of phase oscillators with a scale-free coupling topology endowed with a positive correlation between the node degree and the oscillator's individual frequencies. More precisely, we studied the phenomenon of explosive synchronization which was recently discovered in these networks. Introducing a time delay τ, we have observed higher coherence for larger delays in two different meanings. Solutions for which all groups of identical degrees are synchronized appear for smaller coupling strengths λ, and these solutions have higher order parameters. We have shown that independent of the delay τ, the synchronous state disappears through a saddle-node bifurcation. Due to these bifurcations, all the transitions to synchrony are discontinuous when restricted to the class of rotating wave solutions. Consequently, this approach does not explain the second order transitions observed in simulations of the finite networks for certain values of the delay τ. However, it allows us to eliminate the possibility that in these cases, the solutions leading to synchrony are rotating waves. My supervisor S. Yanchuk brought my attention to the appearance of modulated waves, which could be a possible explanation for the second order transition. These are known to appear in systems with rotational symmetry and bifurcate in a scenario much like a Hopf bifurcation from rotating waves. They were previously observed in lattices of differential equations [**87**] and in certain classes of spatially extended reaction-diffusion equations [**156, 157**]. It turned out that other phenomena inherent to spatially extended reaction-diffusion equations such as Turing instabilities can also be observed in their discrete counterparts [**128**]. Hence, it might be a promising idea to look for bifurcations known from spatially extended systems in this case as well.

In general, it is remarkable that even for this rather simple class of rotating wave solutions, the transitions to synchrony seem to be very complex. This rich

behaviour opens up many more questions than we were able to answer here. For instance, the branch of coherent solutions does not undergo a simple saddle-node bifurcation, but rather a sequence of consecutive saddle-node bifurcations, eventually leading to a state of lower coherence. A further investigation of the locations and number of these bifurcations should be done using the methods introduced here. A main difficulty with the existence of rotating wave solutions was posed by the complex equation which defines their parameters. We could gain much more insight once this equation can be tackled in a more elegant way. As mentioned in the introduction, it is important to treat the question whether solutions of the finite network will converge to solutions of the thermodynamic limit equation in some sense. However, this class of problem proved to be very hard **[32, 33]** even for much simpler systems. Finally, we did not characterize stability properties of the described solutions which will certainly be the subject of future investigations.

CHAPTER 7

Conclusion and Outlook

All the problems I investigated in this thesis have one fundamental question in common: What is the relation between a network's coupling structure and the exhibited dynamics? I have not answered this question for arbitrary networks, and most probably there is not just one answer for the most general setting[1]. However, I have shown that, restricting to certain classes of coupling topologies and local dynamics, answers can indeed be found, leading to new insights and perspectives in the theory and applications of coupled dynamical systems. In chapters 2 and 5 I found fundamental structures in rather general settings. By restricting to smaller classes of networks I was able to describe in much detail the dynamics and bifurcations in these networks in chapters 3 and 4. Finally, chapter 6 constitutes an intermediate case which covers a broad class of networks, but still allows for detailed insights in the existence and bifurcations of special solutions.

In my opinion, one of the great challenges in this young and rapidly growing field of research is its interdisciplinary character. Like any other challenge, this can also be understood as an opportunity - an opportunity for inspiring scientists from other disciplines, for opening up new horizons and for developing new tools together. For instance, we have seen in chapter 2 that certain directed networks can behave essentially different from their undirected counterparts. We have also seen that this fact can be traced back to the spectrum of the graph Laplacian. There is a lot of work from algebraic graph theory about the relation between the spectrum of a symmetric Laplacian and the topology of the underlying (undirected) graph. However, there are few results of this type on directed graphs and even worse, as these communities are traditionally quite far away from each other, there is almost no exchange. This example shows, that a collaboration between algebraic graph theory and dynamical systems could be very fruitful. Indeed, we showed this in chapter 5. In collaboration with K. Knauer we determined equivalent classes of delay coupled dynamical systems and unravelled the connection to the graph theoretical notion of the cycle space of a graph. Furthermore, it turned out that our rough main idea for the reduction algorithm was well known in graph theory. This cooperation also demonstrated the need of a common language. Although it might sound trivial, even the use of different words for the same thing, like link/edge or

[1] In a distant future a very powerful computer might find the answer 42 though.

loop/cycle can be quite cumbersome. Following up directly on this we plan another collaboration which includes yet another discipline, namely statistical physics. It was recently brought to my attention by E. Garibaldi from Campinas (Brazil) that there is a simple formula relating the spectral gap of a symmetric Laplacian to a quantity called "entropy of a graph". The entropy of a graph in turn is closely related to the closed paths in the graph, and therefore to its topology. To my knowledge this connection has never been investigated in the theory of dynamics on networks.

The aforementioned issues were related to rather theoretical questions. In chapter 4 we have seen that questions and ideas from applications such as information processing can lead to equally interesting approaches. Here, such a question led me to the detailed analysis of a system of DDEs. It turned out that the pattern recognition device depends on the size of the basins of attraction of certain synchronous solutions. This leads to another interesting question, not only for this application but also from a theoretical point of view and even for other applications. The term "basin stability" was recently introduced for networks with instantaneous couplings, and relies on the analysis of the size of the attractor basins. Although many networks in applications involve delays, to my knowledge this approach was not extended to the case of delayed couplings yet. Indeed, determining attractor basins turns out to be a hard problem even for finite dimensional systems as it involves the analysis of global invariant manifolds. So one can imagine that for the infinite dimensional case of a DDE this problem is even more involved.

I want to mention another question which subtly resonates in many investigations regarding the dynamics in large networks such as in chapter 6. Is there a correspondence between a large network and some appropriately chosen continuum equation? And if so, can we exploit this relation? As mentioned in the last chapter, it was recently shown by H. Chiba that the bifurcation structure in a PDE, constituting the thermodynamic limit of the Kuramoto model, is the same as in the finite dimensional Kuramoto model. Although the proof turned out to be highly non-trivial, Kuramoto was able to make the right guess by using his intuition from the finite dimensional model. In the other way around, in chapter 3 I have investigated a finite dimensional system which was earlier shown to exhibit a cascade of bifurcations similar to a well known bifurcation structure in spatially extended reaction-diffusion systems called Eckhaus scenario[**191**]. But even when the coupling structure is not regular, such correspondences were discovered. For instance it was shown in [**128**] that Turing instabilities, well known from spatially extended reaction-diffusion equations as well, can be observed in large networks with a random coupling structure. Amongst others, they were observed in scale-free networks, which brings me again to chapter 6. Here, I hypothesized that the appearance of modulated waves could explain the bifurcation scenario observed in the finite dimensional model with a scale-free coupling structure. Once again, modulated waves can

be observed in a very similar bifurcation scenario in reaction-diffusion equations [**156**]. So here, one might wonder whether there is a different approach than the one we used here, in order to rigorously relate the scale-free network structure to a reaction-diffusion equation on a properly chosen heterogeneous medium.

I opened this thesis with the description of a problem raised by S. Smale in 1976. Now let me close with a similar problem, raised almost 40 years later by M. Golubitsky which was recently brought to my attention by M. Wolfrum. Consider a network in the setting of chapter 2. We have seen that the eigenvectors belonging to nonzero eigenvalues of the network Laplacian correspond to transverse directions of the synchronous manifold. Now, the question is whether for any given eigenvector of the Laplacian, the pair $(\boldsymbol{f}, \boldsymbol{H})$ can be chosen such that the synchronous manifold is stable in all eigendirections except for the prescribed one. To my knowledge this problem is still unsolved and indeed, appears to be nontrivial. Using ideas and methods developed in this thesis I believe it is worth a try to tackle it. This problem and many others, some of which I described in this thesis, still await for pioneering work in the field of dynamics on networks. During my time as a PhD student I was always fascinated by the diversity of problems and methods in this field, and I hope that I will keep this fascination as long as possible.

Appendix A

Here, we derive the system of DDEs from the continuity equation by using the Ansatz (6.2.7) in section 6.2. Omitting g which is a factor on both sides of the equation and independent of θ and t, we have

$$\partial_t f = \sum_{n=1}^{\infty} n\left(\partial_t b\right) b^{n-1} e^{-in\theta} + \sum_{n=1}^{\infty} n\left(\partial_t b^*\right)\left(b^*\right)^{n-1} e^{in\theta}$$

and

$$\begin{aligned}\partial_\theta\left(vf\right) &= \left[\lambda\Im\left(-ie^{-i\theta}R\right)\right] f + \left[k + \lambda\Im\left(e^{-i\theta}R\right)\right]\partial_\theta f \\ &= \left[-\frac{\lambda}{2}\left(e^{-i\theta}R + e^{i\theta}R^*\right)\right] f + \left[\omega + \frac{\lambda}{2i}\left(e^{-i\theta}R - e^{i\theta}R^*\right)\right]\partial_\theta f\end{aligned}$$

Furthermore,

$$\begin{aligned}e^{-i\theta}f &= e^{-i\theta} + \sum_{n=1}^{\infty} b\left(\omega,k,t\right)^n e^{-i(n+1)\theta} + \sum_{n=1}^{\infty} b^*\left(\omega,k,t\right)^n e^{i(n-1)\theta} \\ e^{i\theta}f &= e^{i\theta} + \sum_{n=1}^{\infty} b\left(\omega,k,t\right)^n e^{-i(n-1)\theta} + \sum_{n=1}^{\infty} b^*\left(\omega,k,t\right)^n e^{i(n+1)\theta}\end{aligned}$$

and

$$\begin{aligned}\partial_\theta f &= -i\sum_{n=1}^{\infty} nb\left(\omega,k,t\right)^n e^{-in\theta} + i\sum_{n=1}^{\infty} nb^*\left(\omega,k,t\right)^n e^{in\theta} \\ e^{-i\theta}\partial_\theta f &= -i\sum_{n=1}^{\infty} nb\left(\omega,k,t\right)^n e^{-i(n+1)\theta} + i\sum_{n=1}^{\infty} nb^*\left(\omega,k,t\right)^n e^{i(n-1)\theta} \\ e^{i\theta}\partial_\theta f &= -i\sum_{n=1}^{\infty} nb\left(\omega,k,t\right)^n e^{-i(n-1)\theta} + i\sum_{n=1}^{\infty} nb^*\left(\omega,k,t\right)^n e^{i(n+1)\theta}.\end{aligned}$$

Comparing the coefficients of the term $e^{-i\theta}$ in the equation $\partial_t f = -\partial_\theta\left(vf\right)$ finally yields

$$\begin{aligned}\partial_t b &= -\left[-\frac{\lambda}{2}\left(b^2R^* + R\right) - i\omega b + \frac{\lambda}{2i}\left(2ib^2R^*\right)\right] \\ &= \frac{\lambda}{2}\left(b^2R^* + R\right) - \frac{\lambda}{2}\left(2b^2R^*\right) + i\omega b \\ &= -\frac{\lambda}{2}\left(b^2R^* - R\right) + i\omega b.\end{aligned}$$

Doing the same for the coefficients of $e^{i\theta}$ yields the conjugated equation. Surprisingly enough this equation or its conjugation is obtained when comparing the coefficients of any of the $e^{\pm in\theta}$.

Appendix B

Adjacency spectrum for large s

To apply the implicit function theorem and continue roots of the characteristic equation (3.2.5) for the case of large s, we define

$$F(\lambda,\tau,\vartheta)=\tau\lambda^N-\lambda^{\ell-1}-\vartheta. \tag{7.0.1}$$

Then $F\left(\lambda,\frac{1}{s},\frac{1}{s}\right)=0$ is equivalent to (3.2.5). We now apply the implicit function theorem twice to find the two distinct families (3.2.7) and (3.2.8) of small and large solutions of (3.2.5). Let us first compute

$$\begin{aligned}\partial_\lambda F(\lambda,\tau,\vartheta) &= \tau N\lambda^{N-1}-(\ell-1)\lambda^{\ell-2},\\ \partial_\tau F(\lambda,\tau,\vartheta) &= \lambda^N, \qquad \partial_\vartheta F(\lambda,\tau,\vartheta)=-1.\end{aligned} \tag{7.0.2}$$

Consider the equation

$$F(\lambda,0,\vartheta)=-\lambda^{\ell-1}-\vartheta=0. \tag{7.0.3}$$

It possesses $\ell-1$ solutions

$$\lambda_{1,k}(0,\vartheta)=\vartheta^{\frac{1}{\ell-1}}e^{i\frac{\pi}{\ell-1}}\gamma_{\ell-1,k},$$

$k=0,...,\ell-2$. Assuming (we show that below) that for $(\tau,\vartheta)\neq 0$ one can extend these solutions to smooth functions $(\tau,\vartheta)\mapsto\lambda_{1,k}(\tau,\vartheta)$ which solve $F(\lambda_{1,k}(\tau,\vartheta),\tau,\vartheta)=0$. These can be expanded in $\tau=0$ as

$$\begin{aligned}\lambda_{1,k}(\tau,\vartheta) &= \lambda_{1,k}(0,\vartheta)-\partial_\lambda F(\lambda_{1,k}(0,\vartheta),0,\vartheta)^{-1}\partial_\tau F(\lambda_{1,k}(0,\vartheta),0,\vartheta)\tau+\mathcal{O}\left(\tau^2\right)\\ &= \lambda_{1,k}(0,\vartheta)+\left((\ell-1)\lambda_{1,k}^{\ell-2}(0,\vartheta)\right)^{-1}\lambda_{1,k}^N(0,\vartheta)\tau+\mathcal{O}\left(\tau^2\right)\\ &= \lambda_{1,k}(0,\vartheta)+\frac{\lambda_{1,k}^{N-\ell+2}(0,\vartheta)}{\ell-1}\tau+\mathcal{O}\left(\tau^2\right)\end{aligned}$$

and for $\vartheta=\tau$,

$$\lambda_{1,k}(\tau,\tau)=\lambda_{1,k}(0,\tau)+\frac{\lambda_{1,k}^{N-\ell+2}(0,\tau)}{\ell-1}\tau+\mathcal{O}\left(\tau^2\right). \tag{7.0.4}$$

This gives a family of $\ell-1$ solutions of (3.2.5) situated near a small circle of radius $\sim(1/s)^{\frac{1}{\ell-1}}$. For $\tau\neq 0$, the equation

$$F(\lambda,\tau,0)=\tau\lambda^N-\lambda^{\ell-1}=0 \tag{7.0.5}$$

has an $(\ell-1)$-fold root at $\lambda=0$ which corresponds to the solutions of (7.0.3) and $N-\ell+1$ roots

$$\lambda_{2,k}(\tau,0)=|\tau|^{-\frac{1}{N-\ell+1}}\gamma_{N-\ell+1,k} \tag{7.0.6}$$

$k=0,...,N-\ell$. As before, we obtain an asymptotic representation

$$\begin{aligned}\lambda_{2,k}(\tau,\tau) &= \lambda_{2,k}(\tau,0)-\partial_\lambda F(\lambda_{2,k}(\tau,0),\tau,0)^{-1}\partial_\vartheta F(\lambda_{2,k}(\tau,0),\tau,0)\tau+\mathcal{O}\left(\tau^2\right)\\ (7.0.7)&= \lambda_{2,k}(\tau,0)+\chi'_{G_s}(\lambda_{2,k}(\tau,0))^{-1}\tau+\mathcal{O}\left(\tau^2\right)\end{aligned}$$

This is the family of solutions which lie near a larger circle of radius $\sim s^{\frac{1}{N-\ell+1}}$.

Now let us show that the interval of existence of the implicit functions $\tau\mapsto\lambda_{1,k}(\tau,\vartheta_0)$ and $\vartheta\mapsto\lambda_{2,k}(\tau_0,\vartheta)$, respectively, indeed contain the points $\tau=\vartheta_0$ and $\vartheta=\tau_0$, respectively. Let us denote the implicit function in question simply $\lambda(\tau,\vartheta)$. If the implicit function theorem fails to provide an extension of $\lambda(\tau,\vartheta)$ in some point $(\tau_*,\vartheta_*)>0$, we must have

$$\partial_\lambda F(\lambda_*,\tau_*,\vartheta_*)=\tau_* N\lambda_*^{N-1}-(\ell-1)\lambda_*^{\ell-2}=0 \tag{7.0.8}$$

where $\lambda_*=\lambda(\tau_*,\vartheta_*)$. Since $F(0,\tau,\vartheta)=0$ is equivalent to $\vartheta=0$, we may assume $\lambda_*\neq 0$. Thus, (7.0.8) is equivalent to

$$\lambda_*^{N-\ell+1}=\frac{\ell-1}{N\tau_*}. \tag{7.0.9}$$

Furthermore, from (7.0.1)$=0$ we obtain $\tau_*=\lambda^{\ell-1-N}+\vartheta_*\lambda^{-N}$ which we insert into (7.0.8) to obtain

$$\lambda_*^{\ell-1}=-\frac{N}{N-\ell+1}\vartheta_*. \tag{7.0.10}$$

From (7.0.9) and (7.0.10), we obtain

$$\tau_*=\Gamma(\vartheta_*):=\frac{\ell-1}{N}\left(\frac{N-\ell+1}{N}\right)^{\frac{N-\ell+1}{\ell-1}}\vartheta_*^{-\frac{N-\ell+1}{\ell-1}}.$$

Since $\Gamma:\mathbb{R}_{>0}\to\mathbb{R}_{>0}$ is monotonic, we have

$$\partial_\lambda F(\lambda(\tau,\vartheta_*),\tau,\vartheta_*)\neq 0$$

for all $\tau<\tau_*=\Gamma(\vartheta_*)$. Since $\Gamma(\tau)\to\infty$, for $\tau\searrow 0$, there exists $\tau_0>0$ such that $\tau<\Gamma(\tau)$ and $\lambda(\tau,\tau)$ is defined uniquely, for $0<\tau<\tau_0$.

Supercriticality of the Hopf bifurcations

To show that the bifurcations at $\alpha=-\Re(\lambda)$ of system (3.2.1) are supercritical for sufficiently large $s\geq 0$, we use the projection method for center manifolds [**103**]. In the following, we write the vector field of (3.2.1) as

$$f_\alpha(\boldsymbol{z})=\boldsymbol{A}\boldsymbol{z}+\frac{1}{6}\boldsymbol{C}(\boldsymbol{z},\boldsymbol{z},\boldsymbol{z}),$$

where $\boldsymbol{A} = \boldsymbol{I}_N \otimes \boldsymbol{M}_\mu + \boldsymbol{G}_s \otimes \boldsymbol{I}_2$ is the linearization of f_α at $\boldsymbol{z} = 0$ and the trilinear function $\boldsymbol{C}$ contains all cubic terms. Furthermore, let $\boldsymbol{v} \in \mathbb{R}^{2N}$ be an eigenvector of $\boldsymbol{A}$ corresponding to the eigenvalue $\mu + \lambda$, $\lambda \in \sigma(\boldsymbol{G}_s)$. (The case of an eigenvalue $\bar{\mu} + \lambda$ can be treated analogously.) Let $\boldsymbol{w} \in \mathbb{R}^{2N}$ be the normalized adjoint eigenvector corresponding to $\boldsymbol{v}$, i.e. $\boldsymbol{A}^T \boldsymbol{w} = (\bar{\mu} + \bar{\lambda})\boldsymbol{w}$ and $\boldsymbol{w} \cdot \boldsymbol{v} = 1$. We have

$$\boldsymbol{v} = \left(1, \lambda, ..., \lambda^{N-1}\right)^T \otimes (i, 1)^T, \tag{7.0.11}$$

$$\boldsymbol{w} = \frac{1}{\bar{\kappa}} \left(\overline{\lambda}^{\ell-1}, ..., \overline{\lambda}, \overline{\lambda}^N, ..., \overline{\lambda}^\ell\right)^T \otimes (i, 1)^T, \tag{7.0.12}$$

with $\kappa = 2\lambda^{\ell-1}((\ell-1) + (N-\ell+1)\lambda^N)$. A Hopf bifurcation at α is supercritical for a negative and subcritical for a positive first Lyapunov coefficient

$$l_1(0) = \frac{1}{2\omega_0^2} \Re\left(\boldsymbol{w} \cdot \boldsymbol{C}(\boldsymbol{v}, \boldsymbol{v}, \overline{\boldsymbol{v}})\right), \tag{7.0.13}$$

where $\omega_0 = \beta + \Im(\lambda) \neq 0$. Writing $\boldsymbol{C} = (\boldsymbol{C}_{1,1}, \boldsymbol{C}_{1,2}, \ldots, \boldsymbol{C}_{N,1}, \boldsymbol{C}_{N,2})$ we obtain

$$\boldsymbol{C}_{j,1}(\boldsymbol{v}, \boldsymbol{v}, \overline{\boldsymbol{v}}) = -6v_{j,1}|v_{j,1}|^2 - 2\left(2v_{j,1}|v_{j,2}|^2 + v_{j,2}^2 \overline{v}_{j,1}\right) = i\boldsymbol{C}_{j,2}(\boldsymbol{v}, \boldsymbol{v}, \overline{\boldsymbol{v}}), \tag{7.0.14}$$

for $1 \leq j \leq N$. Using this, we get

$$\langle \boldsymbol{w}, \boldsymbol{C}(\boldsymbol{v}, \boldsymbol{v}, \overline{\boldsymbol{v}})\rangle = -8\left(\frac{\sum_{j=1}^{\ell-1}|\lambda|^{2(j-1)} + \lambda^N \sum_{j=\ell}^{N}|\lambda|^{2(j-1)}}{(\ell-1) + (N-\ell+1)\lambda^N}\right). \tag{7.0.15}$$

For large $s > 0$ we distinguish two cases. For the case $|\lambda| \sim s^{1/N-\ell+1}$, we find that

$$\Re\left(\boldsymbol{w} \cdot \boldsymbol{C}(\boldsymbol{v}, \boldsymbol{v}, \overline{\boldsymbol{v}})\right) \to -\infty, \text{ as } s \to \infty,$$

and for the case $|\lambda| \sim s^{-1/\ell-1}$,

$$\Re\left(\boldsymbol{w} \cdot \boldsymbol{C}(\boldsymbol{v}, \boldsymbol{v}, \overline{\boldsymbol{v}})\right) \nearrow 0, \text{ as } s \to \infty.$$

This means that for sufficiently large s, we have $l_1(0) < 0$ for all eigenvalues. Thus, all bifurcations are supercritical.

Supercriticality for an inhomogeneous ring. Consider the case $\ell = 1$ and s arbitrary, i.e. a ring with inhomogeneous coupling strengths. Here, using (7.0.15) and the characteristic equation, $\lambda^N = 1 + s$, we get

$$\boldsymbol{w} \cdot \boldsymbol{C}(\boldsymbol{v}, \boldsymbol{v}, \overline{\boldsymbol{v}}) = -\frac{8\left(1 - (1+s)^2\right)}{N\left(1 - |1+s|^{2/N}\right)}. \tag{7.0.16}$$

Thus, in the case of the inhomogeneous ring the bifurcation is supercritical for arbitrary s.

Expansion of the solution profiles for small perturbations

The linearization of (3.3.8)–(3.3.9) at (3.3.10) is

$$\begin{aligned} 0 &= \left(\alpha + i\left(\beta-\omega\right) - \varepsilon\left|v_j\right|^2\right) + \frac{v_{j+1}}{v_j}, \\ 0 &= \left(\alpha + i\left(\beta-\omega\right) - \varepsilon\left|v_N\right|^2\right) + \frac{v_1}{v_N} + s\frac{v_\ell}{v_N}. \end{aligned} \tag{7.0.17}$$

From these equations we will now find expressions for the first terms of the Taylor expansions of the unknown functions

$$\omega_k\left(\varepsilon,s\right) = \omega_{00} + \varepsilon\omega_{10} + s\omega_{11} + \mathcal{O}\left(\left(\left|\varepsilon\right|+\left|s\right|\right)^2\right)$$

and

$$v_j\left(\varepsilon,s\right) = v_j^{00} + \varepsilon v_j^{10} + s v_j^{01} + \mathcal{O}\left(\left(\left|\varepsilon\right|+\left|s\right|\right)^2\right),\ j=1,...,N.$$

Terms at order $\mathcal{O}\left(1\right)$. Considering the terms in $s=\varepsilon=0$ in (7.0.17) yields the circular equations (let $v_{N+1}^{00} := v_1^{00}$)

$$0 = \alpha^0 + i(\beta-\omega_{00}) + \frac{v_{j+1}^{00}}{v_j^{00}}, \tag{7.0.18}$$

with the shorthand $\alpha^0 = \alpha_k\left(0\right) = -\cos\left(2\pi k/N\right)$. This leads to

$$\left(-\alpha^0 - i\left(\beta-\omega_{00}\right)\right)^N = 1$$

which contains no new information, since it only determines $\alpha^0 = -\Re\left(\lambda_0\right)$ and $\omega_{00} = \beta + \Im\left(\lambda_0\right)$ with an N-th root of unity

$$\lambda_0 = \lambda_k\left(0\right) = e^{i\frac{2\pi k}{N}}.$$

For the profile, (7.0.18) yields

$$v_{j+1}^{00} = \lambda_0^j r_0, \tag{7.0.19}$$

with a hitherto unknown scale factor $r_0 := v_1^{00}$. Without loss of generality, one may choose $v_1\left(\varepsilon,s\right) \in \mathbb{R}_{\geq 0}$, because of the phase shift invariance of (3.3.2). In particular, we then have $r_0 \in \mathbb{R}_+$.

Terms at order $\mathcal{O}\left(\varepsilon\right)$. At first order in ε we obtain another set of circular equations (let again $v_{N+1}^{10} = v_1^{10}$)

$$0 = 1 - i\omega_{10} - r_0^2 + \frac{\lambda_0}{r_0}\left(\frac{v_{j+1}^{10}}{\lambda_0^j} - \frac{v_j^{10}}{\lambda_0^{j-1}}\right)$$

which leads us to the following recursion

$$\frac{v_{j+1}^{10}}{\lambda_0^j} = \left(r_0^2 - \left(1-i\omega_{10}\right)\right)\frac{r_0}{\lambda_0} + \frac{v_j^{10}}{\lambda_0^{j-1}} \tag{7.0.20}$$

Defining $a_j = \frac{v_j^{10}}{\lambda_0^{j-1}}$ and $A = \left(r_0^2 - \left(1-i\omega_{10}\right)\right)\frac{r_0}{\lambda_0}$, Eq. (7.0.20) can be written as $a_{j+1} = A + a_j$ with the solution $a_{j+1} = jA + a_1$. Because of the circularity

$a_{N+1} = a_1$ we then have $a_1 = NA + a_1$ which determines $A = 0$. Therefore, $r_0^2 = (1 - i\omega_{10})$ and finally

$$\omega_{10} = 0 \text{ and } r_0 = 1 \tag{7.0.21}$$

That means at first order the frequency of the oscillations does not depend on ε. For the profiles v_j^{10} it follows (as at order $\mathcal{O}(1)$)

$$v_{j+1}^{10} = \lambda_0^j r_{10}, \tag{7.0.22}$$

with $r_{10} := v_1^{10} \in \mathbb{R}$.

Terms at $\mathcal{O}(s)$. Due to the fact that s perturbs the network symmetry, the equations at order $\mathcal{O}(s)$ are more complex than those at order $\mathcal{O}(\varepsilon)$. Again, the linear terms in s of (7.0.17) give a recursive formula

$$\begin{aligned} \frac{v_{j+1}^{01}}{\lambda_0^j} &= \frac{1}{\lambda_0}\left(i\omega_{01} - \alpha^1\right) + \frac{v_j^{01}}{\lambda_0^{j-1}}, \\ v_1^{01} &= \frac{1}{\lambda_0}\left(i\omega_{01} - \alpha^1\right) - \lambda_0^{\ell-1} + \frac{v_N^{01}}{\lambda_0^{N-1}}, \end{aligned} \tag{7.0.23}$$

where $\alpha^1 = -\frac{d}{ds}\Re\left(\lambda_k(s)\right)|_{s=0}$. For $j < N$ we have $\frac{v_{j+1}^{01}}{\lambda_0^j} = \frac{j}{\lambda_0}\left(i\omega_{01} - \alpha^1\right) + v_1^{01}$. Inserting the resulting expression for v_N^{01} in the second equation gives $v_1^{01} = \frac{N}{\lambda_0}\left(i\omega_{01} - \alpha^1\right) - \lambda_0^{\ell-1} + v_1^{01}$. Therefore, $N\left(i\omega_{01} - \alpha^1\right) = \lambda_0^\ell$ or equivalently

$$\omega_{01} = \frac{1}{N}\Im\left(\lambda_0^\ell\right) \text{ and } \alpha^1 = -\frac{1}{N}\Re\left(\lambda_0^\ell\right). \tag{7.0.24}$$

The perturbations v_{j+1}^{01} of the profile are then determined as

$$v_{j+1}^{01} = \left(\frac{j}{N}\lambda_0^{\ell-1} + r_{01}\right)\lambda_0^j. \tag{7.0.25}$$

up to a scaling $r_{01} := v_1^{01} \in \mathbb{R}$ as above.

Higher order terms. To determine the amplitudes r_{10} and r_{01} of the perturbations v_j^{10} and v_j^{01}, $j = 1, ..., N$, we need to calculate the second order terms $\mathcal{O}\left(\varepsilon^2\right)$, $\mathcal{O}\left(s^2\right)$, and $\mathcal{O}(\varepsilon \cdot s)$ of (7.0.17) due to the nonlinear term. We omit this here and just give the resulting values

$$r_{10} = 0 \text{ and } r_{01} = 0. \tag{7.0.26}$$

The vanishing r_{10} means that at first order the profiles do not depend on ε.

Expansion of the solution profiles for the inhomogeneous ring

A periodic solution of (3.4.5) corresponds to a fixed point in co-rotating coordinates (3.3.7). The stability of this fixed point is governed by its variational

equations

$$\dot{\boldsymbol{x}}_j = \left(\boldsymbol{M}_{\alpha+i(\beta-\omega)} - \varepsilon(s)\left|v_j\right|^2 \begin{bmatrix} 3 & 0 \\ 0 & 1 \end{bmatrix}\right)\dot{\boldsymbol{x}}_j + \boldsymbol{M}_{\frac{v_{j+1}}{v_j}}\dot{\boldsymbol{x}}_{j+1}, \tag{7.0.27}$$

$$\dot{\boldsymbol{x}}_n = \left(\boldsymbol{M}_{\alpha+i(\beta-\omega)} - \varepsilon(s)\left|v_n\right|^2 \begin{bmatrix} 3 & 0 \\ 0 & 1 \end{bmatrix}\right)\dot{\boldsymbol{x}}_n + s\boldsymbol{M}_{\frac{v_1}{v_n}}\dot{\boldsymbol{x}}_1, \tag{7.0.28}$$

Higher order terms of $\omega = \omega(\varepsilon, s)$ and $v_j = v_j(\varepsilon, s)$ can be determined by the equations

$$0 = (\alpha + i(\beta-\omega)) - \varepsilon\left|v_j\right|^2 + \frac{v_{j+1}}{v_j}, \tag{7.0.29}$$

$$0 = (\alpha + i(\beta-\omega)) - \varepsilon\left|v_n\right|^2 + s\frac{v_1}{v_n}, \tag{7.0.30}$$

which are obtained from inserting the solution Ansatz (3.3.2) into (3.4.5). Solving for real and imaginary parts yields the conditions

$$\omega - \beta = \Im\left(\frac{v_{j+1}}{v_j}\right) = s\Im\left(\frac{v_1}{v_n}\right), \tag{7.0.31}$$

$$\alpha = \varepsilon\left|v_j\right|^2 - \Re\left(\frac{v_{j+1}}{v_j}\right) = \varepsilon\left|v_n\right|^2 - s\Re\left(\frac{v_1}{v_n}\right). \tag{7.0.32}$$

Note that we expand the unknown functions only in ε, keeping s arbitrary. Using (7.0.31) and (7.0.32) the variational equations (7.0.27)–(7.0.28) write

$$\dot{\boldsymbol{x}}_j = -\left[\boldsymbol{M}_{\frac{v_{j+1}}{v_j}} + 2\varepsilon \mid v_j \mid^2 \begin{pmatrix} 1 & 0 \\ 0 & 0 \end{pmatrix}\right]\boldsymbol{x}_j + \boldsymbol{M}_{\frac{v_{j+1}}{v_j}}\boldsymbol{x}_{j+1}, \tag{7.0.33}$$

$$\dot{\boldsymbol{x}}_n = -\left[s\boldsymbol{M}_{\frac{v_1}{v_n}} + 2\varepsilon \mid v_n \mid^2 \begin{pmatrix} 1 & 0 \\ 0 & 0 \end{pmatrix}\right]\boldsymbol{x}_n + s\boldsymbol{M}_{\frac{v_1}{v_n}}\boldsymbol{x}_1. \tag{7.0.34}$$

In the rest of this section, we find expressions for $\frac{v_{j+1}}{v_j}(0, s)$ and $\frac{\partial}{\partial\varepsilon}\left[\frac{v_{j+1}}{v_j}(\varepsilon, s)\right]_{|\varepsilon=0}$ which can be inserted into (7.0.33)–(7.0.34) to obtain (3.4.6). Let

$$\omega(\varepsilon, s) = \omega_0(s) + \varepsilon\omega_1(s) + \mathcal{O}\left(\varepsilon^2\right)$$

and

$$v_j(\varepsilon, s) = v_j^0(s) + \varepsilon v_j^1(s) + \mathcal{O}\left(\varepsilon^2\right),\ j = 1, ..., N.$$

For $\varepsilon = 0$, Eqs. (7.0.29)–(7.0.30) yield

$$v_{j+1}^0 = (i(\omega_0 - \beta) - \alpha_0)\, v_j^0 = ... = (i(\omega_0 - \beta) - \alpha_0)^j\, v_1^0,$$

$$v_1^0 = \frac{1}{s}(i(\omega_0 - \beta) - \alpha_0)\, v_n^0,$$

where $\alpha_0 = -\Re(\lambda_k(s)) = -s^{1/n}\cos(2\pi k/n)$ is the critical value at which the periodic solution emerges, $\omega_0 = \beta + \Im(\lambda_k)$ is the initial frequency, and the initial profile is given by $v_j^0 = \lambda_k^{j-1} v_1^0$.

For terms of order $\mathcal{O}(\varepsilon)$ one obtains

$$\omega_1 = 0,\ \left|v_1^0\right|^2 = n\frac{s^{\frac{2}{n}}-1}{s^2-1},\ \text{and}\ v_j^1 = v_j^0\sum_{l=0}^{j-1}\left(|v_{j-l}^0|^2-1\right)+\lambda_k^j v_1^1.$$

To approximate (7.0.33)–(7.0.34), we calculate the first order terms of the quotients v_{j+1}/v_j, which gives at $\mathcal{O}(\varepsilon^0)$

$$\frac{v_{j+1}^0}{v_j^0} = s^{1/n}\gamma_{n,k},$$

and at $\mathcal{O}(\varepsilon)$

$$\left(\frac{v_{j+1}}{v_j}\right)^1 \quad = \quad \left|v_j^0\right|^2 - 1.$$

Appendix C

Here, we show that indeed, a delay differential equation can be interpreted as a hyperbolic PDE. In the general case which includes partial differential equations with delay, we consider $X = C([-\tau, 0], Y)$ as phase space where Y is some Banach space. Furthermore, let $L \in \mathcal{L}(X, Y)$ be a bounded linear operator and $(B, \mathcal{D}(B))$ be the generator of a strongly continuous semigroup $(S(t))_{t\geq 0}$ on Y. This operator can incorporate, for instance, spatial derivatives. Now we consider the abstract delay differential equation (ADDE)

$$\begin{aligned} \dot{u}(t) &= Bu(t) + Lu_t \quad t \geq 0 \\ u_0 &= \varphi \in X \end{aligned} \tag{7.0.35}$$

where u_t is defined as $u_t(s) = u(t+s)$.

Remark. For $Y = \mathbb{R}$ and $B = 0$ we are left with a scalar linear neutral DDE.

Example. For $Y = C(\mathbb{R}^n, \mathbb{R})$, $B = \triangle$, some $\mathcal{D}(B) \subset C(\mathbb{R}^n, \mathbb{R})$ and $L = \delta_{-\tau}$ the ADDE transforms to a heat equation with a time delayed term

$$\begin{aligned} \dot{u}(t) &= \triangle u(t) + u(t-\tau) \quad t \geq 0 \\ u_0 &= \varphi \in X. \end{aligned}$$

In **[51]** (section VI, chapter 6) it is shown that for an appropriate concept of solution, this equation is equivalent to the following abstract Cauchy problem (ACP)

$$\begin{aligned} \dot{\varphi}(t) &= A\varphi \\ \varphi(0) &= \varphi_0 \end{aligned} \tag{7.0.36}$$

where $\varphi \in X$ and the generator A is defined as

$$\begin{aligned} A\varphi &= \varphi' \\ \mathcal{D}(A) &= \left\{ \varphi \in C^1([-\tau, 0], Y) \mid \begin{array}{c} \varphi(0) \in \mathcal{D}(B) \\ \varphi'(0) = B\varphi(0) + L\varphi \end{array} \right\}. \end{aligned}$$

Now, to see that this is indeed a hyperbolic PDE we rewrite it once more. For a solution φ of ACP set $z(t,s) := \varphi(t)(s)$. Then the ACP can be written as

$$\begin{aligned} \frac{\partial}{\partial t} z(t,s) &= \frac{\partial}{\partial s} z(t,s) \\ z(0,s) &= \varphi_0(s). \end{aligned}$$

It is remarkable that the independent variable s now represents the space variable. From this point of view, the delay interval $[-\tau, 0]$ constitutes the space and the flow evolves the initial function on this interval. Hence, DDEs constitute a very special class of hyperbolic PDEs in that they have only one space dimension.

Bibliography

[1] L.F. Abbott and S.B. Nelson. Synaptic plasticity: taming the beast. *Nature neuroscience*, 3:1178–1183, 2000.

[2] D. M. Abrams and S. H. Strogatz. Chimera states for coupled oscillators. *Phys. Rev. Lett.*, 93(17):174102, 2004.

[3] J. A. Acebrón, L. L. Bonilla, C. J. Pérez Vicente, F. Ritort, and R. Spigler. The Kuramoto model: A simple paradigm for synchronization phenomena. *Rev. Mod. Phys.*, 77:137–185, 2005.

[4] R. Albert, H. Jeong, and A.-L. Barabasi. Diameter of the world-wide web. *Nature (London)*, 401:130, 1999.

[5] Y. V. Andreyev, A. S. Dmitriev, L. O. Chua, and C. W. Wu. Associative and random access memory using one-dimensional maps. *Int. J. Bif. Chaos*, 02:483–504, 1992.

[6] D.G. Aronson, G.B. Ermentrout, and N. Kopell. Amplitude response of coupled oscillators. *Physica D*, 41:403–449, 1990.

[7] F.M. Atay, T. Biyikoglu, and J. Jost. Synchronization of networks with prescribed degree distributions. *Circuits and Systems I: Regular Papers, IEEE Transactions on*, 53:92–98, 2006.

[8] F.M. Atay and A. Hutt. Stability and bifurcations in neural fields with finite propagation speed and general connectivity. *SIAM J. Appl. Math.*, 65(2):pp. 644–666, 2004.

[9] P. Baldi and A. Atiya. How delays affect neural dynamics and learning. *IEEE Transactions on Neural Networks*, 5:1045–9227, 1994.

[10] J. Bang-Jensen and G. Gutin. *Digraphs*. Springer, 2009.

[11] A.-L. Barabasi and R. Albert. Emergence of scaling in random networks. *Science*, 5439:509–512, 1999.

[12] M. Barahona and L.M. Pecora. Synchronization in small-world systems. *Phys. Rev. Lett.*, 89:054101, 2002.

[13] R. Barrio and A. Shilnikov. Parameter-sweeping techniques for temporal dynamics of neuronal systems: case study of hindmarsh-rose model. *J. of Math. Neuroscience*, 1, 2011.

[14] J. Bélair and S. Campbell. Stability and bifurcations of equilibria in a multiple-delayed differential equation. *SIAM J. Appl. Math.*, 54(5):1402–1424, 1994.

[15] R. Bellman and K. Cooke. *Differential difference equations*. Academic Press, New-York – London, 1963.

[16] I. Belykh, V. Belykh, and M. Hasler. Synchronization in asymmetrically coupled networks with node balance. *Chaos*, 16:015102, 2006.

[17] A. Berman and R.J. Plemmons. *Nonnegative Matrices in the Mathematical Sciences*. SIAM, 1994.

[18] M. Le Berre, E. Ressayre, A. Tallet, H. M. Gibbs, D. L. Kaplan, and M. H. Rose. Conjecture on the dimensions of chaotic attractors of delayed-feedback dynamical systems. *Phys. Rev. A*, 35:4020–4022, 1987.

[19] T. Biyikoglu, J. Leydold, and P.F. Stadler. *Laplacian Eigenvectors of Graphs*. Springer, 2007.

[20] S. Boccaletti, V. Latora, Y. Moreno, M. Chavez, and D.-U. Hwanga. Complex networks: Structure and dynamics. *Phys. Rep.*, 424:175–308, 2006.

[21] D. Braess. über ein paradoxon aus der verkehrsplanung. *Unternehmensforschung*, 12:258–268, 1968.

[22] D. Braess, A. Nagurney, and T. Wakolbinger. On a paradox of traffic planning. *Transp. Sci.*, 39:446–450, 2005.

[23] P. C. Bressloff, S. Coombes, and B. de Souza. Dynamics of a ring of pulse-coupled oscillators: Group-theoretic approach. *Phys. Rev. Lett.*, 79(15):2791–2794, 1997.

[24] A.E. Brouwer and W. H. Haemers. *Spectra of graphs*. Springer, 2011.

[25] J. Buck. Synchronous flashing of fireflies experimentally induced. *Science*, 81:339–340, 1935.

[26] S.V. Buldyrev, R. Parshani, G. Paul, H.E. Stanley, and S. Havlin. Catastrophic cascade of failures in interdependent networks. *Nature*, 464:08932, 2010.

[27] S.A. Campbell. Time delays in neural systems. In V. Jirsa and A. McIntosh, editors, *Handbook of brain connectivity*, pages 65–90. Springer-Verlag Berlin Heidelberg, 2007.

[28] S.A. Campbell, I. Ncube, and J. Wu. Multistability and stable asynchronous periodic oscillations in a multiple-delayed neural system. *Physica D: Nonlinear Phenomena*, 214(2):101 – 119, 2006.

[29] S.A. Campbell, S. Ruan, and J. Wei. Qualitative analysis of a neural network model with multiple time delays. *Int. J. Bif. Chaos*, 9(08):1585–1595, 1999.

[30] C.C. Canavier and S. Achuthan. Pulse coupled oscillators and the phase resetting curve. *Mathematical biosciences*, 226(2):77–96, 2010.

[31] P.Y. Chebotarev and R.P. Agaev. *Automation and Remote Control*, chapter Coordination in multiagent systems and Laplacian spectra of digraphs, pages 469–483. Springer, 2009.

[32] H. Chiba. A proof of the kuramoto's conjecture for a bifurcation structure of the infinite dimensional kuramoto model. *arXiv:1008.0249*, 2010.

[33] H. Chiba. A proof of the kuramoto conjecture for a bifurcation structure of the infinite dimensional kuramoto model. *Ergo. Theo. Dyn. Sys.*, pages 1–73, 2013.

[34] C. Chicone. Inertial and slow manifolds for delay equations with small delay. *J. Differential Equations*, 190:364–406, 2003.

[35] S.-N. Chow and K. Lu. Invariant manifolds for flows in banach spaces. *J. of Diff. Eq.*, 74:285–317, 1988.

[36] J.J. Collins and I. Stewart. A group-theoretic approach to rings of coupled biological oscillators. *Biol Cybern*, 71(2):95–103, 1994.

[37] J.J. Collins and I.N. Stewart. Coupled nonlinear oscillators and the symmetries of animal gaits. *J. Nonlinear Sci.*, 3:349–392, 1993.

[38] A. Coppel. *Dichotomies in Stability Theory*. Springer, 1978.

[39] H. Daido. Strange waves in coupled-oscillator arrays: Mapping approach. *Phys. Rev. Lett.*, 78(9):1683–1686, 1997.

[40] T. Danino, O. Mondragon-Palomino, L. Tsimring, and J. Hasty. A synchronized quorum of genetic clocks. *Nature*, 463:326–330, 2010.

[41] D. de Solla Price. Networks of scientific papers. *Science*, 149:510–511, 1965.

[42] G. Deco, V. K. Jirsa, and R. McIntosh. Emerging concepts for the dynamical organization of resting-state activity in the brain. *Nature Reviews Neuroscience*, 12:43–56, 2011.

[43] M. Dhamala, V.K. Jirsa, and M. Ding. Enhancement of neural synchrony by time delay. *Phys. Rev. Lett.*, 92, 2004.

[44] A.P. Dias and J. Lamb. Local bifurcation in symmetric coupled cell networks: linear theory. *Physica D*, 223:93–108, 2006.

[45] R. Diestel. *Graph Theory*. Springer-Verlag, Heidelberg, 2010.

[46] E.J. Doedel. *AUTO-07P: Continuation and bifurcation software for ordinary differential equations*. Montreal, Canada, April 2006.

[47] F. Dörfler and F. Bullo. Synchronisation and transient stability in power networks and nonuniform kuramoto oscillators. *SIAM J Cont. Optim.*, 50:1616–1642, 2012.

[48] B. Dorizzi, B. Grammaticos, M. LeBerre, Y. Pomeau, E. Ressayre, and A. Tallet. Statistics and dimension of chaos in differential delay systems. *Phys. Rev. A*, 35:328–339, 1987.

[49] M.G. Earl and S.H. Strogatz. Synchronization in oscillator networks with delayed coupling: A stability criterion. *Phys. Rev. E*, 67:036204, 2003.

[50] W. Eckhaus. *Studies in Non-Linear Stability Theory*, volume 6 of *Springer Tracts in Natural Philosophy*. Springer, New York, 1965.

[51] K.-J. Engel and R. Nagel. *One-Parameter Semigroups for Linear Evolution Equations*. Springer, 2000.

[52] P. Erdös and A. Rényi. On random graphs. *Pub. Mat. Debrecen*, 6:290–297, 1959.

[53] G.B. Ermentrout and N. Kopell. Oscillator death in systems of coupled neural oscillators. *SIAM J. Appl. Math.*, 50:125–146, 1990.

[54] T. Erneux. *Applied Delay Differential Equations*, volume 3 of *Surveys and Tutorials in the Applied Mathematical Sciences*. Springer, 2009.

[55] U. Ernst, K. Pawelzik, and T. Geisel. Synchronization induced by temporal delays in pulse-coupled oscillators. *Phys. Rev. Lett.*, 74(9):1570–1573, Feb 1995.

[56] P. Bonifazi et al. Gabaergic hub neurons orchestrate synchrony in developing hippocampal networks. *Science*, 326:1419–1424, 2009.

[57] H. Farhangi. The path of the smart grid. *Power and Energy Magazine, IEEE*, 8:18–28, 2010.

[58] N. Fenichel. Persistence and smoothness of invariant manifolds for flows. *Indiana Univ. Math. J*, 21(193-226):1972, 1971.

[59] B. Fiedler, V. Flunkert, P. Hövel, and E. Schöll. Delay stabilization of periodic orbits in coupled oscillator systems. *Phil. Trans. R. Soc. A*, 368:319–341, 2010.

[60] B. Fiedler, S. Yanchuk, V. Flunkert, P. Hövel, H.-J. Wünsche, and E. Schöll. Delay stabilization of rotating waves near fold bifurcation and application to all-optical control of a semiconductor laser. *Phys. Rev. E*, 77(6):066207, 2008.

[61] M. Fiedler. Algebraic connectivity of graphs. *Czechoslovak Mathematical Journal*, 23:298–305, 1973.

[62] P. Fries. A mechanism for cognitive dynamics: neuronal communication through neuronal coherence. *Trends in Cogn. Sc.*, 9:474–480, 2005.

[63] P. M. Gade and C.-K. Hu. Synchronous chaos in coupled map lattices with small-world interactions. *Phys. Rev. E*, 62:6409–6413, 2002.

[64] P. Goel and B. Ermentrout. Synchrony, stability, and firing patterns in pulse-coupled oscillators. *Physica D: Nonlinear Phenomena*, 163(3-4):191 – 216, 2002.

[65] M. Golubitsky and D.G. Schaeffer. *Singularities and Groups in Bifurcation Theory. Volume I*, volume 51 of *Applied Mathematical Sciences*. Springer-Verlag, New-York, 1985.

[66] M. Golubitsky, I. Stewart, and D.G. Schaeffer. *Singularities and Groups in Bifurcation Theory. Volume II*, volume 69 of *Applied Mathematical Sciences*. Springer-Verlag, New-York, 1988.

[67] J. Gomez-Gardenes, S. Gomez, A. Arenas, and Y. Moreno. Explosive synchronization transitions in scale-free networks. *Phys. Rev. Lett.*, 106:128701, 2011.

[68] K. Gopalsamy and X.-Z. He. Stability in asymmetric hopfield nets with transmission delays. *Physica D: Nonlinear Phenomena*, 76(4):344–358, 1994.

[69] A. Gosh, Y. Rho, A.R. McIntosh, R. Kötter, and V.K. Jirsa. Noise during rest enables the exploration of the brain's dynamic repertoire. *PLoS Computational Biology*, 2008.

[70] K. Gu, S.-I. Niculescu, and J. Chen. On stability crossing curves for general systems with two delays. *Journal of Mathematical Analysis and Applications*, 311(1):231–253, 2005.

[71] S. Guo, Y. Chen, and J. Wu. Two-parameter bifurcations in a network of two neurons with multiple delays. *Journal of Differential Equations*, 244(2):444–486, 2008.

[72] J. K. Hale and S. M. Verduyn Lunel. *Introduction to Functional Differential Equations*. Springer-Verlag, 1993.

[73] C. Hammond, H. Bergman, and P. Brown. Pathological synchronization in parkinson's disease: networks, models and treatments. *TRENDS in Neuroscience*, 30:357–364, 2007.

[74] J.D. Hart, J.P. Pade, T. Pereira, T.E. Murphy, and R. Roy. Adding connections can hinder network synchronization of time-delayed oscillators. *in preparation*, 2015.

[75] E.N. Harvey. *Living light*. Princeton University Press, 1940.

[76] M. E. Hasselmo, L. M. Giocomo, and M. Yoshida. Cellular dynamical mechanisms for encoding the time and place of events along spatiotemporal trajectories in episodic memory. *Behavioral Brain Research*, 215, 2:261–274, 2010.

[77] D.O. Hebb. *The organization of behavior: A neuropsychological approach*. John Wiley & Sons, 1949.

[78] S. Herculano-Houzel. The human brain in numbers: a linearly scaled-up primate brain. *Front. Hum. Neurosci.*, 3, 2009.

[79] P. Holme, C.R. Edling, and F. Liljeros. Structure and time evolution of an internet dating community. *Social Networks*, 26:155–174, 2004.

[80] J. J. Hopfield. Neural networks and physical systems with emergent collective computational abilities. *Proc Natl Acad Sci U S A*, 79:15541558, 1982.

[81] J. J. Hopfield. Pattern-recognition computation using action-potential timing for stimulus representation. *Nature*, 376(6535):33–36, July 1995.

[82] Y. Horikawa. Exponential dispersion relation and its effects on unstable propagating pulses in unidirectionally coupled symmetric bistable elements. *Communications in Nonlinear Science and Numerical Simulation*, 17(7):2791 – 2803, 2012.

[83] Y. Horikawa and H. Kitajima. Transient chaotic rotating waves in a ring of unidirectionally coupled symmetric bonhoeffer-van der pol oscillators near a codimension-two bifurcation point. *Chaos*, 22(3):033115, 2012.

[84] R.A. Horn and C.R. Johnson. *Matrix analysis*. Cambridge Univ. Press, 1985.

[85] R. Hoyle. *Pattern Formation. An Introduction to Methods*. Cambridge University Press, 2006.

[86] L. Huang, Y. Lai, and R. A. Gatenby. Optimization of synchronization in complex clusterd networks. *Chaos*, 18, 2008.

[87] H.J. Hupkes and B. Sandstede. Modulated wave trains in lattice differential systems. *J. of Dyn. and Diff. Eq.*, 21:417–485, 2009.

[88] T. Ichinomiya. Frequency synchronization in a random oscillator network. *Phys. Rev. E*, 70:026116, 2004.

[89] E. M. Izhikevich. Which model to use for cortical spiking neurons? *IEEE Trans. Neural Netw.*, 15(5):1063–1070, 2004.

[90] E.M. Izhikevich. *Dynamical Systems in Neuroscience: The Geometry of Excitability and Bursting*. The MIT Press, 2005.

[91] E.M. Izhikevich and G.M. Edelman. Large-scale model of mammalian thalamocortical systems. *Proceedings of the national academy of sciences*, 105(9):3593–3598, 2008.

[92] M. Jalili. Enhancing synchronizability of diffusively coupled dynamical networks: a survey. *IEEE TNNLS*, 24:1009–1022, 2013.

[93] J. Jost and M. P. Joy. Spectral properties and synchronization in coupled map lattices. *Phys. Rev. E*, 65(1):016201, 2001.

[94] W. Just, T. Bernard, M. Ostheimer, E. Reibold, and H. Benner. Mechanism of time-delayed feedback control. *Phys. Rev. Lett.*, 78:203–206, 1997.

[95] E.R. Kandel, J.H. Schwartz, and T.M. Jessell. *Principles of Neural Science*. McGraw-Hill Medical, 2000.

[96] I. Kanter, M. Zigzag, A. Englert, F. Geissler, and W. Kinzel. Synchronization of unidirectional time delay chaotic networks and the greatest common divisor. *EPL (Europhysics Letters)*, 93(6):60003, 2011.

[97] W. Klimesch. Memory processes, brain oscillations and eeg synchronization. *Intern. J. of Psychophysiol.*, 24:61–100, 1996.

[98] A. Koseska and J. Kurths. Topological structures enhance the presence of dynamical regimes in synthetic networks. *Chaos: An Interdisciplinary Journal of Nonlinear Science*, 20(4):045111, 2010.

[99] J.B. Kruskal, Jr. On the shortest spanning subtree of a graph and the traveling salesman problem. *Proc. Amer. Math. Soc.*, 7:48–50, 1956.

[100] Y. Kuang. *Delay Differential Equations with Applications in Population Dynamics*, volume 191 of *Mathematics in science and engineering*. Academic Press, 1993.

[101] Y. Kuramoto. In H. Araki, editor, *International Symposium on Mathematical Problems in Theoretical Physics, edited by H. Araki,*, volume 30 of *Lecture Notes in Physics*, page 420. Springer, New York, 1975.

[102] Y. Kuramoto. *Chemical Oscillations, Waves, and Turbulence*. Springer, Berlin, 1984.

[103] Y. Kuznetsov. *Elements of Applied Bifurcation Theory*, volume 112 of *Applied Mathematical Sciences*. Springer-Verlag, 1995.

[104] J. Lamb and I. Melbourne. Bifurcation from discrete rotating waves. *Archive for Rat. Mech. and Anal.*, 149:229–270, 1999.

[105] J. Lamb, I. Melbourne, and C. Wulff. Bifurcation from periodic solutions with spatiotemporal symmetry, including resonances and mode interactions. *J. Differ. Equ.*, 191:377–407, 2003.

[106] P. Lancaster. *The theory of matrices*. Academic Press, 1985.

[107] L. Larger, M. C. Soriano, D. Brunner, L. Appeltant, J. M. Gutierrez, L. Pesquera, C. R. Mirasso, and I. Fischer. Photonic information processing beyond turing: an optoelectronic implementation of reservoir computing. *Opt. Express*, 20(3):3241–3249, Jan 2012.

[108] D.-S. Lee. Synchronization transition in scale-free networks: Clusters of synchrony. *Phys. Rev. E*, 72:026208, 2005.

[109] W. S. Lee, E. Ott, and T. M. Antonsen. Large coupled oscillator systems with heterogeneous interaction delays. *Phys. Rev. Lett.*, 103:044101, Jul 2009.

[110] G.A. Leonov and N.V. Kuznetsov. Time-varying linearization and the perron effects. *Int. J. Bif. Chaos*, 17:1079–1107, 2007.

[111] J. Li and Y. Kuang. Analysis of a model of the glucose-insulin regulatory system with two delays. *SIAM J. Appl. Math.*, 67(3):757–776, 2007.

[112] F. Liljeros, C.R. Edling, L.A.N. Amaral, H.E. Stanley, and Y. Aberg. The web of human sexual contacts. *Nature*, 411:907–908, 2001.

[113] W. Lu and T. Chen. Synchronization of coupled connected neural networks with delays. *IEEE Transactions on Circuits and Systems Part 1: Regular Papers*, 51(12):2491–2503, 2004.

[114] L. Lücken, J. P. Pade, K. Knauer, and S. Yanchuk. Reduction of interaction delays in networks. *EPL (Europhysics Letters)*, 103:10006, 2013.

[115] M. Lysetskiy, A. Lozowski, and J.M. Zurada. Invariant recognition of spatio-temporal patterns in the olfactory system model. *Neural Processing Letters*, 15:225–234, 2002.

[116] M. C. Mackey and L. Glass. Oscillation and chaos in physiological control systems. *Science*, 197:287, 1977.

[117] J. Mallet-Paret and G.R. Sell. The poincaré–bendixson theorem for monotone cyclic feedback systems with delay. *Journal of differential equations*, 125(2):441–489, 1996.

[118] Y. Manor, C. Koch, and I. Segev. Effect of geometrical irregularities on propagation delay in axonal trees. *Biophysical Journal*, 60(6):1424–1437, 1991.

[119] J. Maynard-Smith. *Models in Ecology*. Cambridge Univ. Press, 1974.

[120] P.J. Menck, J. Heitzig, N. Marwan, and J. Kurths. How basin stability complements the linear-stability paradigm. *Nat. Phys.*, 9:89–92, 2013.

[121] R. Milo, S. Shen-Orr, S. Itzkovitz, N. Kashtan, D. Chklovskii, and U. Alon. Network motifs: Simple building blocks of complex networks. *Science*, 298(5594):824–827, 2002.

[122] J. Milton and P. Jung, editors. *Epilepsy as a Dynamic Disease*. Springer, 2003.

[123] R. E. Mirollo and S. H. Strogatz. The spectrum of the locked state for the kuramoto model of coupled oscillators. *Physica D*, 205:249–266, 2005.

[124] J.M. Montoya and R.V. Sole. Small world patterns in food webs. *J. Theor. Biol.*, 214:405–412, 2002.

[125] A. E. Motter, S. A. Myers, M. Anghel, and T. Nishikawa. Spontaneous synchrony in power-grid networks. *Nat. Phys.*, 9:191–197, 2013.

[126] A. E. Motter, C. Zhou, and J. Kurths. Network synchronization, diffusion and the paradox of heterogeneity. *Phys. Rev. E.*, 71, 2005.

[127] T. Nishikawa A.E. Motter, Y.-C. Lai, and F.C. Hoppensteadt. Heterogeneity in oscillator networks: Are smaller worlds easier to synchronize? *Phys. Rev. Lett.*, 91:014101, 2003.

[128] H. Nakao and A.S. Mikhailov. Turing patterns in network-organized activator-inhibitor systems. *Nat. Phys.*, 6:544–550, 2010.

[129] M. E. J. Newman. *Networks: An Introduction*. Oxford Univ Press, 2010.

[130] T. Nishikawa and A.E. Motter. Maximum performance at minimum cost in network synchronization. *Physica D*, 224:77–89, 2006.

[131] R.D. Nussbaum. *Differential-delay equations with two time lags*, volume 16. American Mathematical Society, 1978.

[132] E. Ott and T.M. Antonsen. Low dimensional behavior of large systems of globally coupled oscillators. *Chaos*, 18:037113, 2008.

[133] A. Panchuk, D.P. Rosin, P. Hövel, and E. Schöll. Synchronization of coupled neural oscillators with heterogeneous delays. *Int. J. Bif. Chaos*, 23(12), 2013.

[134] A. A. Papadopoulos, J. A. McCann, and A. Navarra. Connectionless probabilistic (cop) routing: an efficient protocol for mobile wireless ad-hoc sensor networkspapadopoulos2005. In *24th IEEE International IPCCC*, 2005.

[135] R. Pastor-Satorras and A. Vespignani. *Evolution and Structure of the Internet. A Statistical Physics Approach*. Cambridge Univ. Press, 2004.

[136] L.M. Pecora and T.L. Carroll. Master stability functions for synchronized coupled systems. *Phys. Rev. Lett.*, 80:2109–2112, 1998.

[137] T. Pereira, J. Eldering, M. Rasmussen, and A. Veneziani. Towards a theory for diffusive coupling functions allowing persistent synchronization. *Nonlinearity*, 27:501–525, 2014.

[138] P. Perlikowski, S. Yanchuk, O. V. Popovych, and P. A. Tass. Periodic patterns in a ring of delay-coupled oscillators. *Phys. Rev. E*, 82(3):036208, Sep 2010.

[139] P. Perlikowski, S. Yanchuk, M. Wolfrum, A. Stefanski, P. Mosiolek, and T. Kapitaniak. Routes to complex dynamics in a ring of unidirectionally coupled systems. *Chaos*, 20:013111, 2010.

[140] T. K. Peron and F. A. Rodrigues. Explosive synchronization enhanced by time-delayed coupling. *Phys. Rev. E*, 86:016102, 2012.

[141] A. Pikovsky, M. Rosenblum, and J. Kurths. *Synchronization. A Universal Concept in Nonlinear Sciences*. Cambridge University Press, 2001.

[142] O. V. Popovych, S. Yanchuk, and P. A. Tass. Delay- and coupling-induced firing patterns in oscillatory neural loops. *Phys. Rev. Lett.*, 107:228102, 2011.

[143] O.V. Popovych, S. Yanchuk, and P.A. Tass. Self-organized noise resistance of oscillatory neural networks with spike timing-dependent plasticity. *Sci. Rep.*, 3:2926, 2013.

[144] K. Pyragas. Continuous control of chaos by self-controlling feedback. *Physics Letters A*, 170:421–427, 1992.

[145] F. Radicchi and A. Arenas. Abrupt transition in the structural formation of interconnected networks. *Nat. Phys.*, 9:717–720, 2013.

[146] W. Ren and R. Beard. *Distributed consensus in Multi-vehicle Cooperative Control*. Springer, 2007.

[147] J. G. Restrepo and E. Ott. Mean-field theory of assortative networks of phase oscillators. *EPL (Europhysics Letters)*, 107:60006, 2014.

[148] J.G. Restrepo, E. Ott, and B.R. Hunt. Desynchronization waves and localized instabilities in oscillator arrays. *Phys. Rev. Lett.*, 93(11):114101, 2004.

[149] J.G. Restrepo, E. Ott, and B.R. Hunt. Spatial patterns of desynchronization bursts in networks. *Phys. Rev. E*, 69(6):066215, 2004.

[150] J. A. Rogge and D. Aeyels. Stability of phase locking in a ring of unidirectionally coupled oscillators. *Journal of Physics A: Mathematical and General*, 37:11135–11148, 2004.

[151] M. G. Rosenblum, A. S. Pikovsky, and J. Kurths. Phase synchronization of chaotic oscillators. *Phys. Rev. Lett.*, 76:1804–1807, 1996.

[152] D.P. Rosin, D. Rontani, D.J. Gauthier, and E. Schöll. Control of synchronization patterns in neural-like boolean networks. *Phys. Rev. Lett.*, 110:104102, Mar 2013.

[153] O. Rössler. An equation for hyperchaos. *Phys. Letters*, 71A, 1979.

[154] S. Ruan and J. Wei. On the zeros of transcendental functions with applications to stability of delay differential equations with two delays. *Dynamics of Continuous, Discrete and Impulsive Systems Series A*, 10:863–874, 2003.

[155] H. Sakaguchi. Cooperative phenomena in coupled oscillator systems under external fields. *Progr. Theoret. Phys.*, 79:39–46, 1988.

[156] B. Sandstede and A. Scheel. Spectral stability of modulated travelling waves bifurcating near essential instabilites. *Proceedings of the Royal Society of Edinburgh*, 130:419–448, 2000.

[157] B. Sandstede and A. Scheel. On the structure of spectra of modulated travelling waves. *Math. Nachr.*, 232:39–93, 2001.

[158] Y. Shan, D. Huang, W. Singer, and D. Nikolic. A small world of neuronal synchrony. *Cerebral Cortex*, 18:2891 – 2901, 2008.

[159] L.P. Shayer and S.A. Campbell. Stability, bifurcation, and multistability in a system of two coupled neurons with multiple time delays. *SIAM J. Appl. Math.*, 61(2):673–700, 2000.

[160] Y. Shen and J. Wang. Robustness analysis of global exponential stability of recurrent neural networks in the presence of time delays and random disturbances. *IEEE TNNLS*, 23:87–96, 2012.

[161] C. A. Skarda and W. J. Freeman. How brain makes chaos in order to make sense of the world. *Behavioral Brain Sci.*, 10:161–195, 1987.

[162] S. Smale. Differentiable dynamical systems. *Bull. Amer. Math. Soc*, 73:747–817, 1967.

[163] S. Smale. *The Hopf Bifurcation and Its Applications*, chapter 11, pages 354–367. Springer Berlin, 1976.

[164] M.C. Soriano, J. García-Ojalvo, C.R. Mirasso, and I. Fischer. Complex photonics: Dynamics and applications of delay-coupled semiconductors lasers. *Rev. Mod. Phys.*, 85:421–470, 2013.

[165] P. A. Starr, G. M. Rau, V. Davis, W. J. Marks, J. L. Ostrem, D. Simmons, N. Lindsey, and R. S. Turner. Spontaneous pallidal neuronal activity in human dystonia: Comparison with parkinson's disease and normal macaque. *J. of Neurophysiol.*, 93:3165–3176, 2005.

[166] N. Strelkowa and M. Barahona. Transient dynamics around unstable periodic orbits in the generalized repressilator model. *Chaos*, 21(2):023104, 2011.

[167] S.H. Strogatz. Exploring complex networks. *Nature*, 410:268 – 276, 2001.

[168] S.H. Strogatz and R. E. Mirollo. Stability of incoherence in a population of coupled oscillators. *J. of Stat. Phys.*, 63:613–635, 1991.

[169] A. Takamatsu, R. Tanaka, H. Yamada, T. Nakagaki, T. Fujii, and I. Endo. Spatiotemporal symmetry in rings of coupled biological oscillators of physarum plasmodial slime mold. *Phys. Rev. Lett*, 87(7):078102, Jul 2001.

[170] T. Tao and V. Vu. Random matrices have simple spectrum. *arXiv:1412.1438v1*, 2014.

[171] R. Temam. *Infinite-Dimensional Dynamical Systems in Mechanics and Physics*. Springer, 1997.

[172] L.S. Tuckerman and D. Barkley. Bifurcation analysis of the Eckhaus instability. *Physica D*, 46:57–86, 1990.

[173] A. M. Turing. The chemical basis of morphogenesis. *Philosophical Transactions of the Royal Society of London. Series B, Biological Sciences*, 237(641):37–72, 1952.

[174] P. Van Den Driessche and X. Zou. Global attractivity in delayed hopfield neural network models. *SIAM J. Appl. Math.*, 58(6):1878–1890, 1998.

[175] Guy Van der Sande, Miguel C. Soriano, Ingo Fischer, and Claudio R. Mirasso. Dynamics, correlation scaling, and synchronization behavior in rings of delay-coupled oscillators. *Phys. Rev. E*, 77:055202, 2008.

[176] N. van Kampen. *Stochastic processes in physics and chemistry*. North-Holland, 1981.

[177] R. Vicente, S. Tang, J. Mulet, C.R. Mirasso, and J.-M. Liu. Synchronization properties of two self-oscillating semiconductor lasers subject to delayed optoelectronic mutual coupling. *Phys. Rev. E*, 73:047201, 2006.

[178] A. Vishwanathan, G. Bi, and H.C. Zeringue. Ring-shaped neuronal networks: a platform to study persistent activity. *Lab Chip*, 11(6):1081–8, 2011.

[179] I. Waller and R. Kapral. Spatial and temporal structure in systems of coupled nonlinear oscillators. *Phys. Rev. A*, 30(4):2047–2055, 1984.

[180] L. Wang and X. Zou. Capacity of stable periodic solutions in discrete-time bidirectional associative memory neural networks. *IEEE Trans. Circuits Syst, Express Briefs*, 51:315–319, 2004.

[181] N. Wiener. *Nonlinear Problems in Random Theory*. MIT Press, 1958.

[182] A. T. Winfree. Biological rhythms and the behavior of populations of coupled oscillators. *Journal of Theoretical Biology*, 16:15–42, 1967.

[183] D. Witthaut and M. Timme. Braess's paradox in oscillator networks, desynchronization and power outage. *New J. Phys.*, 14:083036, 2012.

[184] A. Wu and Z. Zeng. Lagrange stability of memristive neural networks with discrete and distributed delays. *IEEE TNNLS*, 25:690–703, 2014.

[185] J. Wu. *Introduction to neural dynamics and signal transmission delayat*, volume 6. Walter de Gruyter, 2001.

[186] L. Wu and Z. Feng. Stability and synchronization of discrete-time neual networks with switching parameters and time-varying delays. *IEEE TNNLS*, 24:1957–1972, 2013.

[187] H.-J. Wünsche, S. Bauer, J. Kreissl, O. Ushakov, N. Korneyev, F. Henneberger, E. Wille, H. Erzgräber, M. Peil, W. Elsäßer, and I. Fischer. Synchronization of delay-coupled oscillators: A study of semiconductor lasers. *Phys. Rev. Lett.*, 94:163901, 2005.

[188] S. Yanchuk and G. Giacomelli. Pattern formation in systems with multiple delayed feedbacks. *Phys. Rev. Lett.*, 112:174103, 2014.

[189] S. Yanchuk and P. Perlikowski. Delay and periodicity. *Phys. Rev. E*, 79(4):046221, 2009.

[190] S. Yanchuk, P. Perlikowski, O. V. Popovych, and P. A. Tass. Variability of spatio-temporal patterns in non-homogeneous rings of spiking neurons. *Chaos*, 21:047511, 2011.

[191] S. Yanchuk and M. Wolfrum. Destabilization patterns in chains of coupled oscillators. *Phys. Rev. E*, 77(2):026212, 2008.

[192] H. Ye, A.N. Michel, and K. Wang. Qualitative analysis of cohen-grossberg neural networks with multiple delays. *Physical Review E*, 51(3):2611, 1995.

[193] M. K. Stephen Yeung and Steven H. Strogatz. Time delay in the kuramoto model of coupled oscillators. *Phys. Rev. Lett.*, 82(3):648–651, Jan 1999.

[194] W. Zou and M. Zhan. Splay states in a ring of coupled oscillators: From local to global coupling. *SIAM J. Appl. Dyn. Syst.*, 8:1324–1340, 2009.